NUMERICAL STUDY OF ENHANCEMENT OF PLASTIC ROTATION CAPACITY OF SEISMIC STEEL MOMENT CONNECTIONS BY FIBER REINFORCED POLYMER MATERIALS

A Thesis Submitted to
The Graduate School of Engineering and Sciences of
İzmir Institute of Technology
in Partial Fulfillment of the Requirements for the Degree of

MASTER OF SCIENCE

in Civil Engineering

by
Deniz ALKAN

October 2008

İZMİR

We approve the thesis of **Deniz ALKAN**

Assist. Prof. Dr. O. Özgür EĞİLMEZ
Supervisor

Assist. Prof. Dr. Cemalettin DÖNMEZ
Committee Member

Assoc. Prof. Dr. Metin TANOĞLU
Committee Member

14 October 2008

Prof. Dr. Gökmen TAYFUR
Head of the Civil Engineering Department

Prof. Dr. Hasan BÖKE
Dean of the Graduate School of Engineering and Science

ACKNOWLEDGEMENTS

I would like to express my sincere gratitude to my supervisor Assist. Prof.Dr.O. Özgür EĞİLMEZ for his guidance, supervision, patience, and support throughout this study. I also wish to express my thanks to Assist. Prof.Dr. Cemalettin DÖNMEZ and Assoc.Prof.Dr. Metin TANOĞLU for their all kind of support and help.

I also would like to thank to gratefully acknowledge The Scientific and Technical Research Council of Turkey (TUBITAK - Project Number 106Y309) for their supports.

I would also like to thank to research assistant Can Ali GÜVEN for his contribution to my thesis and my friends Nisa KARTALTEPE and Eyyüb KARAKAN for their supports.

Lastly, I offer sincere thanks to my family members for their endless support, encouragement and love.

ABSTRACT

NUMERICAL STUDY OF ENHANCEMENT OF PLASTIC ROTATION CAPACITY OF SEISMIC STEEL MOMENT CONNECTIONS BY FIBER REINFORCED POLYMER MATERIALS

Flange and web local buckling in beam plastic hinge regions of welded Steel Moment Frames (SMF) can prevent the beam-column connections to achieve adequate plastic rotations under earthquake induced forces. Reducing the web-flange slenderness ratios is the most effective way in preventing local member buckling as stipulated in the latest earthquake specifications. However, older steel beam-column connections that lack the adequate slenderness ratios stipulated for new SMFs are vulnerable to local plastic buckling. This study investigates postponing the formation of local buckles in beam flanges and webs at the plastic hinge region of modified SMF connections (welded haunch) by the use of externally bonded Glass Fiber Reinforced Polymers (GFRP). The research includes finite element (FE) modeling. The energy dissipation capacity of existing SMF connections is anticipated to increase with GFRP laminates bonded to flanges of beams in plastic hinge locations. Cantilever beams with and without GFRP were analyzed under quasi-static cyclic loading and the effects to the plastic local buckling of the GFRP laminates added to the steel beams were observed. Both geometric and material nonlinearities are considered. The mechanical properties of the GFRP material were obtained through standard ASTM tests and were utilized directly in the FE model. Steel beams with flange slenderness ratios of 8 to 12 and web slenderness ratios of 40-60-80 were analyzed. Results indicate that GFRP strips can effectively delay the formation of local plastic buckling in the plastic hinge region.

ÖZET

SİSMİK ÇELİK MOMENT BİRLEŞİMLERİNİN PLASTİK DÖNME KAPASİTELERİNİN ELYAF POLİMER MALZEMELER KULLANILARAK ARTIRILMASININ NÜMERİK MODELLEME İLE İNCELENMESİ

Moment aktaran süneklik düzeyi yüksek çelik çerçevelerin (SDYÇ) bir deprem esnasında kiriş plastik mafsal bölgelerinde oluşabilecek başlık ve gövde mevzi burkulmaları, bu sistemlerin arzu edilen plastik dönme değerlerine ulaşmalarını engelleyebilir. Mevzi burkulmaların önüne geçebilmenin başlıca yolu, güncel deprem şartnamelerinin de öngördüğü gibi, başlık ve gövde narinlik oranlarının küçültülmesidir. Ancak yeni yapılacak SDYÇ'ler için şart koşulan narinlik oranlarına sahip olmayan mevcut çelik çerçeve kiriş-kolon birleşimleri başlık ve gövde mevzi burkulmalarına karşı korunmasız durumdadırlar. Mevcut çalışmada modifiye edilmiş SDYÇ'lerin (kaynaklı kemer takviyesi) plastik mafsal bölgesindeki başlık ve gövde mevzi burkulmaların Cam Elyaf Takviyeli Polimer (CTP) malzemeler ile önlenmesi veya ötelenmesi sonlu elemanlar (SE) modeli kullanılarak araştırılmıştır. CTP malzemesinin kiriş plastik mafsal bölgelerine şeritler halinde kiriş başlıklarına yerleştirilmesi ile mevcut SDYÇ'lerin depremler esnasındaki enerji absorbsiyon değerlerinin arttırılacağı öngörülmektedir. CTP takviyeli ve takviyesiz konsol I-kirişler bir sonlu eleman analiz programı kullanılarak tekrarlı yüklere tabi tutulmuştur ve kirişlere eklenen CTP'lerin plastik mafsalda oluşacak yerel plastik burkulmalara etkileri incelenmiştir. Çözümlemelerde doğrusal olmayan geometri ve malzeme modeli kullanılmıştır. CTP malzemesinin ASTM standart test sonuçlarından elde edilen mekanik özellikleri doğrudan sonlu elemanlar modelinde kullanılmıştır. Başlık narinlik oranları 8 ile 12 arasında değişen ve gövde narinlik oranları 40–60–80 olan çelik kirişlerin CTP şeritlerle birlikte ve CTP şeritler olmadan analizleri yapılmıştır. Analiz sonuçları göstermiştir ki CTP şeritler, plastik mafsal bölgesinde oluşan yerel plastik burkulmaları etkili bir şekilde öteleyebilmektedir.

TABLE OF CONTENTS

LIST OF FIGURES

Figure **Page**

LIST OF TABLES

CHAPTER 1

INTRODUCTION

1.1. General

Seismic design of welded steel moment frames (SMF) is generally based on the strong column-weak beam concept, in which the majority of the energy dissipation is anticipated to occur by inelastic deformations in the beams through the formation of plastic hinges near beam-column connections. In general, the philosophy behind seismic design of new SMF is to maintain a total (elastic plus plastic) interstory drift angle of at least 0.02~0.04 radians (for intermediate and special moment frames, respectively) in magnitude without significant strength degradation or development of instability; thereby providing a ductile behavior under earthquake induced forces (AISC 2005b, BİB 2006, Eurocode-8 2003, FEMA 2000a). Interstory drift angle is defined as interstory displacement divided by story height (Figure 1.1). However, during these plastic rotations, inelastic local buckling that frequently occurs in beam flanges and webs is a threat for the ductility and stability of the structural system.

The ductility of welded beam-to-column connections depends on the following failure modes: 1) fracture of the beam flange to column groove weld, 2) lateral torsional buckling (LTB), and 3) flange and web local buckling (FLB and WLB). Most of the research conducted after the 1994 Northridge (US) and 1995 Kobe (Japan) earthquakes focused primarily on stress reduction methodologies and improvement of welding procedures to overcome the brittle weld fractures in order to enhance the plastic rotation capacity of welded connections (Nakashima, et al. 1998, SAC 1996). Based on the findings from these researches new design guidelines and modification methods including Reduced Beam Section (RBS) and Welded Haunch (WH) connections have been developed for new and existing SMFs (AISC 2001, FEMA 2000a, FEMA 2000b). However, inelastic local buckling can still prevent beam-column connections to achieve adequate plastic rotations. This threat is especially valid for existing SMFs that need to

be rehabilitated. Figure 1.2.a depicts a typical exterior welded flange-bolted web pre-Northridge connection where the girder flanges are welded and girder web is bolted to the column flange. Figure 1.2.b shows the typical failure modes of such connections (Fracture of weld and local buckling). Beam-to column connection can also collapse due to LTB. In this study it is assumed that LTB is prevented by sufficiently spaced lateral bracings and therefore is not considered.

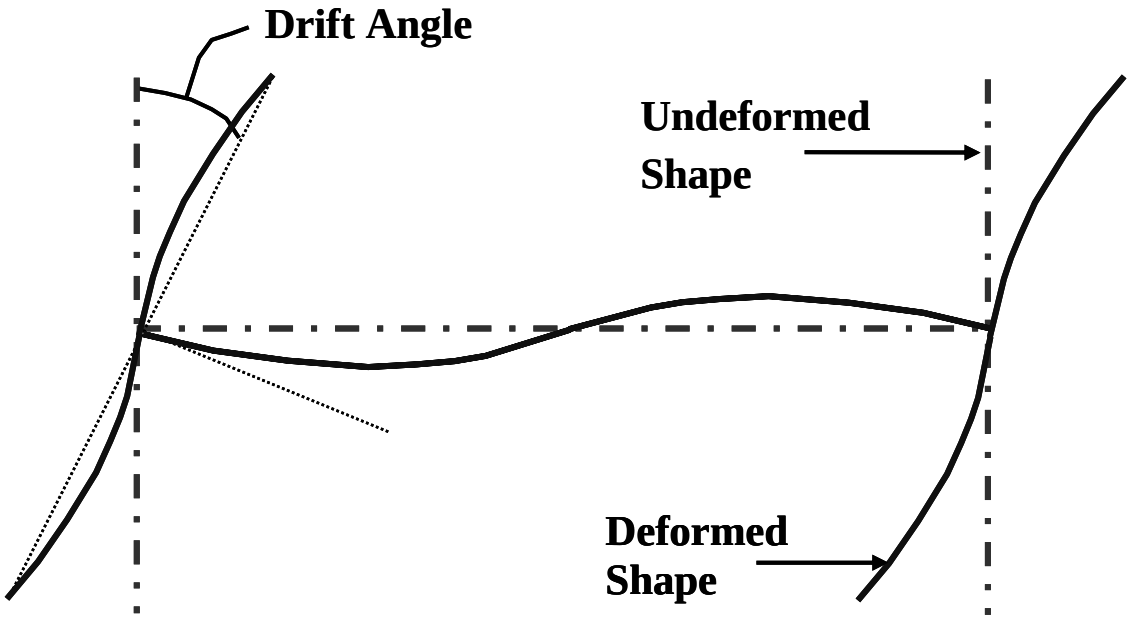

Figure 1.1. Interstory Drift Angle
(Source: FEMA 2000a)

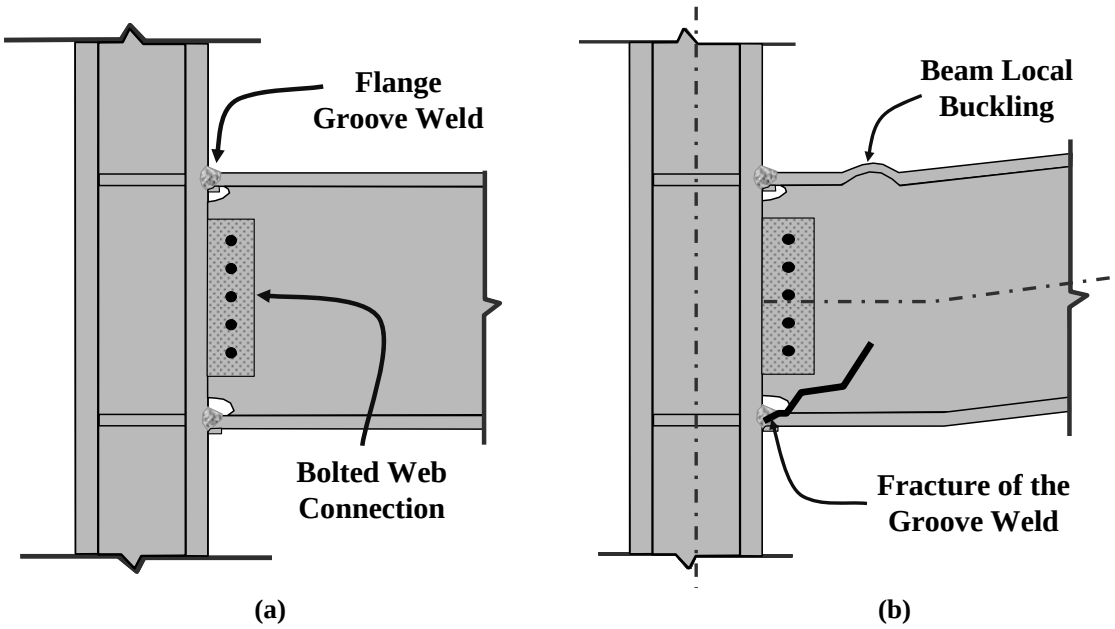

Figure 1.2. a) Typical Welded Flange-Bolted Web Exterior Connection (Prior to 1994)
b) Typical Failure Modes of WSMF Connections (Source: FEMA 2000b)

In current seismic design codes (AISC 2005b, Eurocode-8 2003), lateral-torsional buckling and local instabilities are controlled by limiting the unbraced length between lateral supports and flange-web slenderness ratios, respectively. However, not only these code limits were primarily established for monotonically loaded structures (AISC 1971), but the rotation capacities expected from beam-column connections have increased significantly as a result of post-Northridge and post-Kobe research. This means that especially older structures with poor detailing are vulnerable to local member buckling and thereby system wise instability due to overloads such as earthquakes or other extreme events prior to reaching the required plastic rotation capacities specified for new buildings. Okazaki et al. (2006) and Nakashima et al. (2002 and 2003) have investigated the stability requirements for beams in steel special moment frames under earthquake induced forces and proposed more stringent limits for unbraced length and width-thickness ratios to control instabilities during large plastic rotations. Furthermore, even higher levels of plastic rotations than those stipulated in provisions may also be needed for buildings in soft soils, irregular buildings, and important structures. In addition, the repair of local buckles is an expensive and

challenging application. Therefore, the mitigation of local inelastic instabilities in steel frame I-beams is an important task, which will not only improve the structural ductility and energy dissipation capacity of the structure, but will also minimize cumbersome repair works in the aftermath of extreme events.

1.2. Research Overview and Objectives

In this study it is aimed to improve the ductility of existing SMF connections by preventing or delaying the formation of local buckles in beam flanges or webs at the plastic hinge region of SMF connections modified by a welded haunch (WH) or reduced beam section (RBS) through the use of externally bonded Glass Fiber Reinforced Polymers (GFRP). Figure 1.3 shows GFRP strips placed on top of the bottom beam flange out of the WH region and bottom of the top beam flange in and out of the WH region; considering the presence of a concrete slab over the top flange in a real structure.

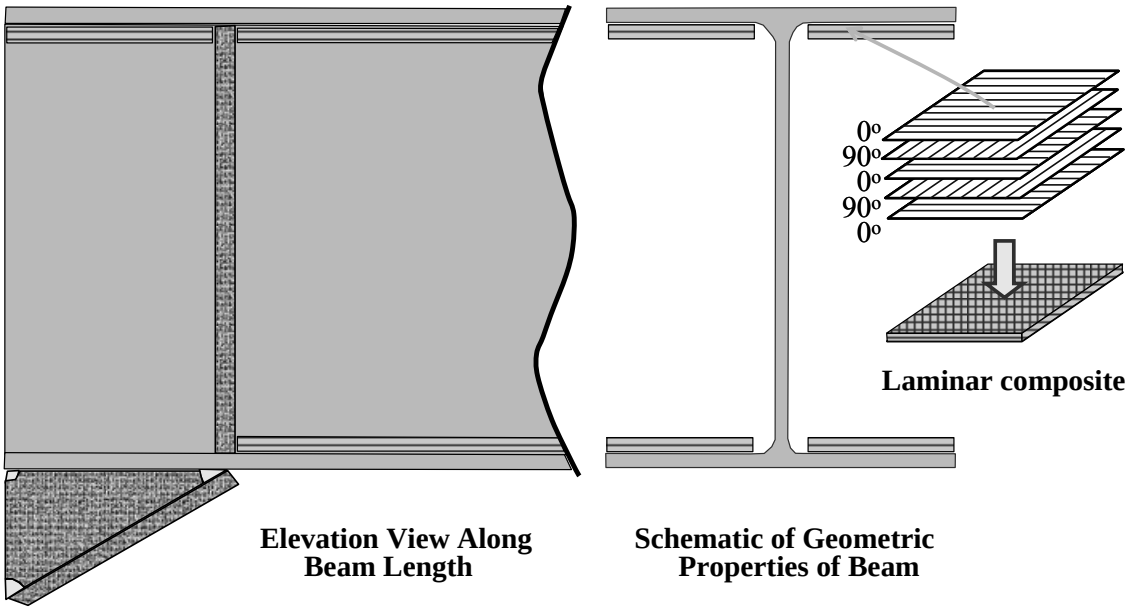

Figure 1.3. The Hybrid System of Beam-GFRP Material

The high stiffness-to-weight and strength-to-weight ratios of FRP materials, combined with their resistance to corrosion have increased their use in repair and strengthening of steel structures. Generally, high modulus carbon FRP laminates, with elastic modulus similar to that of steel, are preferred in repair and strengthening applications of steel members. On the other hand, in a steel-GFRP composite system, the low modulus of GFRP as compared to that of steel can be an asset in stabilizing flange and web local buckling during plastic hinge formations. While the low modulus of GFRP will not allow a significant strength increase in the steel section, its compressive strength will enable GFRP strips to maintain their flexural strength to provide bracing to the underlying steel (Accord and Earls 2006). In a modification application of an SMF a strength increase in the beam section is not desired because such an increase will result in higher forces in the beam-column welds, which can lead to weld fractures. This type of a composite action can enhance the plastic rotation capacity of the plastic hinge region; provided that an early debonding or GFRP fracture do not control the behavior.

Using FRP for stabilization of local buckling will have many advantages over traditional methods such as welding or bolting additional steel to the section. FRPs are very light, easily applicable, corrosion resistant, and will eliminate problems associated with conventional methods, such as introduction of unknown residual stresses and erection difficulties. However, understanding the distribution of material inelastic deformations in the steel beam section, the unique material properties of GFRP and the bonding between GFRP and steel member is essential to leverage the qualities of each material to develop an efficient FRP laminated steel member with enhanced plastic rotation capacities.

A research study has been conducted at the İzmir Institute of Technology (İYTE) to determine the ability of GFRP laminates to brace beam local buckling during large plastic rotations. The research investigation included both laboratory tests and computational studies using finite element analysis. The main goal of this study was to investigate the behavior of steel-GFRP systems under reversed cyclic loading. Experimental study consisted of cantilever I-beam tests with and without GFRP laminates. Fixed ends of the beams were modified by either an RBS or WH detail as stipulated in BİB (2006) and AISC (2005b) and loaded cyclically consistent with AISC standard loading protocol (AISC 2000a). Finite element analyses were also conducted

to investigate the effects of width, thickness, length, and location of GFRP laminates to inelastic local buckling of flanges and web.

1.3. Scope

This thesis reports the results from finite element analysis of beams with only WH detail. The finite element analytical (FEA) work consisted of studying the behavior of several beam sections with web and flange slenderness ratios ranging between 40-80 and 8-12, respectively. The verification of the FEA model was done by comparing the behavior of the model by that of different laboratory tests from literature.

This thesis is divided into five chapters. Following this introduction, Chapter 2 presents background information that is necessary to understand the behavior of modified existing steel I-beams reinforced with glass fiber reinforced polymer (GFRP) laminates. Chapter 3 presents an overview of the finite element model that was used for the SMF systems, a description of sections that were used in the analyses, as well as a set of correlation studies between experimental data and numerical results. After obtaining good correlation between the FE models and the literature data, parametric studies were conducted on modified existing steel I-beams reinforced with and without glass fiber reinforced polymer (GFRP). The results from the parametrical studies are presented in Chapter 4 and a summary of the study and findings is presented in Chapter 5.

CHAPTER 2

BACKGROUND

2.1. Introduction

Seismic design of SMF connections have been significantly changed after the 1994 Northridge and 1995 Kobe earthquakes. In order to provide adequate seismic performance of the pre-Northridge connections, National Institute of Standards and Technology (NIST), the American Institute of Steel Construction (AISC), the Federal Emergency Management Agency (FEMA), the University of California at San Diego, the University of Texas at Austin, and Lehigh University have initiated comprehensive research projects that include experimental, analytical and numerical studies (SAC 1996, AISC 2001, Uang, et al. 2000, Yu, et al. 2000). As a consequence, new design guidelines have been proposed for new constructions and modification methods have been developed for existing SMFs in order to improve the seismic performance that includes strength, stiffness, ductility, and deformation capacity of the connections (FEMA 2000b).

Three main design strategies that include strengthening or weakening the beams have been proposed in new design guidelines so that the plastic hinging of the beam could occur away from the face of the column: Reduced Beam Section (RBS), Welded Haunch (WH), and Bolted Bracket (BB) modifications (AISC 2001). Forcing the plastic hinge to occur away from the face of the column limits the maximum moment at the column face and thereby reduces the risk of brittle weld fractures near the edge of the beam flange to column groove weld. In this thesis only the WH modifications are considered. Gross et al. (AISC 2001) reported that strengthening the connection was generally employed by using the haunch on the bottom side of the beam for WH modifications and weakening methodology was provided by reducing the beam section near the column face in conjunction with increasing the weld quality.

Although the stress reduction and better weld quality at the beam-column connections of existing SMFs can now be satisfactorily accomplished to overcome the brittle weld fractures observed during the 1994 Northridge and 1995 Kobe earthquakes; mitigation of inelastic instabilities has not been resolved completely yet and local member buckling can still prevent the connection to achieve adequate plastic rotations. As the use of advanced composite materials is rapidly increasing in steel structures, utilizing FRP composite materials in mitigation of local buckling to increase the plastic rotation capacities is also of interest (Accord and Earls 2006).

This chapter provides background information on three main topics. First part discusses the SMF modified connection types, which are WH and RBS connection methods. Second part contains general information on steel-FRP composite hybrid systems and the mechanical properties of FRP composite materials used to enhance the seismic performance of beam-column connections. Finally, information on previous works related to steel-FRP composite hybrid systems is presented.

2.2. Post-Northridge SMF Connection Background

2.2.1. Welded Haunch (WH) Modification Method

Figure 2.1 shows the details of welded haunch (WH) connection technique. As shown in this figure, in order to strengthen the beam near the welded connection, a triangular haunch is welded to the beam bottom flange. SAC (1996) reported that when the welded haunch is used in both top and bottom flanges of the beam, beam showed better seismic performance than one-sided welded haunch connection type. However, execution of top flange WH connection and top flange welding application is difficult for both existing structures and also new constructions owing to the presence of the concrete slab. Removing the concrete slab around the column requires additional cost and workmanship.

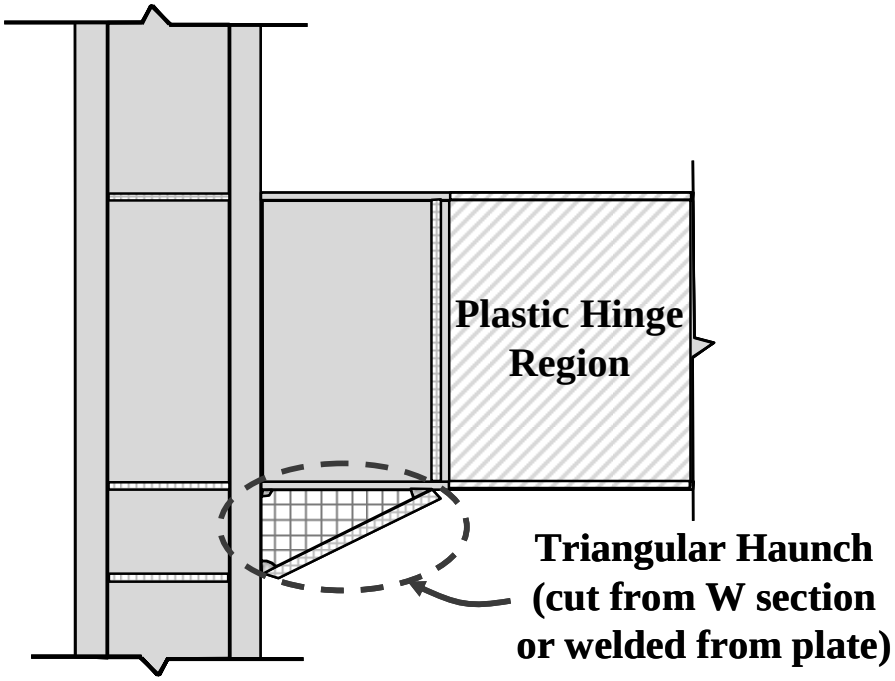

Figure 2.1. Details of Welded Haunch Connection

(Source: AISC 2001)

According to SAC 1996 test results, the addition of a welded bottom haunch also resulted in significantly improved cyclic performance of the connections. In addition, Uang et al. (2000) and Yu et al. (2000) demonstrated that there was no need to modify the existing groove welds when welded bottom haunch connection is used. In view of these findings, adding a triangular haunch only at the bottom side of the beam is selected in this study.

The tapered haunch is consisted of a flange and web plate or it could be cut from a structural tee or wide flange section (AISC 2001). Yu et al. (2000) conducted both theoretical and experimental study at University of California San Diego (UCSD) (Uang, et al. 2000, Yu, et al. 2000). They found that the beam shear force transfer mechanism changes with the presence of a welded haunch. The welded haunch behaves as a “diagonal strut”. In this way, the majority of shear force is transferred within the haunch flange to the column. In addition, Gross, et al. reported in the AISC Design Guide No. 12 (AISC 2001) that in order to distribute the vertical load that is carried by

the welded haunch to the beam web, a pair of beam web stiffeners should be provided at the end of the haunch.

If the welded haunch is designated with adequate stiffness and strength, plastic hinge of the beam would occur at the end of the welded haunch. Therefore, tensile stress in the beam-to-column connection weld is reduced.

2.2.2. Reduced Beam Section (RBS) Modification Method

The reduced beam section (RBS) type connection is an alternative to the welded haunch connection. RBS moment resisting connections are economical and practical connections than the WH connections. This type of connections does not necessitate the additional steel plate or welding in the connection reinforcement region. The other beneficial features of the RBS is that providing the strong column-weak beam requirements are easier because of weakened beam section and the demands of the continuity plates and panel zone requirements are lessened (Uang, et al. 2000, AISC, 2001, Jin and El-Tawil 2004).

Three main RBS cutouts exist, including a constant cut, a tapered cut, and radius cut. Many researches have been conducted on the RBS cutouts, such as Engelhardt (1998), Popov et al. (1998), Jones et al. (2002), Uang et al. (2001), Lee et al. (2005). Test results showed that the radius cut RBS connections provided suitable levels of ductility and better performance than the other type cutouts. Figure 2.2 briefly depicts a radius cut RBS connection.

In the radius cut RBS connection, a maximum of 50 percent flange portion is cut from the total flange area at a short distance from the column face. This weakening strategy forces the inelastic action in the beam to occur outside the connection region by moving the plastic hinge away from the column face and thereby limiting the stress levels around the connection welds. The plastic hinging of the beam is anticipated to occur within the reduced section (AISC 2001).

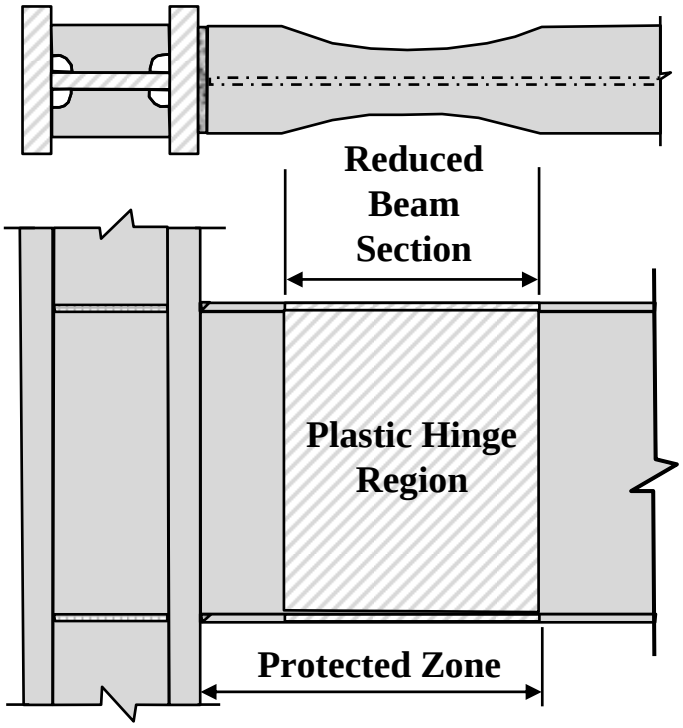

Figure 2.2. Details of Reduced Beam Section Connection

(Source: AISC 2001)

The application of RBS in new constructions differs from that for modifying existing structures. When the existing connection is modified with RBS, only the bottom flange is trimmed on account of the presence of a floor slab in beam top flange. On the other hand, both top and bottom flange of the beam can be reduced for new constructions. Civjan et al. (2000) conducted laboratory tests and indicated that the RBS connections for new construction showed good performance.

2.3. Steel-FRP Composite Hybrid System Background

2.3.1. Introduction

No matter what the usage purpose is, it is necessary to understand the individual properties of the constituent materials in order to evaluate the working principle of steel-fiber composite hybrid systems. This section presents basic information on

mechanical properties of fiber itself, matrix material, binding material that binds composite material to steel and steel-GFRP hybrid systems.

2.3.2. Properties of Fiber Material

Polymer composite materials strengthened with fiber consist of two components: a) fiber, b) binding matrix. Generally, carbon, glass and aramid fibers are used in the application area of industry. Carbon has the highest stiffness and strength values than other fibers mentioned (Cadei, et al. 2004). The elastic modulus of carbon fiber ranges between 230 GPa and 640 GPa (Setunge, et al. 2002). The main reason of utilizing the carbon fiber composites in strengthening and repair applications is its high modulus values.

Aramid has high strength and high modulus, but it has mid-degree stiffness. Glass fibers on the other hand have the least stiffness and the least strength than both carbon and aramid fibers. However, glass fibers are cheaper than other mentioned fibers (Cadei, et al. 2004). The elastic modulus value of glass fibers changes from 70 GPa to 85 GPa (Setunge, et al. 2002).

2.3.3. Properties of Matrix Material

Polymeric matrix is the main constituent of composite materials that binds the fibers and maintains the integrity of the composite. The load transfer between the fibers and the matrix is provided by the interfacial shear stresses. Besides these mentioned properties, matrix protects the composite material against environmental effects (Gibson 1994, Schwartz 2002). Other features of composite materials, such as heat and fire chemical resistance depend on the properties of the polymeric matrix (Cadei, et al. 2004).

The principle polymer matrix materials that are commonly used are epoxies and polyester resins (Gibson 1994). The elastic modulus of matrixes range between 2.5 GPa and 4 GPa, whereas their tensile strength is between 50-85 MPa (Cadei, et al. 2004).

2.3.4. Properties of Fiber Composite Material

The mechanical properties of fiber composites depend on the properties of the fiber and matrix, fiber-matrix volume fraction, direction of the fibers, and manufacturing methods. Laminates are the most common form in which fiber-reinforced composites are stacked together in a number of layers. According to the usage purpose, 0°/90°, 0°/+45°/-45°/90° orientations of fibers are generally used in structural applications (Hull and Clyne 2000, Schwartz 2002). Figure 2.3 illustrates some simple cross-ply laminates.

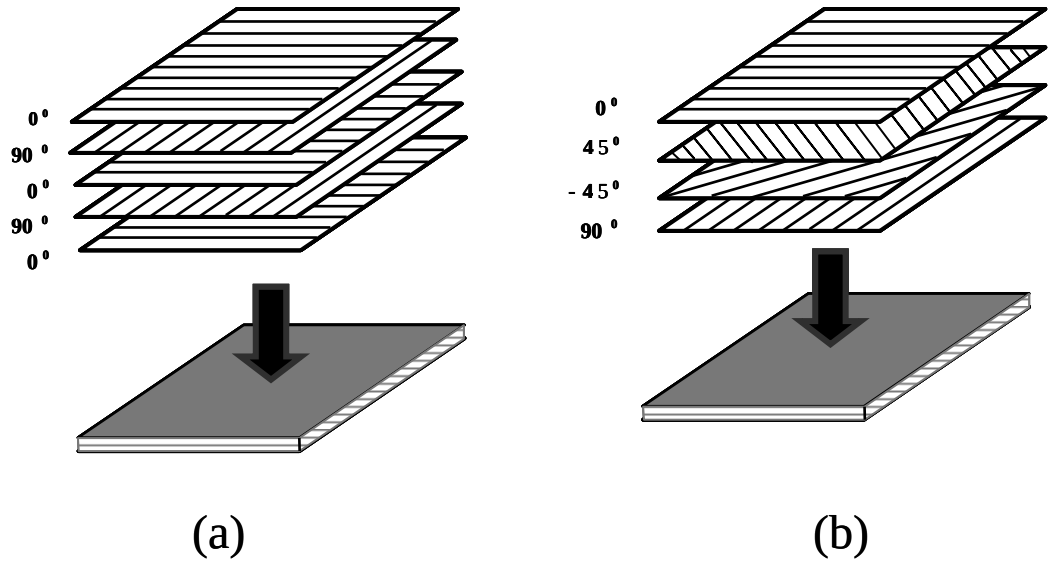

Figure 2.3. a) Arrangement of plies in the fiber orientation of 0°/90° b) Arrangement of plies in the fiber orientation 0°/+45°/-45°/90° (Source: Hull and Clyne 2000)

2.4. Literature Review of Steel-GFRP Composite Hybrid System

Fiber reinforced polymer (FRP) composite materials have been used in strengthening of steel members in past decades (Schnerch, et al. 2007, Photiou, et al. 2006, Tavakkolizadeh and Saadatmanesh 2003). Generally, high modulus carbon and

aramid fiber materials, with elastic modulus similar to that of steel are preferred for this type of applications. Recently, in addition to strengthening applications researches have also started to be interested in enhancing the plastic rotation capacity of steel elements by using GFRP materials. However, limited number of studies exists in literature on this subject.

The most significant work on stability of local buckling of steel members utilizing GFRP composites is a finite element based study conducted by Accord et al. (2006). In this study Accord performed 3-D finite element analyses on cantilever steel I-beams with GFRP strips under static loading and investigated the contribution of GFRP strips to the plastic rotation capacity and flexural strength in the section. It is confirmed that steel beams with GFRP strips had higher plastic rotation capacities than plastic rotation capacities of bare steel beams, besides a %25 increase of the flexural strength. In this study, the GFRP strips were modeled as traditional shell elements. The interface material and the GFRP strips were perfectly bonded to each other and they were modeled as isotropic elastic materials.

Ekiz et al. (2004) conducted an experimental study investigating the energy dissipating capacity of double channel members, which were wrapped by carbon fiber reinforced polymers (CFRP) around the plastic hinge regions, under reversed cyclic loading. Two different wrapping were applied to the members. In the first application, CFRP strips were bonded to the bottom side of the member in the plastic hinge region. The other application is that the beam was fully wrapped around the plastic hinge region. The test results showed that CFRP wrapping can increase the size of the yielded plastic hinge region and inhibit occurrence of local buckling.

Sayed-Ahmed (2006) also performed a finite element study in which CFRP strips were placed on the compression region of the web of I-beams and investigated the contribution of CFRP strips in delaying local web buckling. Steel I-section beams having different web slenderness ratios were analyzed by linear buckling and nonlinear finite element analyses. The results of the parametrical study showed that through the use of CFRP strips the local buckling of the web can be delayed resulting in critical load and strength increase. The ratio of the critical load increase changed from 20% to 48% for different web slenderness ratios.

Photiou et al. (2006) performed an experimental study that includes steel beams strengthened with hybrid composites. In this study, the flexural strength capacity of four

steel rectangular cross-section beams was tested under four-point loading. Two beams were retrofitted with U-shaped units and the other beams were strengthened with the flat plate units to its tension flange. All units used to increase the flexural capacity of the steel beams consisted of hybrid lay-up of CFRP and GFRP composites. Photiou et al. (2006) reported that the flexural load carrying capacity of a steel girder was significantly improved by utilizing the hybrid lay-up of CFRP and GFRP composites.

In addition to Photiou et al. (2006), Schnerch et al. (2007) conducted an analytical study to demonstrate the flexural behavior of steel-concrete composite bridge girders with high modulus CFRP bonded to the tension flange of composite beams using a structural epoxy adhesive. A flexural design procedure was presented as a consequence of this study. The research findings showed that flexural-strengthening beams displayed a capacity increase at their stiffness and strength.

A similar project was conducted on strengthening of steel-concrete composite sections by the use of epoxy-bonded CFRP sheets under static loading (Tavakkolizadeh and Saadatmanesh 2003). This study was both experimental and analytical. Three large-scale composite girders with one, three, and five-layered CFRP laminates bonded to the tension flange of beams were tested. According to the results of the experimental investigation, ultimate load-carrying capacity of the girders increased by a ratio ranging between 44% and 76% depending on the different number of CFRP layers.

Besides these mentioned works, various studies have been conducted on strengthening of steel and steel-concrete composite sections by the use of CFRP (Lenwari, et al. 2005, Rizkalla and Dawood 2006, etc.); all of which showed that the flexural strength of steel sections can be significantly improved by utilizing externally bonded CFRP composite materials.

In addition, studies investigating the properties and fracture modes of adhesives utilized in steel-composite systems also exist (Buyukozturk, et al. 2003, Damatty, et al. 2003, Fawzai, et al. 2006, Taib, et al. 2005a and 2005b, Dawood and Rizkalla 2006). These studies investigated the fracture stresses of adhesive materials and showed that adhesive materials can be modeled using elastic elements.

CHAPTER 3

FINITE ELEMENT ANALYTICAL (FEA) STUDIES

3.1. Introduction

Three-dimensional finite element program ANSYS (2007) was used to perform parametric studies on the behavior of modified existing steel I-beams reinforced with and without glass fiber reinforced polymer (GFRP) laminates by using the program code in the program. Steel I-sections, beam web stiffeners, and triangular haunches were modeled using 8-noded quadrilateral shell elements, SHELL93, with 6 degrees of freedom per node; while GFRPs were modeled using full integrated 4-noded layered shell elements, SHELL181, with 6 degrees of freedom per node. Both shell elements have in-plane inelastic deformations along with out-of-plane bending capabilities. The rigid column was modeled using rigid link elements, named as MPC184 in ANSYS. Figure 3.1 shows a description of the finite element model. Non-linear analysis with respect to both material and geometry was considered. The accuracy of the finite element model was checked by comparing the analysis results with cantilever beam test results from literature. This verification, along with the basic features of the model is presented in the following sections.

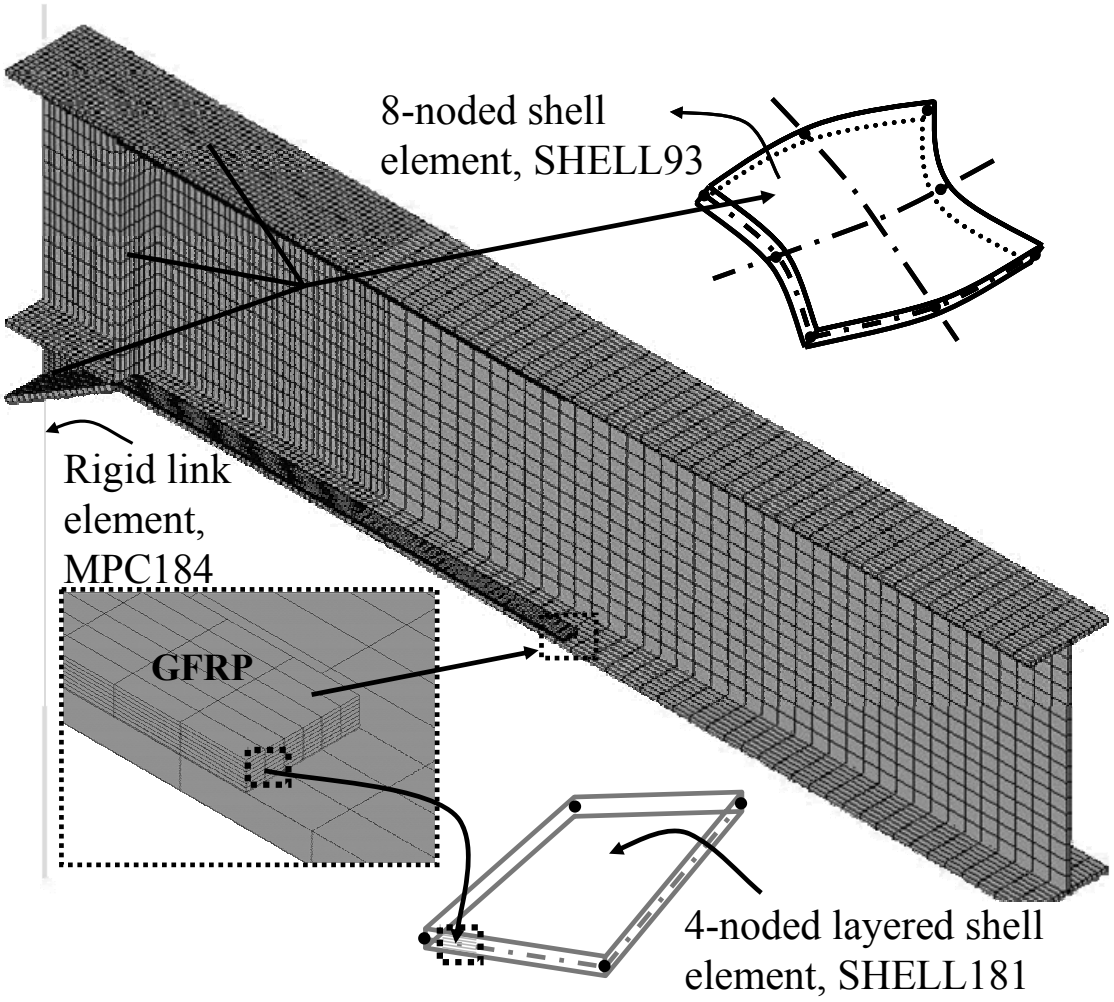

Figure 3.1. Finite Element Model Representation of Steel-GFRP System

3.2. Steel Material Model

The inelastic behavior of steel members under reversed cyclic loading can be modeled by several different material models that include strain hardening, which is known as the yield stress increase with further plastic straining. Figure 3.2 simulates the typical stress-strain behavior of monotonically loaded mild steel in tension (Chen and Han 1988, ANSYS Help 2007, Richard 2004).

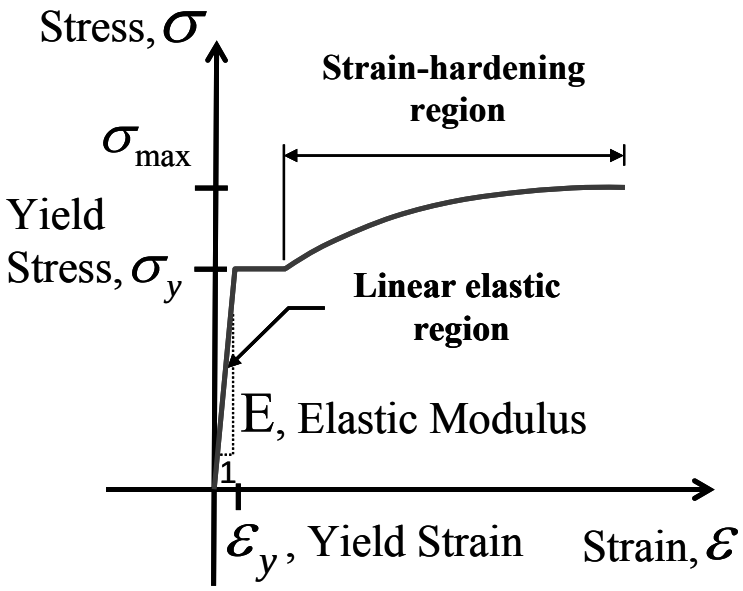

Figure 3.2. Monotonic Curve for Mild Reinforcing Steel in Tension
(Source: Chen and Han 1988)

Metals exhibit yielding, σ_y^{II}, at lower load than the original yield limit, σ_y, and also much lower than the subsequent yield limit, σ_y^{I}, under unloading followed by a reversed loading. This effect of the material is known as Bauschinger effect (Chen and Han 1988, ANSYS Help 2007, Richard 2004). Figure 3.3 illustrates the Bauschinger effect.

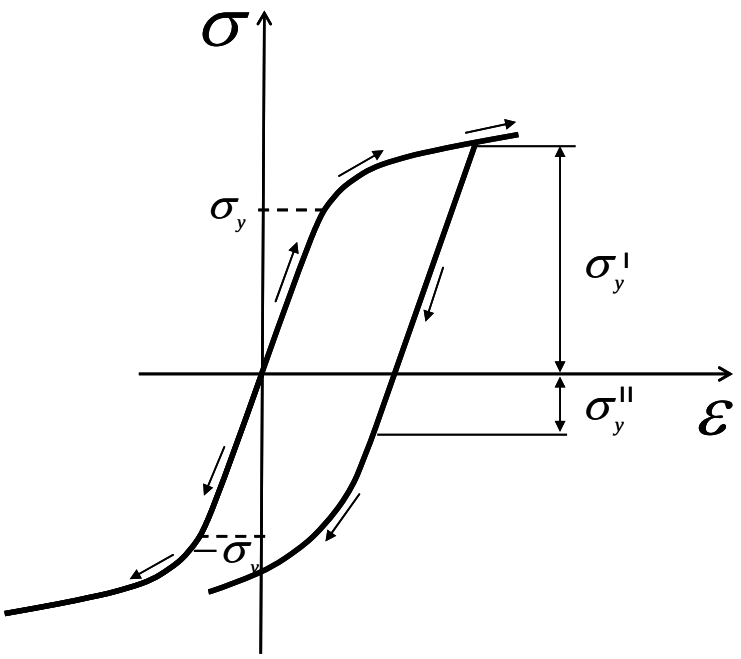

Figure 3.3. Plastic Hardening: Bauschinger Effect

(Source: Chen and Han 1988)

In literature, generally Bilinear Kinematic Hardening (BKIN) or Multilinear Kinematic Hardening (MKIN) material models, which both consider the Bauschinger effect (Kim and Engelhardt 1995, Okazaki, et al. 2006), are used. It can be observed from these past investigations that both models can predict the reversed cyclic behavior of steel members with high accuracy. Figure 3.4.a and Figure 3.4.b shows the typical representation of BKIN material model, where the total stress range is equal to twice the yield stress, and MKIN material model, where the material response is represented by multiple layers of perfectly plastic material, respectively. Both of these models were used in the verification study and it was decided to use the BKIN model for this study as explained in the following sections. The BKIN model follows the Von Misses yielding criterion. The second stiffness was taken as 1/100 of the Young's modulus. The material yield stress and Young's modulus of the steel were inputted in the model as 345 MPa and 205 GPa, respectively. To observe the local buckling of finite element model, the beam elements were sized 16.5 mm by 20 mm in the region where plastic hinge occurs and the remainder of the beam elements was sized with bigger elements in order to shorten the computation time.

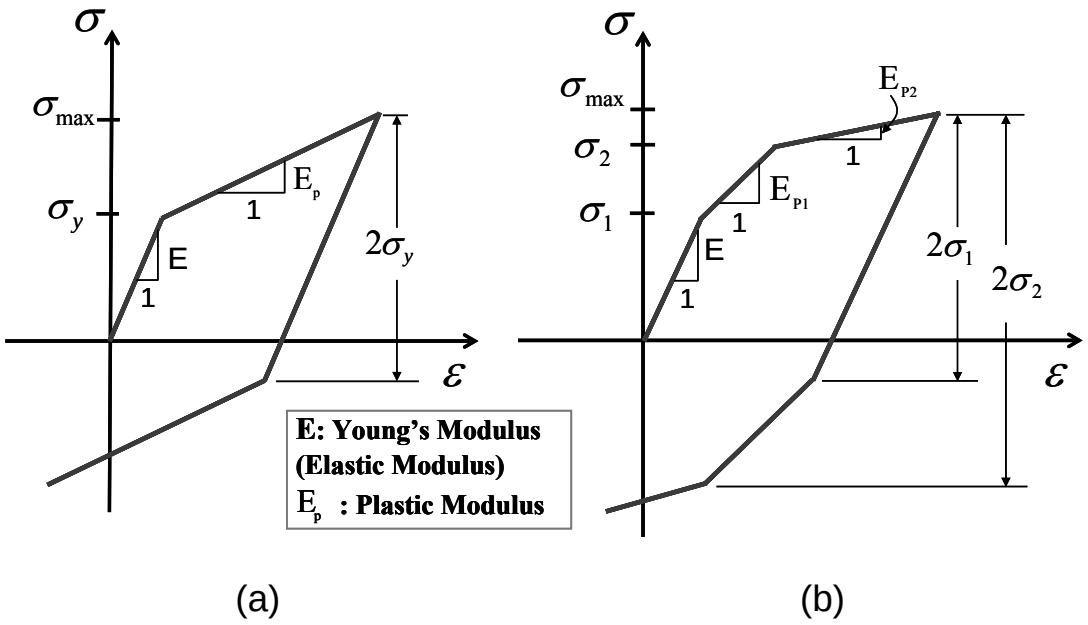

Figure 3.4. a) Bilinear Kinematic Hardening (BKIN) Material Model b) Multilinear Kinematic Hardening (MKIN) Material Model (Source: Chen and Han 1988, ANSYS Help 2007, Richard 2004)

3.3. Glass Fiber Reinforced Polymer Material Model

Fiber reinforced polymer materials generally behave linear up to a specific stress value under tension or compression loads and then fracture suddenly (Buyukozturk, et al. 2004, Photiou, et al. 2006, Setunge, et al. 2002) (Figure 3.5). The maximum strain and Tsai-Hill criteria are commonly applied failure criteria of composite materials (Jones 1998). In steel-GFRP systems, the mechanical properties of both polymer matrix, which is used as the binder, and the GFRP materials having 0°/-45°/90°/+45° fiber orientations in each layer were determined firstly through small scale standard tests. The results from standard tests performed on both GFRP and polymer matrix are presented in Table 3.1 (Guven 2008). Table 3.1 includes the modulus of elasticity; tensile strength, and compressive strength of both 0°/-45°/90°/+45° oriented GFRP with 1250 gr/m^2 unit weight and the modulus of elasticity; tensile strength, and shear strength of polymer matrix (Duratek epoxy). The modulus of elasticity and tensile strength of the epoxy material is provided by the manufacturer.

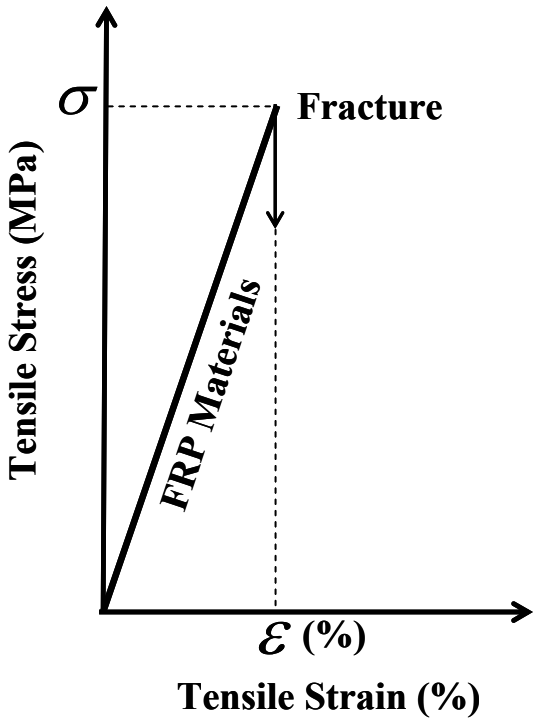

Figure 3.5. Stress-Strain Behavior of FRP Materials
(Source: Buyukozturk, et al. 2004, Photiou, et al. 2006, Setunge, et al. 2002)

Table 3.1. Mechanical Properties of GFRP and Polymer Matrix (Epoxy Resin)
(Source: Guven 2008)

Mechanical Properties	$0^o/-45^o/90^o/+45^o$ Oriented GFRP with 1250 gr/m^2 Fiber Compactness	Polymer Matrix (Epoxy)
Elastic Modulus (MPa)	10000	2600
Tensile Strength (MPa)	230	70
Compressive Strength (MPa)	260	-
Shear Strength (MPa)	-	5.5

In addition, inter-laminar shear strength and shear modulus of the GFRP materials (1250 gr/m^2 unit weight per area for 0/-45/90/+45 fiber orientation) were determined through ASTM D 5379M (2005) standard (V-notch beam method) tests (Guven 2008). The test apparatus that was used in these tests and a specimen that was placed between the compression jaws of the Mechanical Test Apparatus are shown in Figure 3.6.

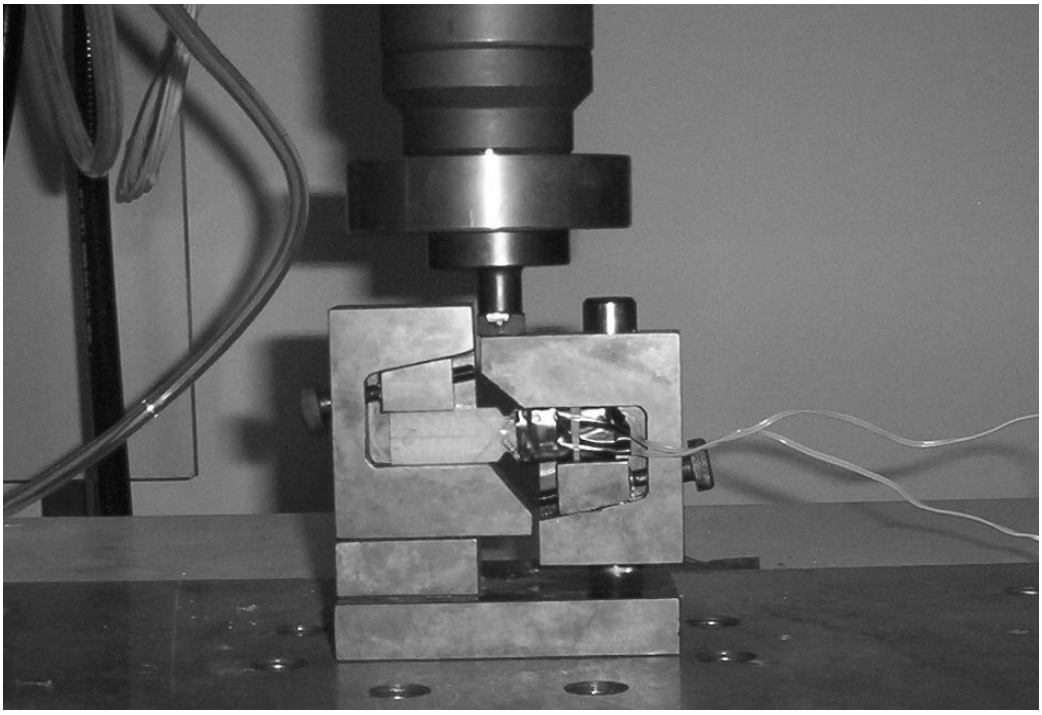

Figure 3.6. V-Notch Beam Test Apparatus and Specimen
(Source: Guven 2008)

The global coordinate system used in ANSYS is shown in Figure 3.7. The X-axis is parallel to the longitudinal axis of the beam, Z-axis is along the width of the flanges, and Y-axis is parallel to the axis of the beam web. The orientation of the tested specimens with respect to the global axes is shown in Figure 3.8. Since X-axis is parallel to the longitudinal axis of the beam, the shear modulus and shear strength in the XZ direction are not determined. In the cantilever tests, force is applied at the tip of the

beam in the Y- direction and therefore the shear force in the XZ direction is minimal, if not zero. The shear modulus and shear strength of the GFRP materials in the XY and YZ directions determined through standard tests is presented in Table 3.2. Since the orientation of the laminates is 0°/-45°/90°/+45°, the shear modulus in XY and YZ directions has to be equal to each other, which is verified through the standard tests (Table 3.2). On the other hand the shear strengths in these directions are not the same due to the fact that in the YZ direction failure occurs at the polymer matrix.

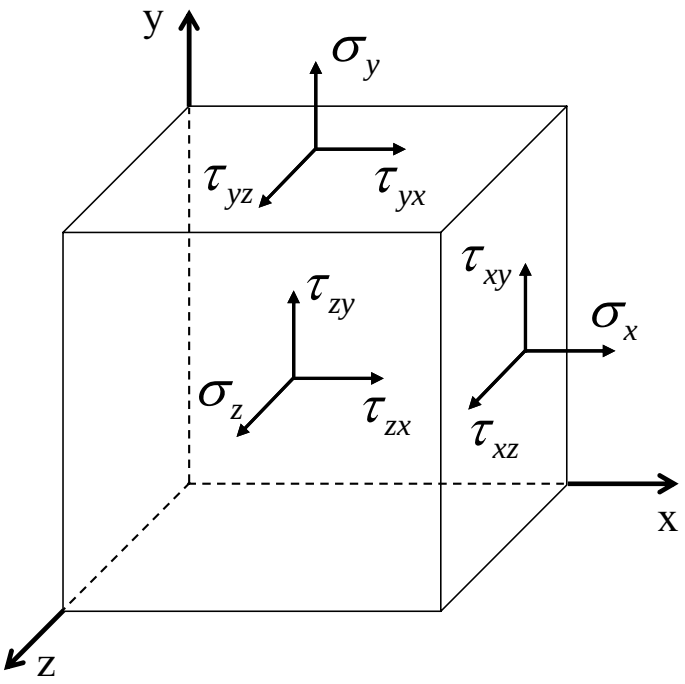

Figure 3.7. Global Coordinate System and Stresses

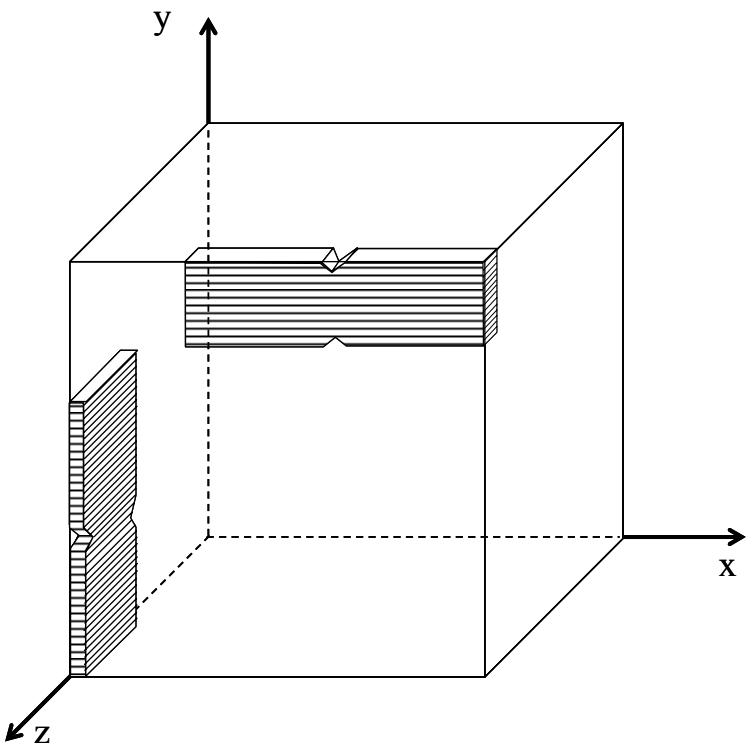

Figure 3.8. Representation of Test Specimens in the Global Coordinate System

Table 3.2. V-Notch Beam Test Results

(Source: Guven 2008)

Specimen Direction	Maximum Stress (Mpa)	Shear Modulus (Mpa)
XY	43.61	2655
YZ	13.00	2440

In the existing study, the results obtained from the small scale standard tests were inputted to FE model of GFRP laminates in order to model the GFRP as an orthotropic element. Layered shell elements, SHELL181, taken from the ANSYS

composite element model library were adopted to model the GFRP strips including 0°/-45°/90°/+45° fiber direction in each layer. The nodes of this element are located at the middle of the shell thickness. The numerical model of GFRP strips was assumed to be linearly elastic and perfectly bonded to the flanges. The adhesive that bonds GFRP to steel was not modeled.

3.4. Verification of Finite Element Analyses

Cantilever I-beam test results from literature were used to verify the bare steel finite element model. The first correlation study between the model and experimental data was based on experimental results from cyclic tests on the behavior of steel bar coupons (Aktan, et al. 1973) (Figure 3.9). The data that was used in the correlation belongs to # 6 bar coupon from test 9. The steel bar coupon was modeled as a link element, depicted as LINK1 in ANSYS. Figure 3.10.a and Figure 3.10.b shows the cyclic stress-strain response of the test coupon and the FE model for both BKIN and MKIN material models, respectively.

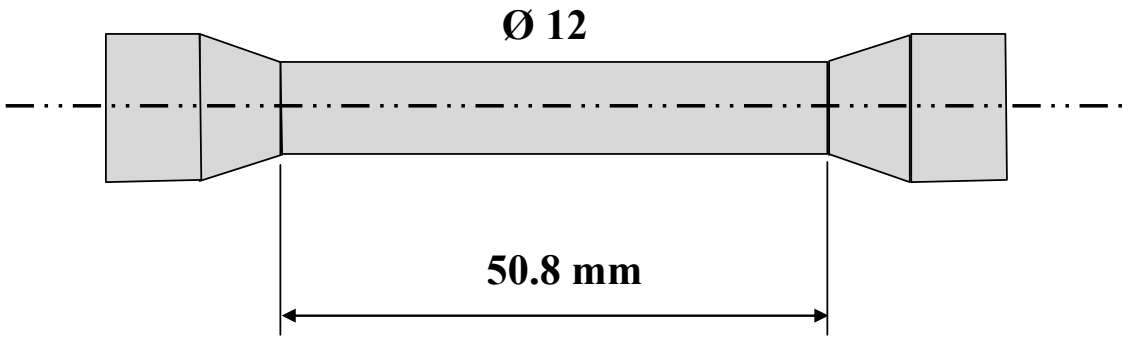

Figure 3.9. Steel Bar Coupon tested by Aktan (1973), Test 9, # 6
(Source: Aktan, et al. 1973)

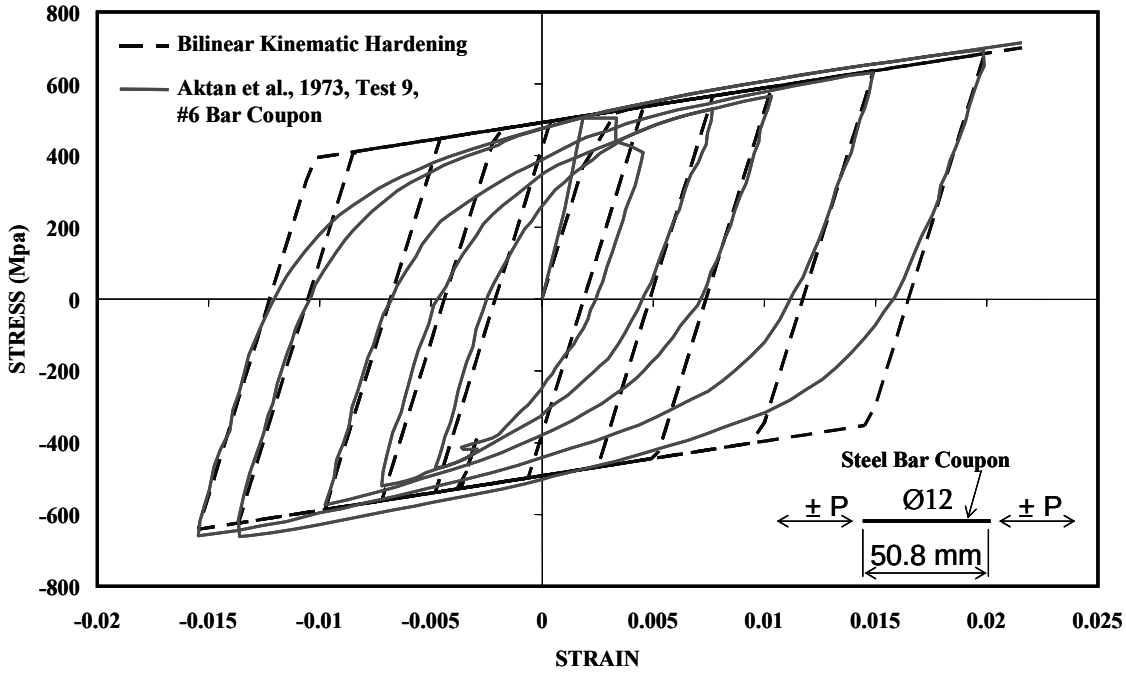

(a)

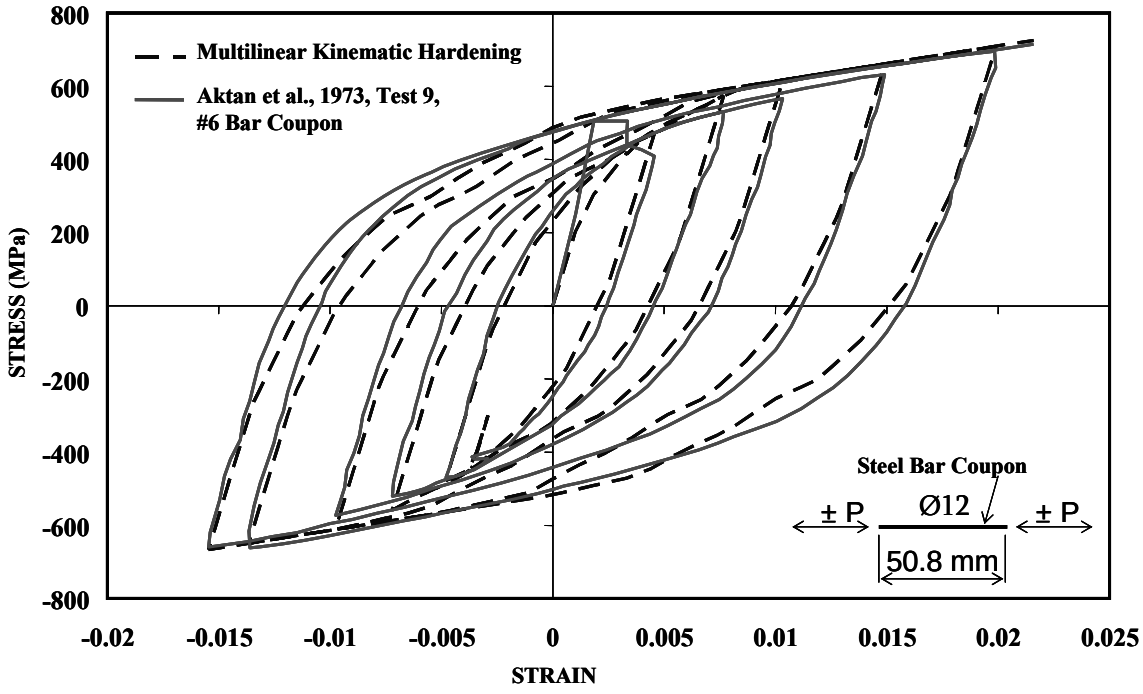

(b)

Figure 3.10. a) Aktan et al. (1973), Test 9, # 6 Bar Coupon Test Data – BKIN Model Comparison, b) Aktan et al. (1973), Test 9, # 6 Bar Coupon Test Data – MKIN Model Comparison

As it can be seen in Figure 3.10, the stress-strain response of both BKIN and MKIN models provided a good agreement with the stress-strain response of the test data. However, MKIN model matched with test data better than BKIN model.

The second test that was used in the verification belongs to a cantilever test conducted by Engelhardt and Husain (1992). The FE model of the beam-column connection is shown in Figure 3.11. The cantilever beam was a welded, 4 m long W530×85 (American section). The load was applied as load controlled until plastic moment capacity was reached and displacement controlled from there on. The load cycles were: +/- 0.008, +/- 0.0095, +/-0.011, +/-0.013 rad. Although failure of this beam occurred at about 0.012 rad by bottom flange weld fracture with no sign of local buckling, this beam is still a valuable source for verifying the material model adopted. The test results of this cantilever beam (Load versus tip displacement) were compared with two finite element analyses, where BKIN and MKIN material models were used (Figure 3.12.a and Figure 3.12.b).

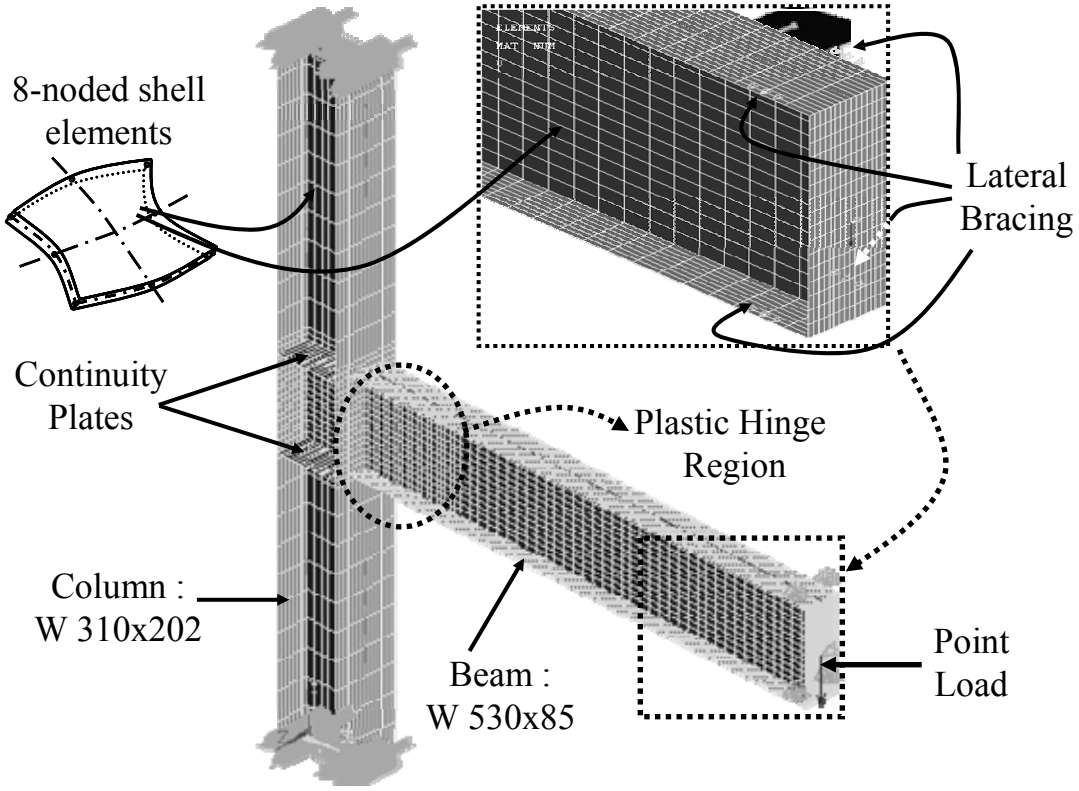

Figure 3.11. FE model for Engelhard's (1992) Test Set Up

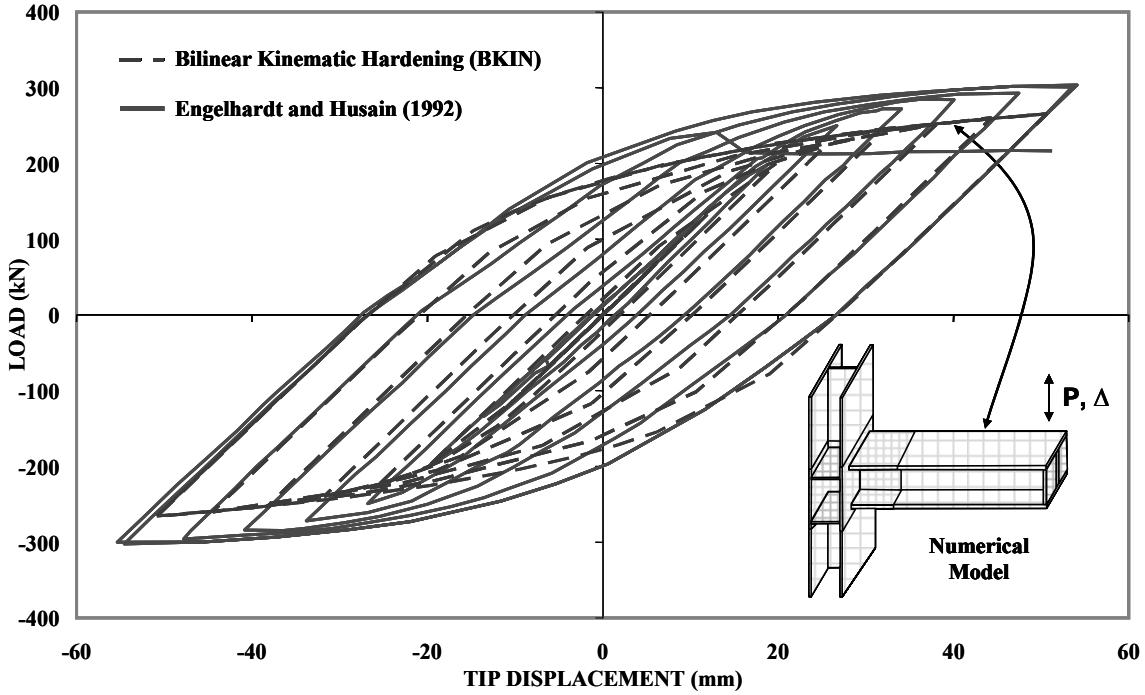

(a)

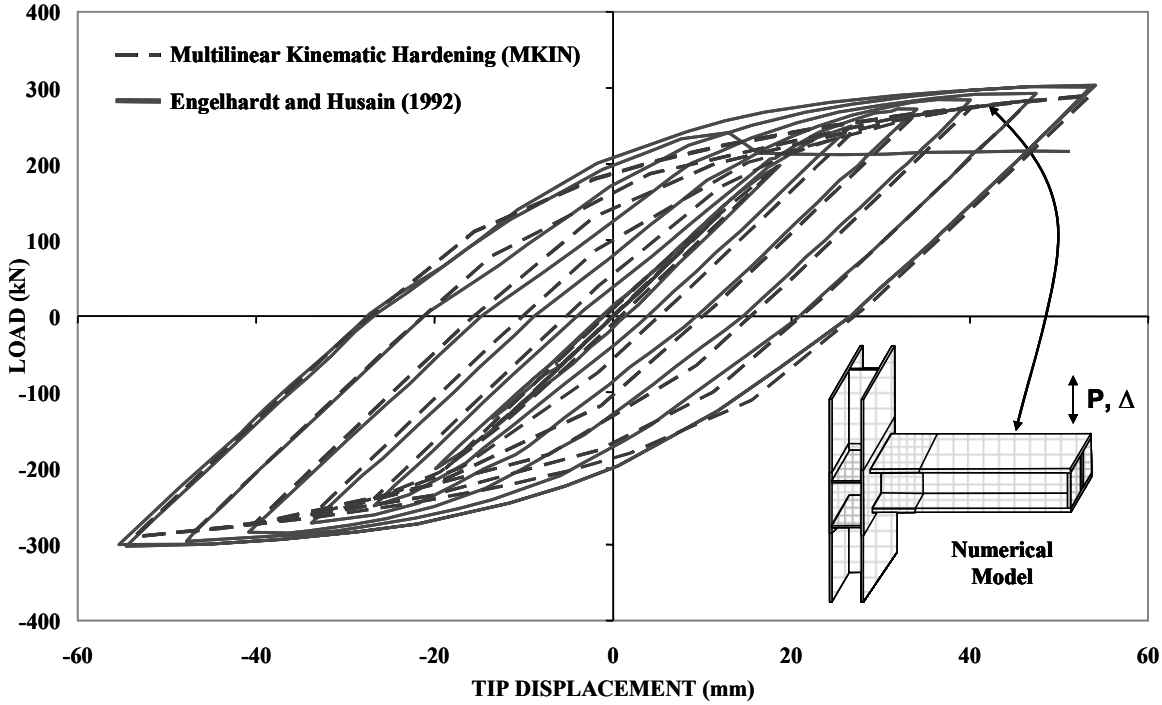

(b)

Figure 3.12. a) Engelhardt and Husain (1992) Test Data – BKIN Model Comparison, b) Engelhardt and Husain (1992) Test Data – MKIN Model Comparison

It can be observed from Figure 3.12 that both models predict the behavior of the cantilever beam closely. The MKIN model was able to reach %95 of the moment achieved by the test beam, whereas for the BKIN model this value was %88. Although the accuracy of the MKIN model is better than that of the BKIN model, the computation times of the two models are not comparable. The computation time of the MKIN model is far greater than that of the BKIN model. Due to this reason BKIN model is chosen for the FE studies.

The last test utilized in the verification of FE model was a cantilever beam test conducted by Nakashima et al. (1998). The beam adopted in this test was an H-500x200x10x16 Japan's medium section and was 3 m long as shown in Figure 3.13. The cantilever beam was loaded cyclically with two cycles repeated for each increment of +/- 0.015, +/- 0.03, +/- 0.045, and +/- 0.06 radians. The results of the study were presented in the form of normalized moment vs. rotation (Θ-radian) plot. Figure 3.14 compares the behavior of the test beam with that of the FE model. The results of the BKIN model with a secondary stiffness equal to 1/100 of the elastic modulus matched the measured data well. Figure 3.15 shows the local buckling observed by the BKIN model at 0.06 rad; similar to the local buckling observed during the test at this rotation level.

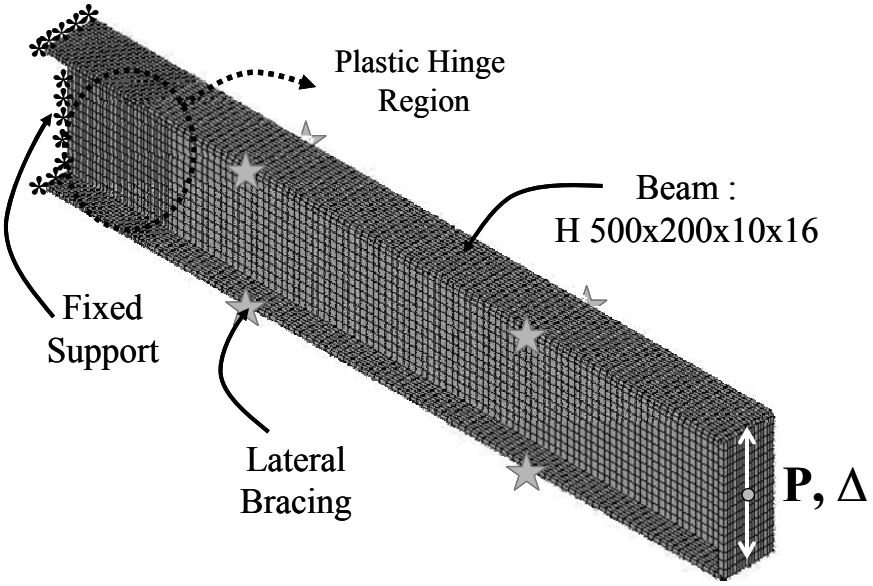

Figure 3.13. FE model for Nakashima's (1998) Test Set Up

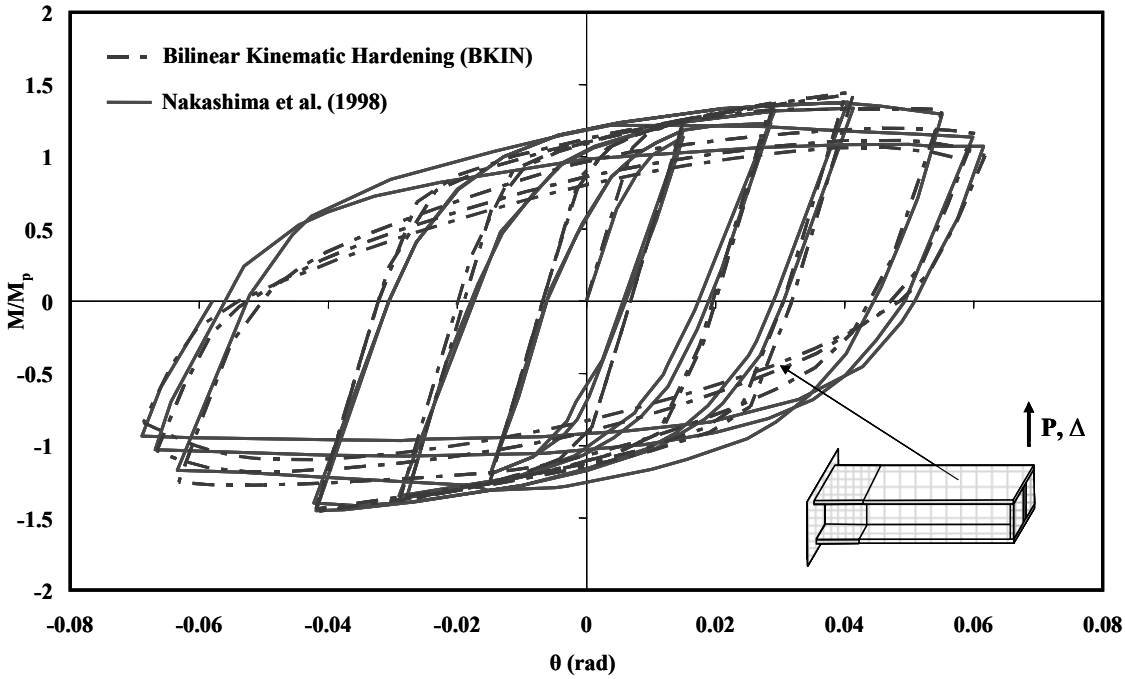

Figure 3.14. Nakashima et al. (1998) Test Data – BKIN Model Comparison

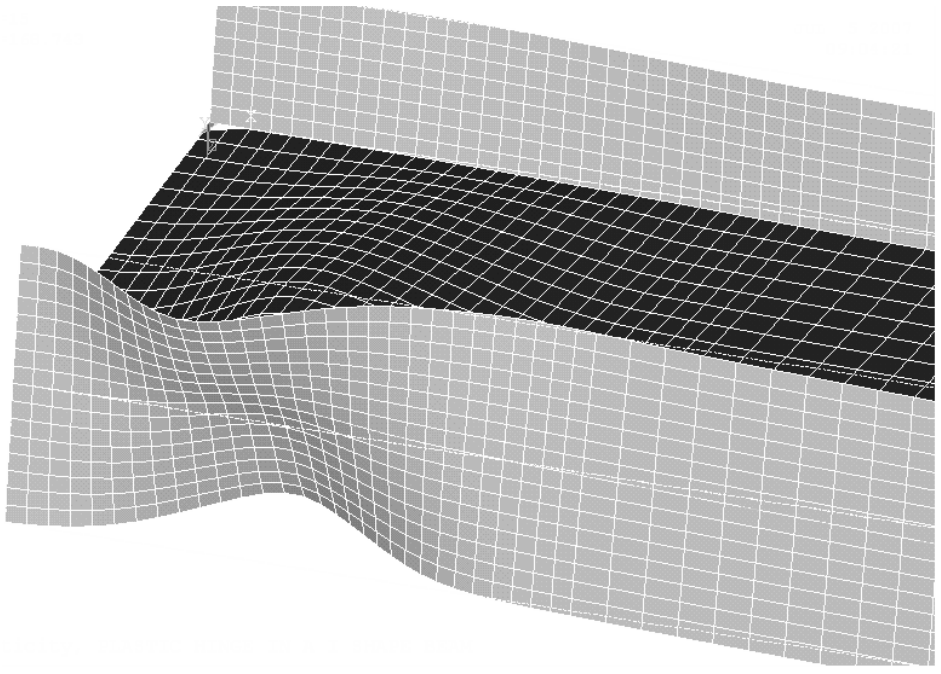

Figure 3.15. BKIN Model of Nakashima et al. (1998) Beam - Local Buckling

3.5. Sections Used in FE Studies

Web and flange local buckling are directly related with flange and web slenderness ratios. In American (AISC 2005b, AISC 2005c), European (Eurocode-8 2003) and Turkish (BİB 2006) codes, the slenderness ratios are limited in order to counteract the web and flange local buckling. In this research study the behavior of older steel structures built outside these code limits is studied. For this reason, the sections that are used in the finite element studies were determined according to the following criteria:

a) Sections with slenderness ratios exceeding code limits;

b) Sections that are commonly used in multi storey steel structures.

Table 3.3 and Table 3.4 present the slenderness ratios (formulas and actual values, respectively) set by the American, European and Turkish codes. In these codes it is stated that beams with slenderness ratios lower than those given in the Tables are expected to reach 0.04 radians of rotation with a measured moment resistance at the face of the column of at least 80% of the plastic moment capacity of the section at that target rotation amplitude.

Table 3.3. Limiting Slenderness Ratio Formulas for Flanges and Webs

Description of Element	Width-Thickness Ratio	Limiting Width-Thickness Ratios			
		AISC LRFD (Specification 2005)		TURKISH SEISMIC CODE	EUROCODE 3 (Design 2003)
		Seismically Compact	Compact		
Flexure in flanges of rolled I-shaped sections	b/t_f	$0.30\sqrt{E/F_y}$	$0.38\sqrt{E/F_y}$	$0.3\sqrt{E_s/\sigma_a}$	9ε
Flexure in webs of doubly symmetric I-shaped sections	h/t_w	$2.45\sqrt{E/F_y}$	$3.2\sqrt{E_s\sigma_a}$	$3.2\sqrt{E_s\sigma_a}$	72ε

$\varepsilon = \sqrt{235/F_y}$

F_y, σ_a Specified minimum yield stres steel,

E_s, E Modulus of elasticity of steel E = 200000 MPa,

b/t_f Flange slenderness refers to the ratio of half flange width to thickness,

h/t_w Web slenderness refers to the ratio of twice the depth between the neutral axis and fillet radious.

Table 3.4. Slenderness Ratio Limit Values (F_y = 345 MPa)

Description of Element	Slenderness Ratio	AISC (Seismically compact)	AISC (compact)	TURKISH SEISMIC CODE	EUROCODE-8
Flexure in flanges of rolled I-shaped sections	b/t_f	7.1	9.0	7.1	7.2
Flexure in webs of doubly symmetric I-shaped sections	h/t_w	58.2	89.2	76.0	58.6

In this study the yield strength of steel is taken as 345 MPa, which is a widely used yield strength in the steel industry. As it can be seen from Table 3.4 for steel I-

beams with yield strength of 345 MPa the limit for flange and web slenderness ratios are approximately 7 and 60, respectively (except for Turkish BİB 2006 Code).

The web and flange buckling are not independent from each other. If two sections with same flange slenderness ratios (FSR), but different web slenderness ratios (WSR) are investigated, it will be seen that the section with higher web slenderness ratio will have more local buckling compared to the section with lower WSR under the action of same loads (Okazaki, et al. 2006).

Taking into consideration all of the above facts, the following FSR and WSR values are decided to be investigated in the FEA studies:

a) Flange Slenderness Ratios: 8-9-10-11-12

b) Web Slenderness Ratios: 40-60-80

Consequently, for each flange slenderness ratio there are 3 analyses with WSR of 40, 60, and 80. The highest web slenderness ratio for rolled sections is around 60 (American-W or European-HE-I sections). The upper limit for WSR in this study is taken as 80; partly covering build-up sections (plate girders) that do not need stiffeners to carry shear loads.

In addition to slenderness ratios, section sizes also need to be determined. In general, deep beams such as W920×223, W760×147, W840×226, and W690×265 are used in steel special moment frames. To be consistent with the sections generally used in special moment frames the following section dimensions are used for all slenderness ratios:

a) Flange width = 265 mm;

b) Web height = 753 mm (close to sections W760×147 and W760×134).

The desired FSR and WSR values are obtained by changing the flange and web thicknesses. The dimensions and section properties of the 15 beam sections used in the FEA study are presented in Table 3.5 as d = depth of beam, h = height of section, b_f = width of flange, t_w = thickness of web, t_f = thickness of flange, Z_b = plastic section modulus of section, M_{pr} = maximum moment expected in plastic hinge region $b_f/2t_f$ = flange slenderness of beam, h/t_w = web slenderness of beam, A_b = cross-section area of beam, I_x = moment of inertia of beam, r_y = radius of gyration, S_x = elastic section modulus of section.

Table 3.5. Properties of the Specimens used in FEA

Specimen	$b/2t_f$	h/t_w	d (mm)	b_f (mm)	t_f (mm)	t_w (mm)	h (mm)	A_b ($/10^3$) (mm^2)	I_x ($/10^6$) (mm^4)	r_y (mm)	S_x ($/10^3$) (mm^3)	Z_b ($/10^3$) (mm^3)	M_{pr} ($/10^6$) (N-mm)
Beam 1	8	40	753	265	16.56	17.20	686.9	21.3	1748.9	49.2	4645.1	5523.9	2191.6
Beam 2	8	60	753	265	16.56	11.45	686.9	17.2	1570.9	54.7	4172.4	4782.4	1897.4
Beam 3	8	80	753	265	16.56	8.59	686.9	15.1	1482.0	58.3	3936.1	4411.6	1750.3
Beam 4	9	40	753	265	14.72	17.26	690.6	20.3	1633.1	47.4	4337.6	5207.0	2065.9
Beam 5	9	60	753	265	14.72	11.51	690.6	16.3	1451.5	53.0	3855.2	4453.8	1767.0
Beam 6	9	80	753	265	14.72	8.63	690.6	14.2	1360.6	56.7	3613.9	4077.2	1617.6
Beam 7	10	40	753	265	13.25	17.34	693.5	19.8	1539.7	45.7	4089.5	4952.4	1964.9
Beam 8	10	60	753	265	13.25	11.56	693.5	15.6	1355.0	51.4	3599.0	4189.8	1662.3
Beam 9	10	80	753	265	13.25	8.67	693.5	13.5	1262.7	55.2	3353.8	3808.5	1511.0
Beam 10	11	40	753	265	12.05	17.40	695.2	19.2	1462.8	44.2	3885.1	4743.4	1882.0
Beam 11	11	60	753	265	12.05	11.60	695.2	15.0	1275.6	49.9	3388.0	3973.1	1576.3
Beam 12	11	80	753	265	12.05	8.70	695.2	12.9	1182.0	53.8	3139.5	3588.0	1423.5
Beam 13	12	40	753	265	11.04	17.45	697.9	18.8	1398.2	42.9	3713.8	4568.8	1812.7
Beam 14	12	60	753	265	11.04	11.63	697.9	14.5	1208.9	48.6	3211.1	3792.0	1504.5
Beam 15	12	80	753	265	11.04	8.72	697.9	12.4	1114.4	52.9	2959.8	3403.6	1350.4

3.6. Finite Element Model

To investigate the behavior of the plastic moment region of steel beams, a half span steel frame was modeled to be used in FEA studies. The model is shown in Figure 3.16 for a beam with welded haunch modification. The column is modeled as a rigid bar and the coinciding nodes of the beam flange and web shell elements are coupled to column nodes in all directions (3 displacements: UX, UY, UZ, and 3 rotations: ROTX, ROTY, ROTZ). Rigid column member is taken as 4.15 m long. The motion of the column top end is prevented in Z direction only and bottom of the column is pinned support. The beam is connected to the mid point of the column and the length of the cantilever beam is taken as 3.50 m (half of typical beam spans used in steel moment frames). The free end of the beam is supported by a roller; it is unconstrained in the longitudinal direction, however the vertical displacement is constrained. Beams used in analyses are laterally supported at locations consistent with spacing limits stipulated by the AISC Code Provisions (AISC 2005b) so as to prevent lateral-torsional buckling. The dimensions of the welded triangular haunches added to the bottom flange of the beams

are calculated by following the suggestions in AISC Design Guide Series (DGS) 12 (AISC 2001). The determination of the welded haunch size for the beam with flange and web slenderness ratios of 10 and 60 (Beam 8 in Table 3.5), respectively, are presented in Appendix A.

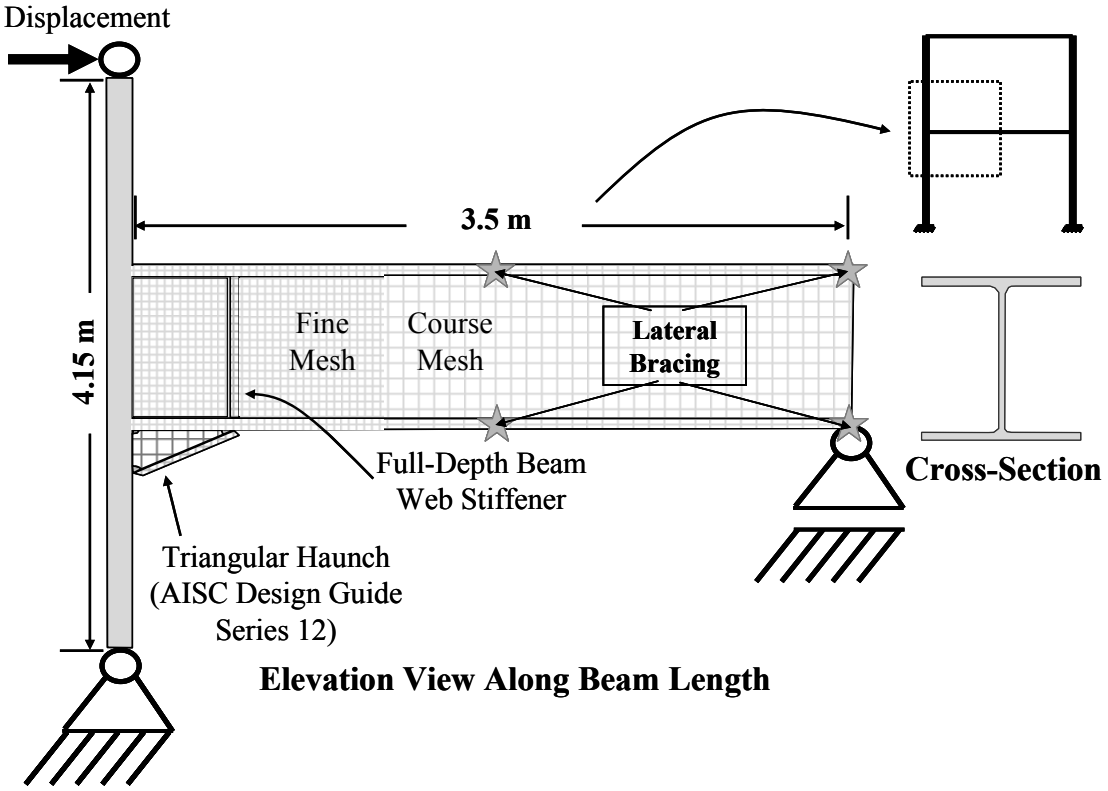

Figure 3.16. Half Span Beam Model with Welded Haunch Modification

In the plastic hinge region of the beam, small finite elements are used in order to follow local buckling (fine mesh size: 16.56 ^{mm} × 20 ^{mm}). However, towards the cantilever end of the beam, the element sizes are enlarged to reduce the computation time (course mesh size: 16.56 ^{mm} × 40 ^{mm}). In this model the load is applied as drift to the tip of the column. Column tip displacements are arranged so that the following drift angles are achieved as specified in 2005 AISC seismic provisions (except that initial elastic cycles were ignored):

1) 2 cycles at 0.01 radians
2) 2 cycles at 0.015 radians
3) 2 cycles at 0.02 radians
4) 2 cycles at 0.03 radians
5) 2 cycles at 0.04 radians

CHAPTER 4

FEA RESULTS AND DISCUSSION

4.1. Introduction

In this chapter, the criteria to be used for assessing the results of the analyses are described first. Then, FEA results of both bare steel sections and steel sections retrofitted with GFRP materials are presented. The chapter concludes with a discussion of results.

4.2. Criteria used in Evaluation of Analysis Results

In order to get an indication of the benefit of using GFRP, it is needed to have an idea about the expected behavior of SMF connections. The performance of steel beam-column connections strengthened by GFRP will be evaluated according to the following three criteria: 1) The design moment of the connection need not be exceeded; 2) the ratio of the moment carried by the connection divided by the plastic moment of the section need not be lower than 0.80 for special moment frames (SMF) at 0.04 radians of rotation; and 3) whether local buckling that occurs in beams is postponed or not. These criteria are covered below.

4.2.1. Maximum Design Moment of the Connection

The moment value used in designing the beam-column connections generally is named as the maximum moment value expected, M_{pr} (AISC 2005a). ANSI/AISC 358-05 (AISC 2005a) specification suggests using the following equation to calculate the maximum plastic moment expected in the plastic hinge region of beams (ANSI/AISC 358-05 Equation 3-1):

$$M_{pr} = C_{pr} R_y F_y Z_e \tag{4.1}$$

where:

C_{pr} = factor to account for peak connection strength, including strain hardening, local restraint, other connection conditions:

$$C_{pr} = \frac{F_y + F_u}{2F_y} \leq 1.2 \; (ANSI / AISC 358-05 \; Equation \; 2.4.3-2) \tag{4.2}$$

R_y = ratio of the expected yield stress to the specified minimum yield stress (ANSI/AISC 341-05 (AISC 2005b) Table I-6-1)

F_u = specified minimum tensile strength of steel (MPa)

$F_y Z_e = M_p$ = Plastic moment of section (N-mm)

Z_e = effective plastic modulus of the section at the location of the plastic hinge (mm^3)

F_y = specified minimum yield stress of steel (MPa)

As previously stated in Chapter 3 Bilinear Kinematic Hardening (BKIN) model was adopted for the stress-strain relation of the steel material in this study. After reaching the yield strength, the elastic modulus of steel was decreased by a ratio of 1/100. Assuming that steel ruptures at 10% elongation, which is a realistic value when the real stress-strain behaviors are examined, the C_{pr} value for the model is calculated as around 1.2. Hence, C_{pr} is taken as 1.2 in this study.

R_y value was not considered in the numerical study or in other words this value is taken as 1 and yield stress of steel was taken as F_y = 345 MPa in the FEA model.

In the light of the above explanations, the maximum design moment of the beam-column connection in this study is accepted to be:

$$M_{pr} = C_{pr} R_y F_y Z_e = 1.2 M_p \tag{4.3}$$

In other words:

$$\frac{M_{pr}}{M_p} = 1.2 \tag{4.4}$$

It is clear from mechanics of materials that the addition of GFRP strips will increase the moment carrying capacity of the beams. However, any increase beyond the design moment of the connection will cause the connection to fail. Therefore, the increase in the moment carrying capacity of the beams should be kept under 20% with the addition of the GFRP strips.

4.2.2. Measured Flexural Resistance of the Connection at 0.04 Radians of Rotation

One of the main criteria in the design of special moment frames is that the beam-column connection shall be capable of sustaining an interstory drift angle of at least 0.04 radians and a measured moment resistance at the face of the column of at least 80% of the plastic moment capacity of the section. The required inter-story drift angle is 0.02 for intermediate moment frames (AISC 2005b); however there is no specified moment resistance at the face of the column at this rotation. Figure 4.1 shows the M/M_p - θ behavior of the bare beam having FSR of 8 and WSR of 40 together with these limits.

The contribution of GFRP strips to the moment resistance of the face of the column is currently unclear. It will be seen in the following section that there is generally an increase in the moment resistance at the end of the last cycle for beams with GFRP as compared to bare beams. However, this is not a reliable increase since local buckling generally occurs before the last cycle of loading and whether the GFRP

strips are still bonded to the flanges or not after local buckling is not clear and needs to be verified through laboratory testing. Therefore, no conclusion will be drawn about whether the GFRP strips still contribute to the moment capacity of beams beyond local buckling.

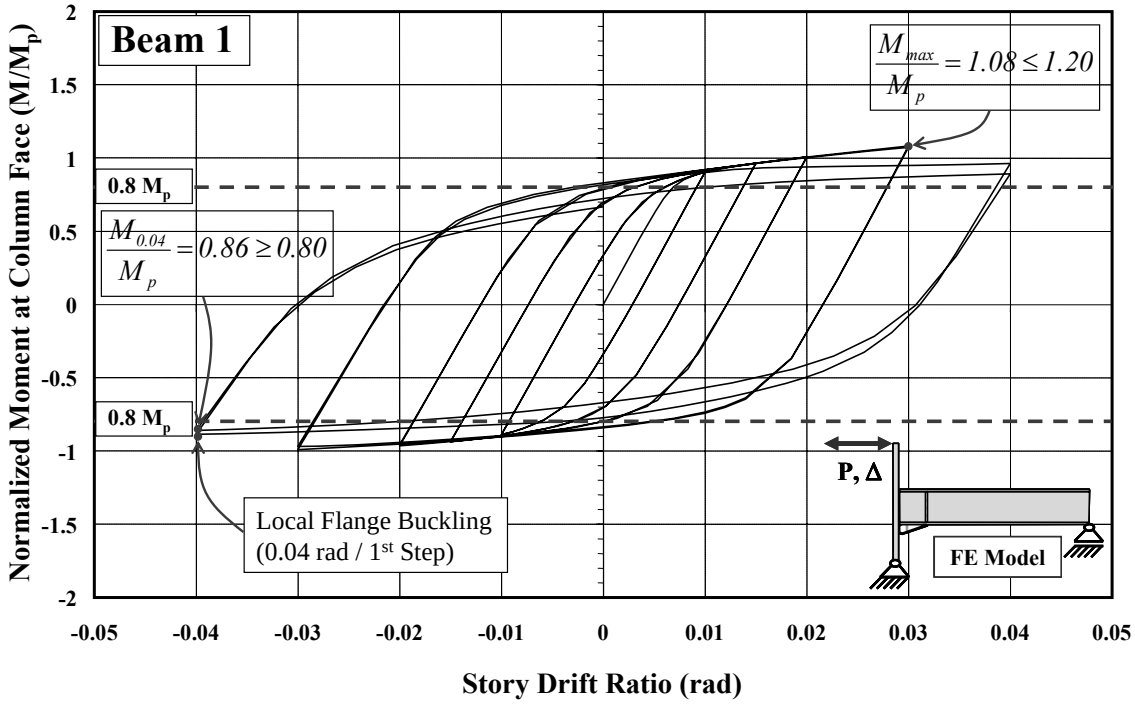

Figure 4.1. Criteria used in Evaluation of Analysis Results (FSR = 8, WSR = 40)

4.2.3. Local Buckling

The other criterion that is used to evaluate the FEA results is whether local buckling can be postponed or even prevented. Postponing local buckling will increase the energy dissipation capacity of connections. However, postponing local buckling will happen by an increase in the moment resisting capacity of beams and it should be checked that the maximum moment at the connection is below $1.2\ M_p$ (Max design moment of the connection).

4.3. Finite Element Analyses

4.3.1. Introduction

The results presented in this section contain M/M_p vs. interstory drift angle, Θ, behavior of modified existing beam-column connections with and without GFRP strips, where M is the moment at the column face and M_p is the nominal plastic flexural strength of the section (AISC 2005b). The modification consists of a welded haunch detail at the bottom flange. The detailing of the welded haunches was discussed in Chapter 3 and an example is presented in Appendix A. Yield strength of steel, F_y, was taken as 345 MPa in analyses.

Moment at the column face, M, is calculated as the reaction force of the roller support times the length of the beam minus the moments occurred by the forces within the haunch flange. Beam sections were all analyzed under quasi-static cyclic loading using the loading history shown in Figure 4.2, consistent with the loading protocol stated in the AISC Seismic Provision (2005a) for beam-column moment connections.

Finite element analyses for bare steel sections are presented first, followed by analyses for steel sections reinforced with GFRP strips.

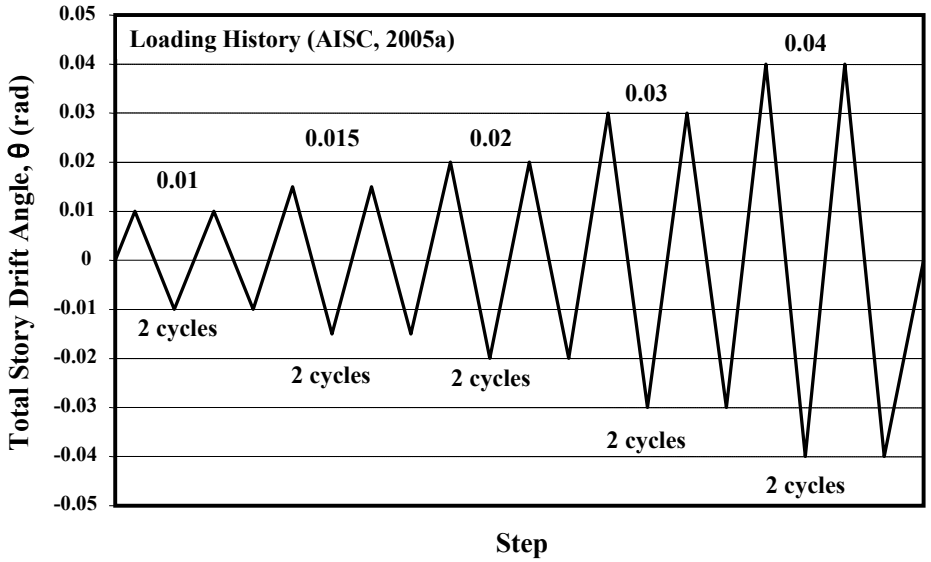

Figure 4.2. Loading History
(Source: AISC 2005a)

4.3.2. FEA Results for Bare Steel Beams with Welded Haunch Modification

The FEA results of bare beams retrofitted by welded haunch (WH) beneath the beam bottom flange are presented first. Normalized moment at the column face (M_f/M_p) versus total (elastic plus plastic) story drift ratio (radian) behavior of specimens with flange slenderness ratios of 8 to 12 and web slenderness ratios of 40, 60, and 80 are shown in Figure 4.3 – 4.17.

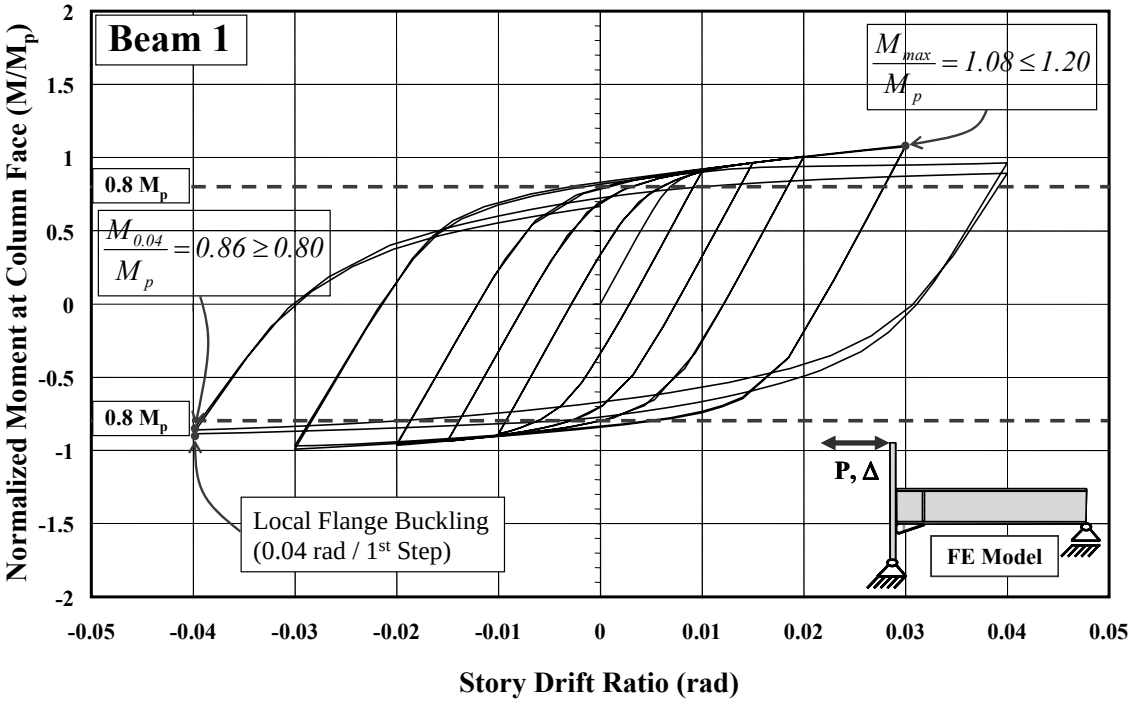

Figure 4.3. Normalized Moment-Total Story Drift Angle (FSR=8, WSR=40)

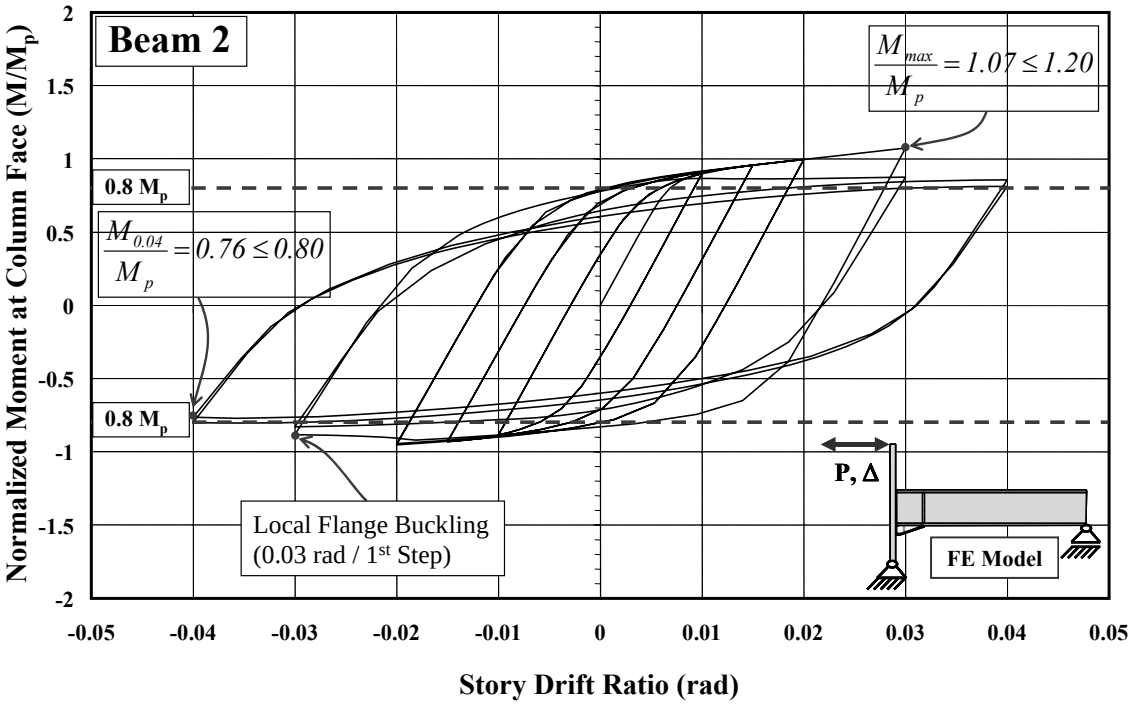

Figure 4.4. Normalized Moment-Total Story Drift Angle (FSR=8, WSR=60)

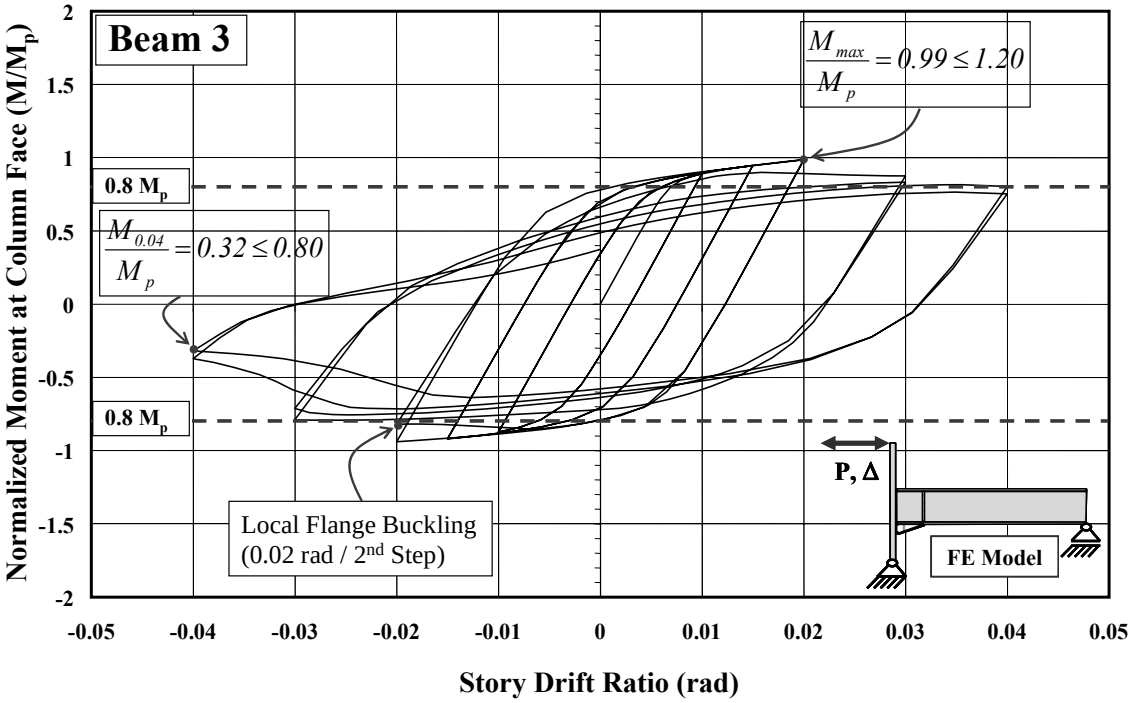

Figure 4.5. Normalized Moment-Total Story Drift Angle (FSR=8, WSR=80)

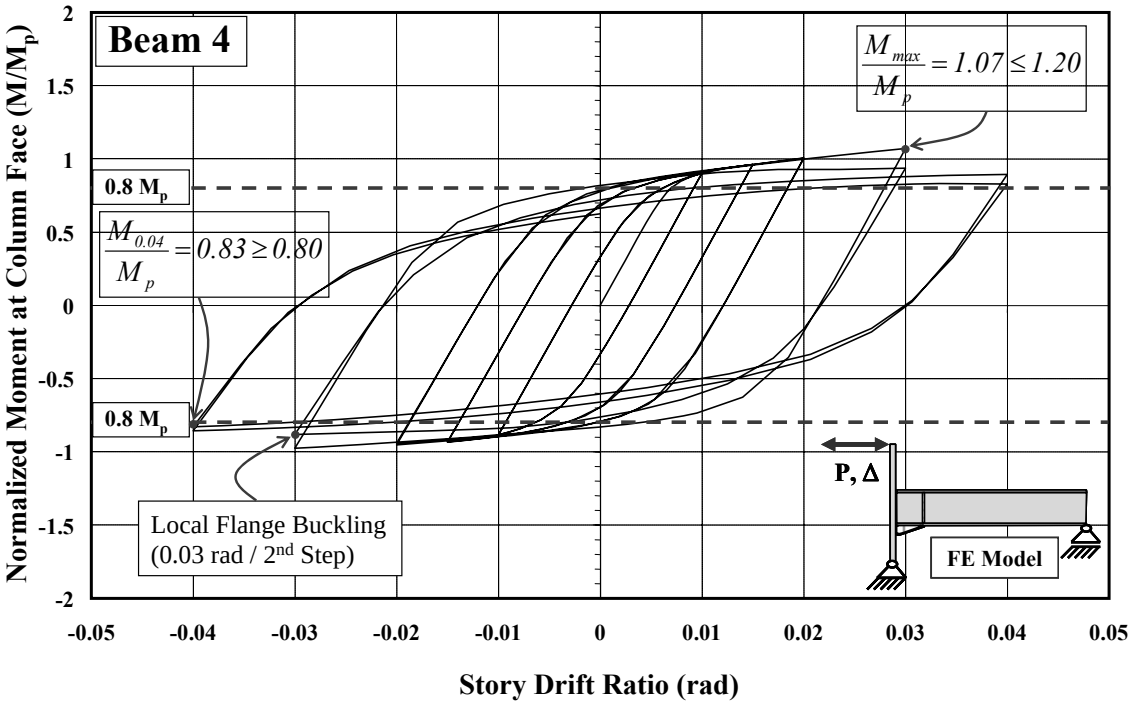

Figure 4.6. Normalized Moment-Total Story Drift Angle (FSR=9, WSR=40)

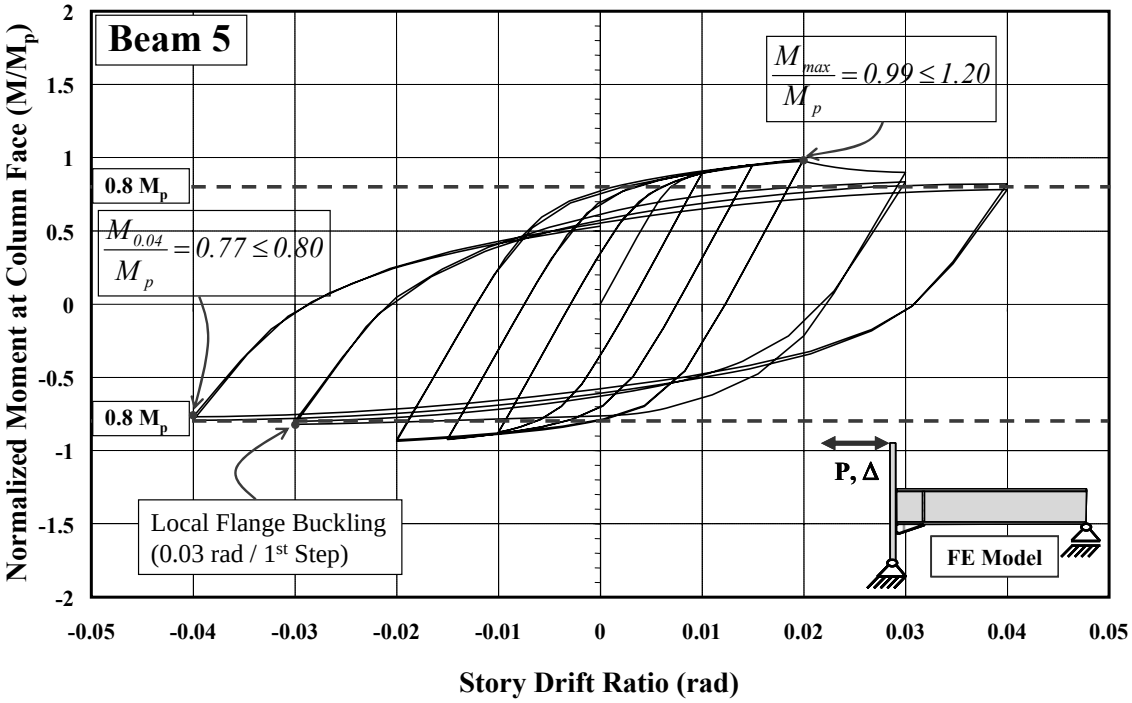

Figure 4.7. Normalized Moment-Total Story Drift Angle (FSR=9, WSR=60)

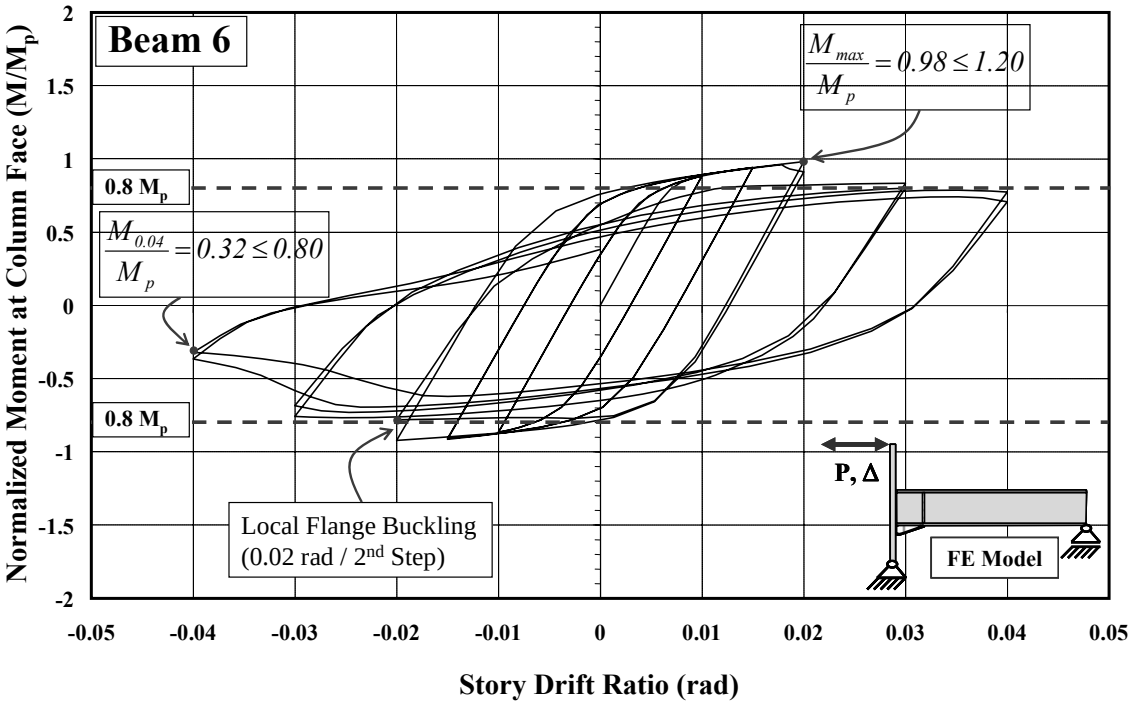

Figure 4.8. Normalized Moment-Total Story Drift Angle (FSR=9, WSR=80)

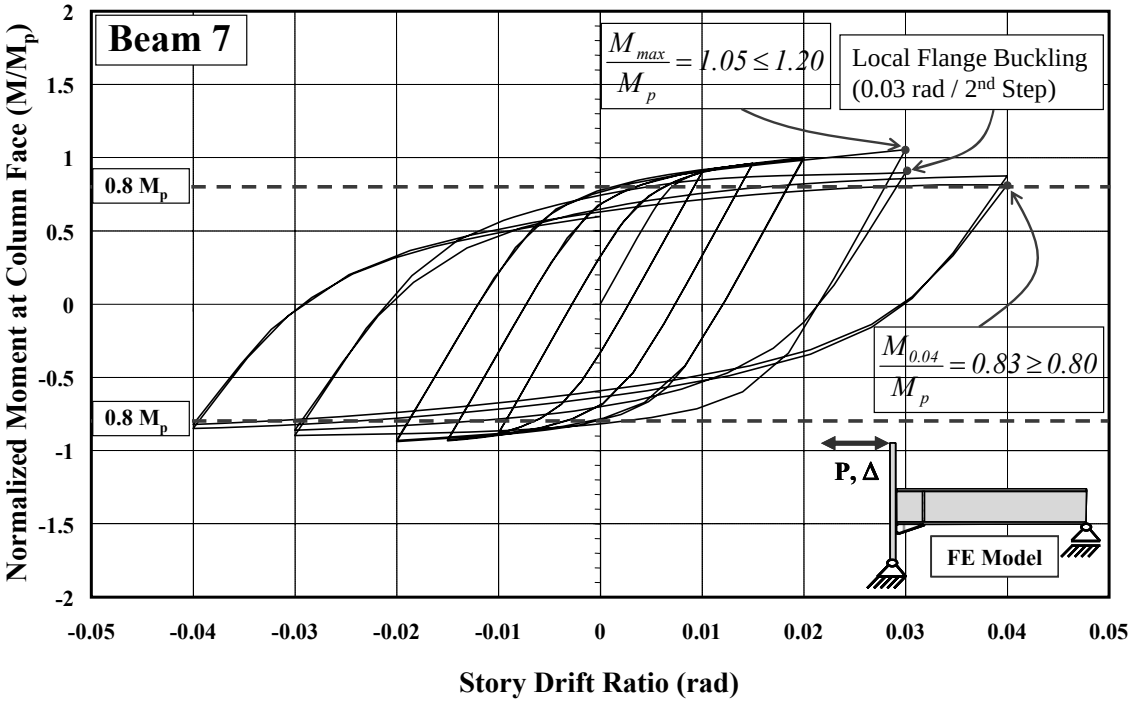

Figure 4.9. Normalized Moment-Total Story Drift Angle (FSR=10, WSR=40)

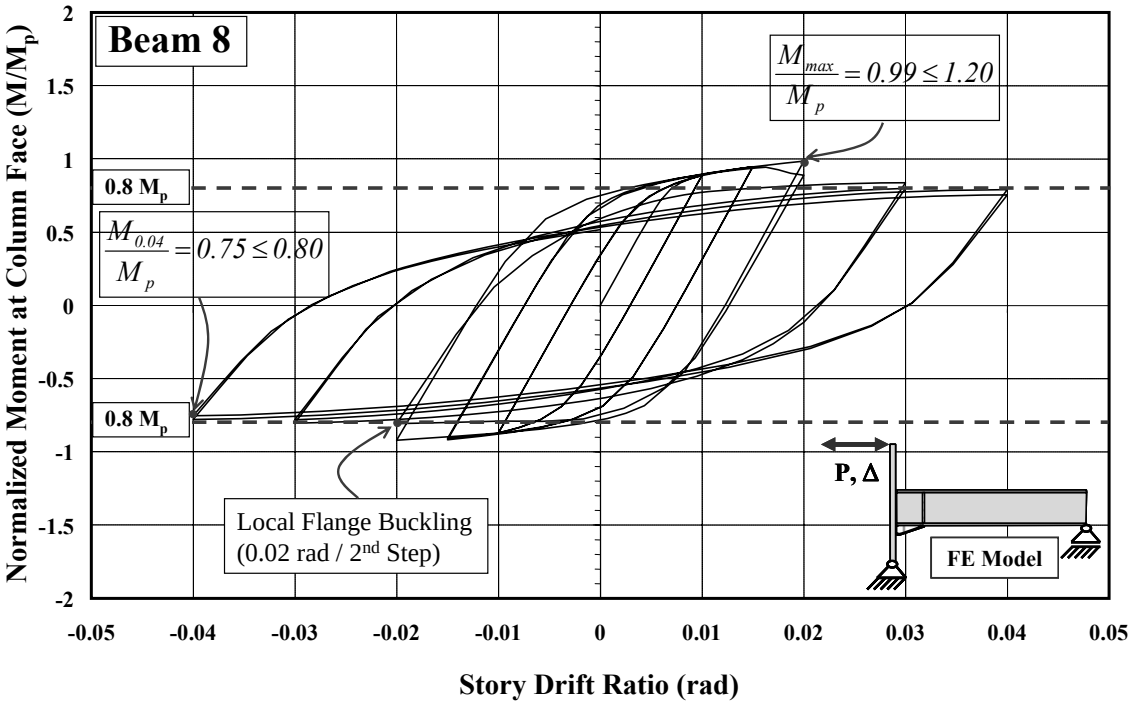

Figure 4.10. Normalized Moment-Total Story Drift Angle (FSR=10, WSR=60)

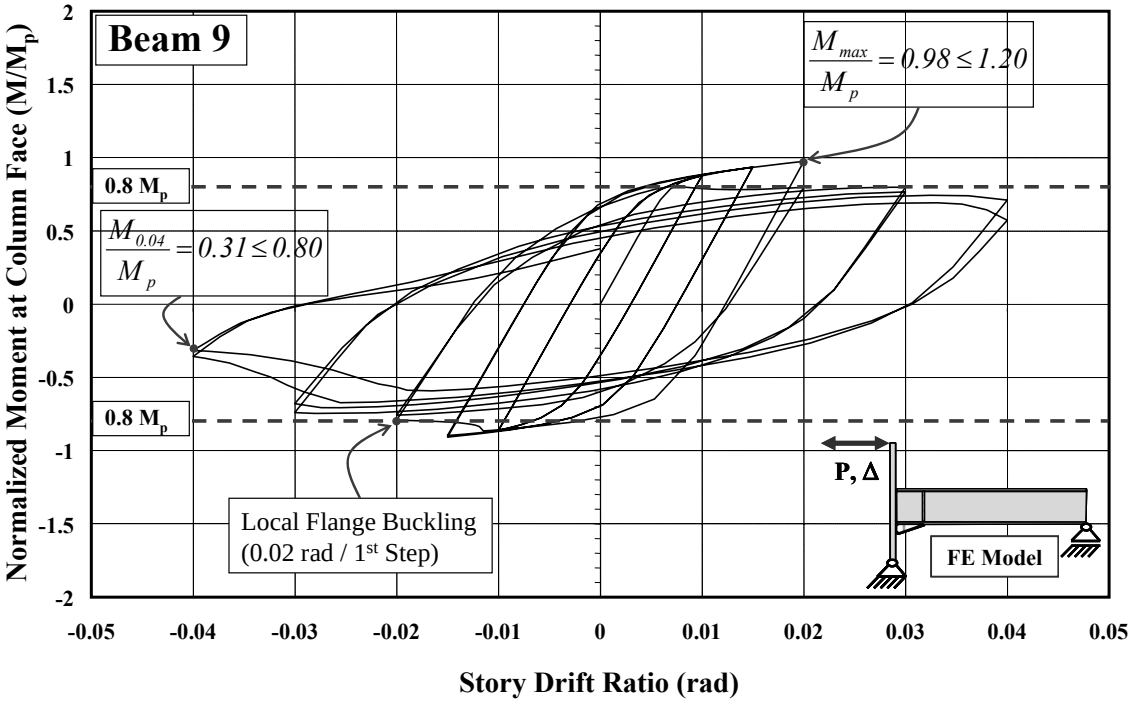

Figure 4.11. Normalized Moment-Total Story Drift Angle (FSR=10, WSR=80)

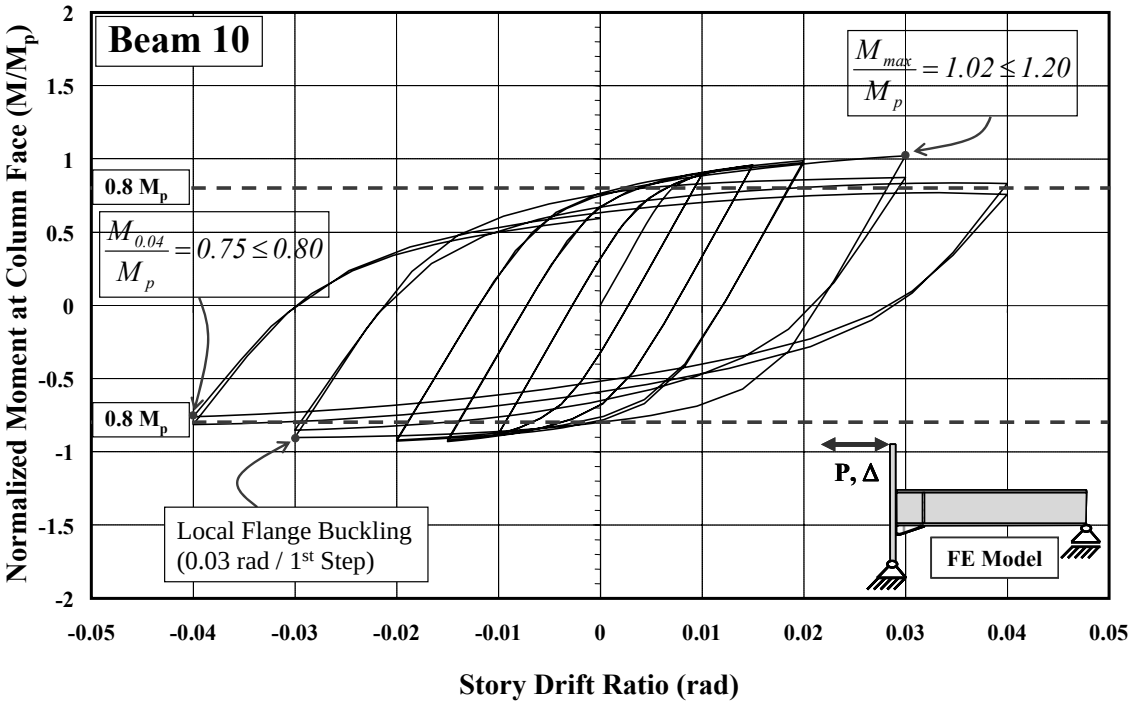

Figure 4.12. Normalized Moment-Total Story Drift Angle (FSR=11, WSR=40)

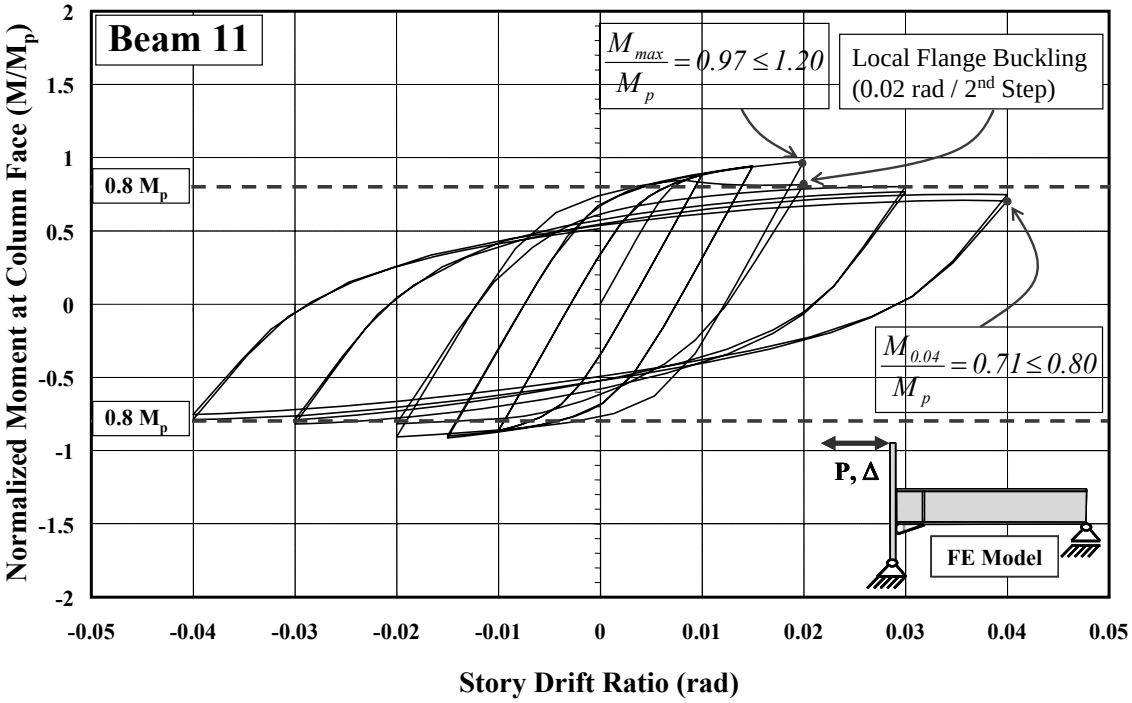

Figure 4.13. Normalized Moment-Total Story Drift Angle (FSR=11, WSR=60)

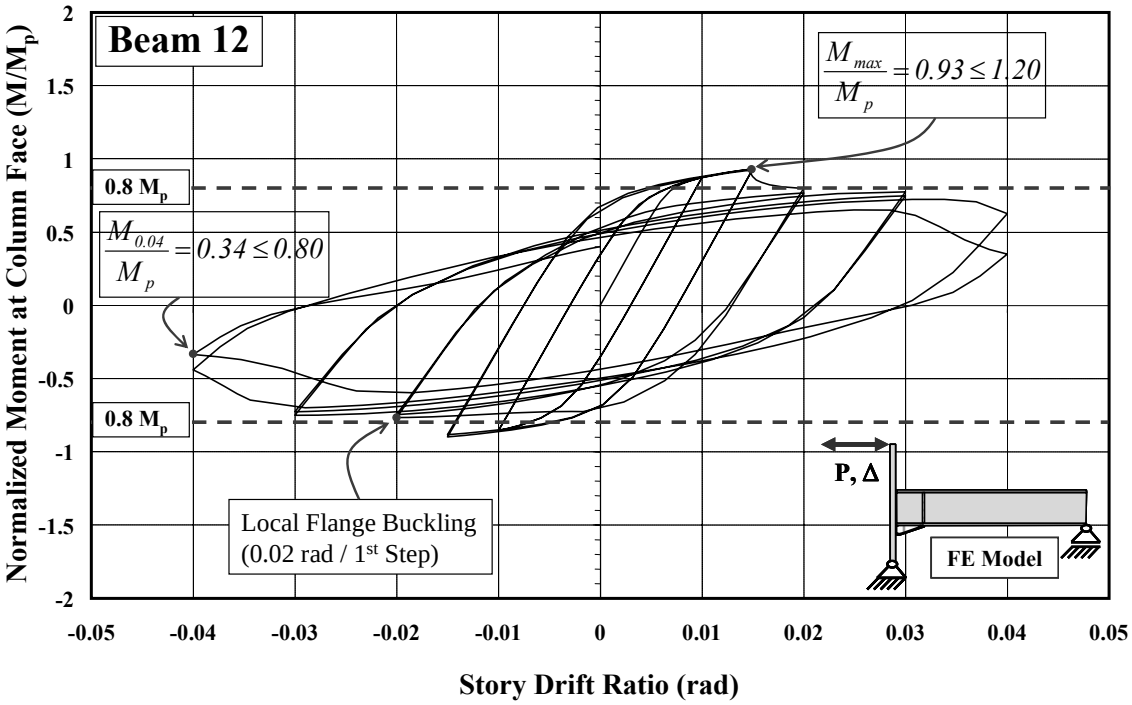

Figure 4.14. Normalized Moment-Total Story Drift Angle (FSR=11, WSR=80)

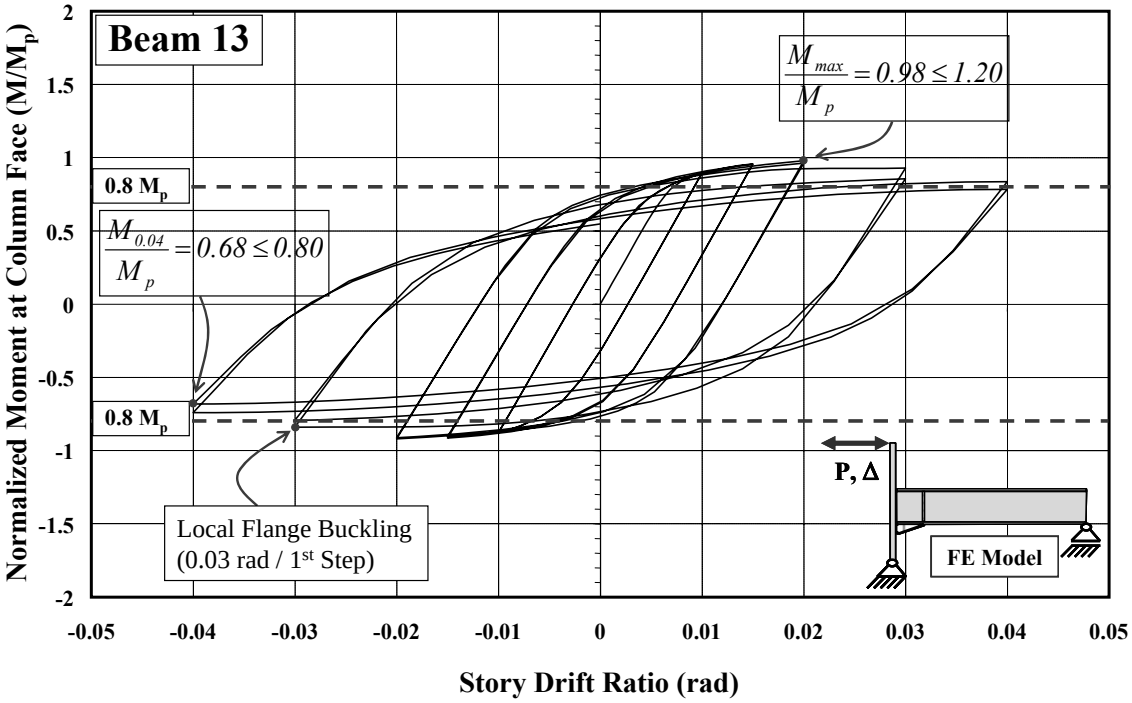

Figure 4.15. Normalized Moment-Total Story Drift Angle (FSR=12, WSR=40)

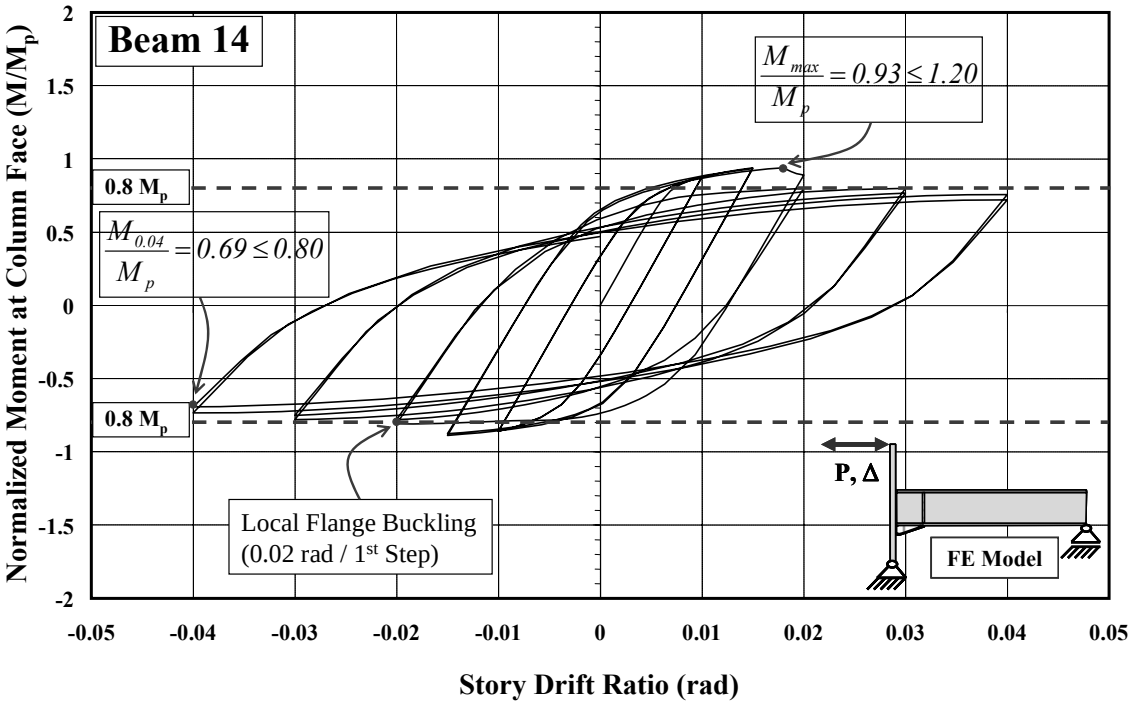

Figure 4.16. Normalized Moment-Total Story Drift Angle (FSR=12, WSR=60)

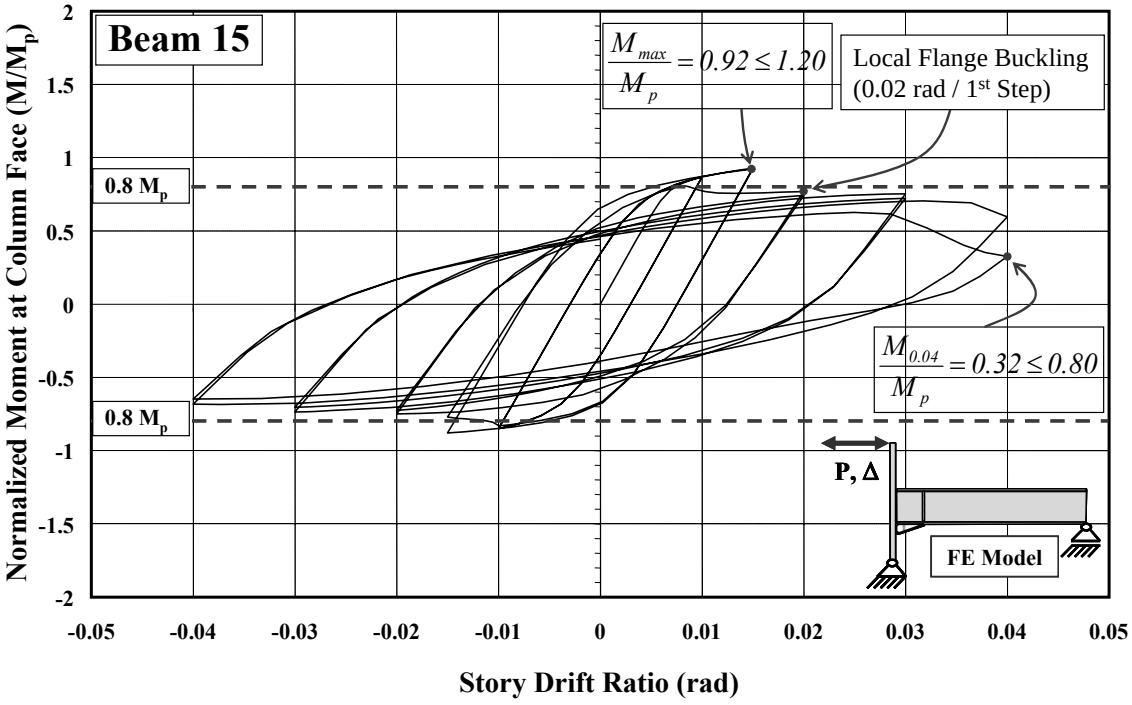

Figure 4.17. Normalized Moment-Total Story Drift Angle (FSR=12, WSR=80)

Some key results of the analyses are briefly summarized in Table 4.1. The first column of Table 1 gives the beam number, the second and third columns give the flange and web slenderness ratios of the beams, respectively, the fourth and fifth columns list the section properties of the beams and welded haunch, the sixth column gives the load cycle at which severe capacity loss occurs, column seven gives the M_f/M_p value at the end of the last cycle, column eight gives the maximum M_f/M_p value reached by the beam, and column nine includes some comments about the behavior of the beams. It can be seen in Table 4.1 that all specimens except Beams 1, 4, and 7 experience strength degradation resulting from local buckling with more than the 20% capacity losses.

Table 4.1. Summary of the FE Analysis Results for the Welded Haunch

1	2	3	4	5	6	7	8	9
Specimen	Flange Slenderness (b/t_f)	Web Slenderness (h/t_w)	Rehabilitation Details		Severe Capacity Loss at θ (%)	Strength Obtained at the End of the Loading ($M_{0.04}/M_p$)	The Largest Strength Obtained During All the Cycles (M_{max}/M_p)	Comments
			Web	Welded Haunch Connection				
Beam 1	8	40	Beam Web Stiffiners A Pair of 20 X 132.5 mm Plates A572 Gr. 50 $F_{y,s}$ = 345 Mpa b_s = 132.5 mm t_s = 20 mm	Welded Haunch A572 Gr. 50 $F_{y,wh}$ = 345 Mpa b_{hw} = 265 mm t_{hf} = 19.5 mm t_{hw} = 12 mm A_{hf} = 5165.5 mm^2 a = 0.5d = 376.5 mm b = a$\tan\theta_{wh}$ = 226.2 mm θ_{wh} = 31°	4	0.86	1.08	Minor bottom flange local buckling with minor strength loss in the second step of 0.02 rad rotation amplitude, and severe web and bottom flange local buckling with severe strength degradation in the first step of 0.04 rad amplitude at negative bending.
Beam 2		60	Beam Web Stiffiners A Pair of 20 X 132.5 mm Plates A572 Gr. 50 $F_{y,s}$ = 345 Mpa b_s = 132.5 mm t_s = 20 mm	Welded Haunch A572 Gr. 50 $F_{y,wh}$ = 345 Mpa b_{hw} = 265 mm t_{hf} = 18 mm t_{hw} = 12 mm A_{hf} = 4770 mm^2 a = 0.5d = 376.5 mm b = a$\tan\theta_{wh}$ = 226.2 mm θ_{wh} = 31°	3	0.76	1.07	Minor bottom flange local buckling with minor strength loss in the second step of 0.02 rad rotation amplitude, and severe web and bottom flange local buckling with severe strength degradation in the first step of 0.03 rad amplitude at negative bending.
Beam 3		80	Beam Web Stiffiners A Pair of 20 X 132.5 mm Plates A572 Gr. 50 $F_{y,s}$ = 345 Mpa b_s = 132.5 mm t_s = 20 mm	Welded Haunch A572 Gr. 50 $F_{y,wh}$ = 345 Mpa b_{hw} = 265 mm t_{hf} = 18 mm t_{hw} = 12 mm A_{hf} = 4770 mm^2 a = 0.5d = 376.5 mm b = a$\tan\theta_{wh}$ = 226.2 mm θ_{wh} = 31°	2	0.32	0.99	Minor bottom flange local buckling with minor strength loss in the first step of 0.02 rad rotation amplitude, and severe web and bottom flange local buckling with severe strength degradation in the second step of 0.02 rad amplitude at negative bending.

(cont. on next page)

Table 4.1. (cont.) Summary of the FE Analysis Results for the Welded Haunch

1	2	3	4	5	6	7	8	9
Specimen	Flange Slenderness (b/t_f)	Web Slenderness (h/t_w)	Rehabilitation Details: Web	Rehabilitation Details: Welded Haunch Connection	Severe Capacity Loss at θ (%)	Strength Obtained at the End of the Loading ($M_{0.04}/M_p$)	The Largest Strength Obtained During All the Cycles (M_{max}/M_p)	Comments
Beam 4	9	40	Beam Web Stiffiners A Pair of 20 X 132.5 mm Plates A572 Gr. 50 $F_{y,s}$ = 345 Mpa b_s = 132.5 mm t_s = 20 mm	Welded Haunch A572 Gr. 50 $F_{y,wh}$ = 345 Mpa b_{hw} = 265 mm t_{hf} = 19 mm t_{hw} = 12 mm A_{hf} = 5035 mm^2 a = 0.5d = 376.5 mm b = a$\tan\theta_{wh}$ = 226.2 mm θ_{wh} = 31°	3	0.83	1.07	Minor bottom flange local buckling with minor strength loss in the first step of 0.02 rad rotation amplitude, and severe web and bottom flange local buckling with severe strength degradation in the second step of 0.03 rad amplitude at negative bending.
Beam 5		60	Beam Web Stiffiners A Pair of 20 X 132.5 mm Plates A572 Gr. 50 $F_{y,s}$ = 345 Mpa b_s = 132.5 mm t_s = 20 mm	Welded Haunch A572 Gr. 50 $F_{y,wh}$ = 345 Mpa b_{hw} = 265 mm t_{hf} = 18 mm t_{hw} = 12 mm A_{hf} = 4770 mm^2 a = 0.5d = 376.5 mm b = a$\tan\theta_{wh}$ = 226.2 mm θ_{wh} = 31°	3	0.77	0.99	Minor bottom flange local buckling with minor strength loss in the first step of 0.02 rad rotation amplitude, and severe web and bottom flange local buckling with severe strength degradation in the first step of 0.03 rad amplitude at negative bending.
Beam 6		80	Beam Web Stiffiners A Pair of 20 X 132.5 mm Plates A572 Gr. 50 $F_{y,s}$ = 345 Mpa b_s = 132.5 mm t_s = 20 mm	Welded Haunch A572 Gr. 50 $F_{y,wh}$ = 345 Mpa b_{hw} = 265 mm t_{hf} = 18 mm t_{hw} = 12 mm A_{hf} = 4770 mm^2 a = 0.5d = 376.5 mm b = a$\tan\theta_{wh}$ = 226.2 mm θ_{wh} = 31°	2	0.32	0.98	Minor bottom flange local buckling with minor strength loss in the first step of 0.02 rad rotation amplitude, and severe web and bottom flange local buckling with severe strength degradation in the second step of 0.02 rad amplitude at negative bending.

(cont. on next page)

Table 4.1. (cont.) Summary of the FE Analysis Results for the Welded Haunch

1	2	3	4	5	6	7	8	9
Specimen	Flange Slenderness (b/t_f)	Web Slenderness (h/t_w)	Rehabilitation Details		Severe Capacity Loss at θ (%)	Strength Obtained at the End of the Loading ($M_{0.04}/M_p$)	The Largest Strength Obtained During All the Cycles (M_{max}/M_p)	Comments
			Web	Welded Haunch Connection				
Beam 7	10	40	Beam Web Stiffiners A Pair of 20 X 132.5 mm Plates A572 Gr. 50 $F_{y,s}$ = 345 Mpa b_s = 132.5 mm t_s = 20 mm	Welded Haunch A572 Gr. 50 $F_{y,wh}$ = 345 Mpa b_{hw} = 265 mm t_{hf} = 18.5 mm t_{hw} = 12 mm A_{hf} = 4902.5 mm^2 a = 0.5d = 376.5 mm b = a tanθ_{wh} = 226.2 mm θ_{wh} = 31°	3	0.81	1.05	Minor bottom flange local buckling with minor strength loss in the second step of 0.02 rad rotation amplitude, and severe web and bottom flange local buckling with severe strength degradation in the second step of 0.03 rad amplitude at positive bending.
Beam 8		60	Beam Web Stiffiners A Pair of 20 X 132.5 mm Plates A572 Gr. 50 $F_{y,s}$ = 345 Mpa b_s = 132.5 mm t_s = 20 mm	Welded Haunch A572 Gr. 50 $F_{y,wh}$ = 345 Mpa b_{hw} = 265 mm t_{hf} = 18 mm t_{hw} = 12 mm A_{hf} = 4770 mm^2 a = 0.5d = 376.5 mm b = a tanθ_{wh} = 226.2 mm θ_{wh} = 31°	2	0.75	0.99	Minor bottom flange local buckling with minor strength loss in the second step of 0.015 rad rotation amplitude, and severe web and bottom flange local buckling with severe strength degradation in the second step of 0.02 rad amplitude at negative bending.
Beam 9		80	Beam Web Stiffiners A Pair of 20 X 132.5 mm Plates A572 Gr. 50 $F_{y,s}$ = 345 Mpa b_s = 132.5 mm t_s = 20 mm	Welded Haunch A572 Gr. 50 $F_{y,wh}$ = 345 Mpa b_{hw} = 265 mm t_{hf} = 18 mm t_{hw} = 12 mm A_{hf} = 4770 mm^2 a = 0.5d = 376.5 mm b = a tanθ_{wh} = 226.2 mm θ_{wh} = 31°	2	0.31	0.98	Minor bottom flange local buckling with minor strength loss in the second step of 0.015 rad rotation amplitude, and severe web and bottom flange local buckling with severe strength degradation in the first step of 0.02 rad amplitude at negative bending.

(cont. on next page)

Table 4.1. (cont.) Summary of the FE Analysis Results for the Welded Haunch

1	2	3	4	5	6	7	8	9
Specimen	Flange Slenderness (b/t_f)	Web Slenderness (h/t_w)	Rehabilitation Details: Web	Rehabilitation Details: Welded Haunch Connection	Severe Capacity Loss at θ (%)	Strength Obtained at the End of the Loading ($M_{0.04}/M_p$)	The Largest Strength Obtained During All the Cycles (M_{max}/M_p)	Comments
Beam 10	11	40	Beam Web Stiffiners A Pair of 20 X 132.5 mm Plates A572 Gr. 50 $F_{y,s}$ = 345 Mpa b_s = 132.5 mm t_s = 20 mm	Welded Haunch A572 Gr. 50 $F_{y,wh}$ = 345 Mpa b_{hw} = 265 mm t_{hf} = 18.5 mm t_{hw} = 12 mm A_{hf} = 4902.5 mm^2 a = 0.5d = 376.5 mm b = a tanθ_{wh} = 226.2 mm θ_{wh} = 31^o	3	0.76	1.02	Minor bottom flange local buckling with minor strength loss in the second step of 0.015 rad rotation amplitude, and severe web and bottom flange local buckling with severe strength degradation in the first step of 0.03 rad amplitude at negative bending.
Beam 11		60	Beam Web Stiffiners A Pair of 20 X 132.5 mm Plates A572 Gr. 50 $F_{y,s}$ = 345 Mpa b_s = 132.5 mm t_s = 20 mm	Welded Haunch A572 Gr. 50 $F_{y,wh}$ = 345 Mpa b_{hw} = 265 mm t_{hf} = 18 mm t_{hw} = 12 mm A_{hf} = 4770 mm^2 a = 0.5d = 376.5 mm b = a tanθ_{wh} = 226.2 mm θ_{wh} = 31^o	2	0.71	0.97	Minor top flange local buckling with minor strength loss in the first step of 0.02 rad rotation amplitude, and severe web and top flange local buckling with severe strength degradation in the second step of 0.02 rad amplitude at positive bending.
Beam 12		80	Beam Web Stiffiners A Pair of 20 X 132.5 mm Plates A572 Gr. 50 $F_{y,s}$ = 345 Mpa b_s = 132.5 mm t_s = 20 mm	Welded Haunch A572 Gr. 50 $F_{y,wh}$ = 345 Mpa b_{hw} = 265 mm t_{hf} = 18 mm t_{hw} = 12 mm A_{hf} = 4770 mm^2 a = 0.5d = 376.5 mm b = a tanθ_{wh} = 226.2 mm θ_{wh} = 31^o	2	0.34	0.93	Minor bottom flange local buckling with minor strength loss in the second step of 0.015 rad rotation amplitude, and severe web and bottom flange local buckling with severe strength degradation in the first step of 0.02 rad amplitude at negative bending.

(cont. on next page)

Table 4.1. (cont.) Summary of the FE Analysis Results for the Welded Haunch

1	2	3	4	5	6	7	8	9
Specimen	Flange Slenderness (b/t_f)	Web Slenderness (h/t_w)	Rehabilitation Details		Severe Capacity Loss at θ (%)	Strength Obtained at the End of the Loading ($M_{0.04}/M_p$)	The Largest Strength Obtained During All the Cycles (M_{max}/M_p)	Comments
			Web	Welded Haunch Connection				
Beam 13	12	40	Beam Web Stiffiners A Pair of 20 X 132.5 mm Plates A572 Gr. 50 $F_{y,s}$ = 345 Mpa b_s = 132.5 mm t_s = 20 mm	Welded Haunch A572 Gr. 50 $F_{y,wh}$ = 345 Mpa b_{hw} = 265 mm t_{hf} = 18 mm t_{hw} = 12 mm A_{hf} = 4770 mm^2 a = 0.5d = 376.5 mm b = a tanθ_{wh} = 226.2 mm θ_{wh} = 31^o	3	0.68	0.98	Minor bottom flange local buckling with minor strength loss in the first step of 0.015 rad rotation amplitude, and severe web and bottom flange local buckling with severe strength degradation in the first step of 0.03 rad amplitude at negative bending.
Beam 14		60	Beam Web Stiffiners A Pair of 20 X 132.5 mm Plates A572 Gr. 50 $F_{y,s}$ = 345 Mpa b_s = 132.5 mm t_s = 20 mm	Welded Haunch A572 Gr. 50 $F_{y,wh}$ = 345 Mpa b_{hw} = 265 mm t_{hf} = 18 mm t_{hw} = 12 mm A_{hf} = 4770 mm^2 a = 0.5d = 376.5 mm b = a tanθ_{wh} = 226.2 mm θ_{wh} = 31^o	2	0.69	0.93	Minor top flange local buckling with minor strength loss in the first step of 0.015 rad rotation amplitude, and severe web and top flange local buckling with severe strength degradation in the first step of 0.02 rad amplitude at negative bending.
Beam 15		80	Beam Web Stiffiners A Pair of 20 X 132.5 mm Plates A572 Gr. 50 $F_{y,s}$ = 345 Mpa b_s = 132.5 mm t_s = 20 mm	Welded Haunch A572 Gr. 50 $F_{y,wh}$ = 345 Mpa b_{hw} = 265 mm t_{hf} = 18 mm t_{hw} = 12 mm A_{hf} = 4770 mm^2 a = 0.5d = 376.5 mm b = a tanθ_{wh} = 226.2 mm θ_{wh} = 31^o	2	0.32	0.92	Severe web and bottom flange local buckling with severe strength degradation in the first step of 0.02 rad amplitude at positive bending.

(cont. on next page)

Table 4.1. (cont.) Summary of the FE Analysis Results for the Welded Haunch

Notes:

All specimens are bare steel.

Lateral bracings in all models were provided at mid-span and both ends of the beams.

Notations:

a = haunch length

b = haunch depth

θ_{wh} = angle of sloped haunch

θ = total story drift angle (interstory displacement divided by story height, radians).

d = beam depth

b_s = beam web stiffener width

t_s = beam web stiffener thickness

b_{hw} = haunch flange width

t_{hf} = haunch flange thickness

t_{hw} = haunch web thickness

A_{hf} = haunch flange area

F_{y_s} = web stiffener yield stress

F_{y_wh} = welded haunch yield stress for both flange and web

Figure 4.18 and 4.19 shows the strength degradations and story drift ratios achieved at the end of the last cycle, respectively. The highest strength degradation resulting from severe flanges and web local buckling was observed in Beam 9 with 31% strength at the 0.04 radians of rotation. Beam 1, 4, and 7 achieved total (elastic plus plastic) story drift ratios of at least 0.04 radians in magnitude before experiencing 20% strength degradation (with 86, 83, and 81% strength capacities, respectively). Only Beam 1 performed the most suitable result of all the beams analyzed under reversed quasi-static cyclic loading. Beam 4 and Beam 7 experienced severe web and flange local buckling at the second step of the story drift angle of 0.03 radians, but they reached the story drift of 0.04 rad with 83% and 81% strength, respectively.

The maximum strength at the last step is considerably less for beams that have higher WSR (Figure 4.18). It can be concluded from the analyses results that the slenderness ratio of the web plays a more critical role in local buckling than the slenderness ratio of the flanges.

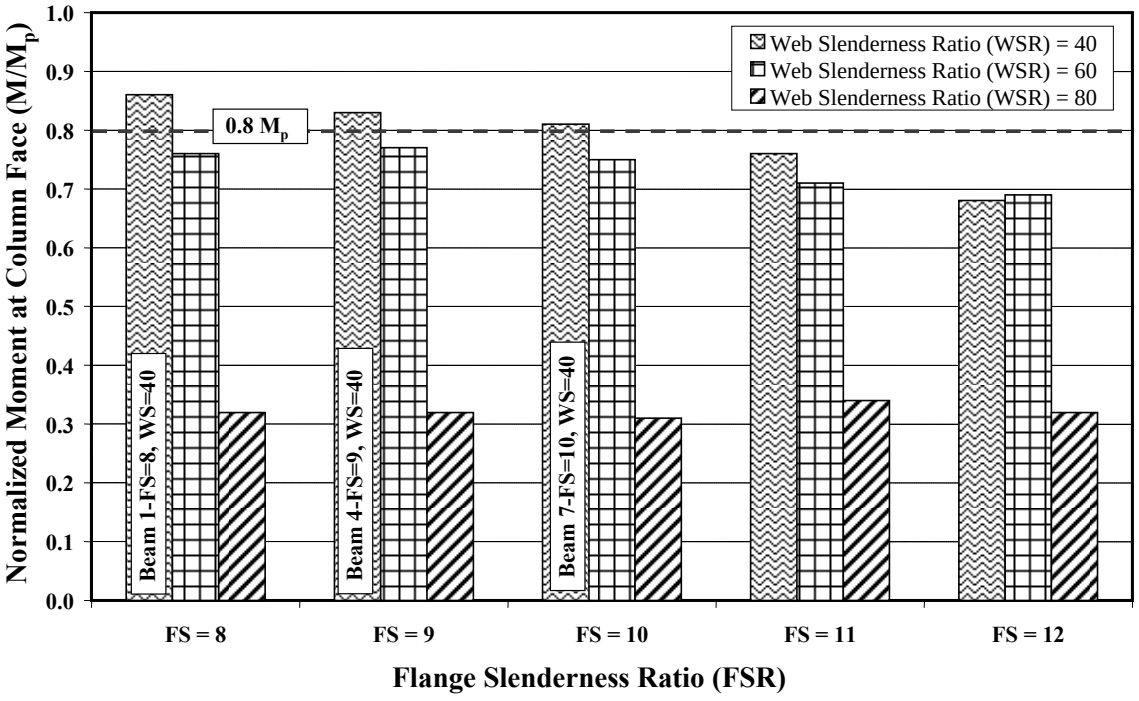

Figure 4.18. Comparisons of Moment Capacities

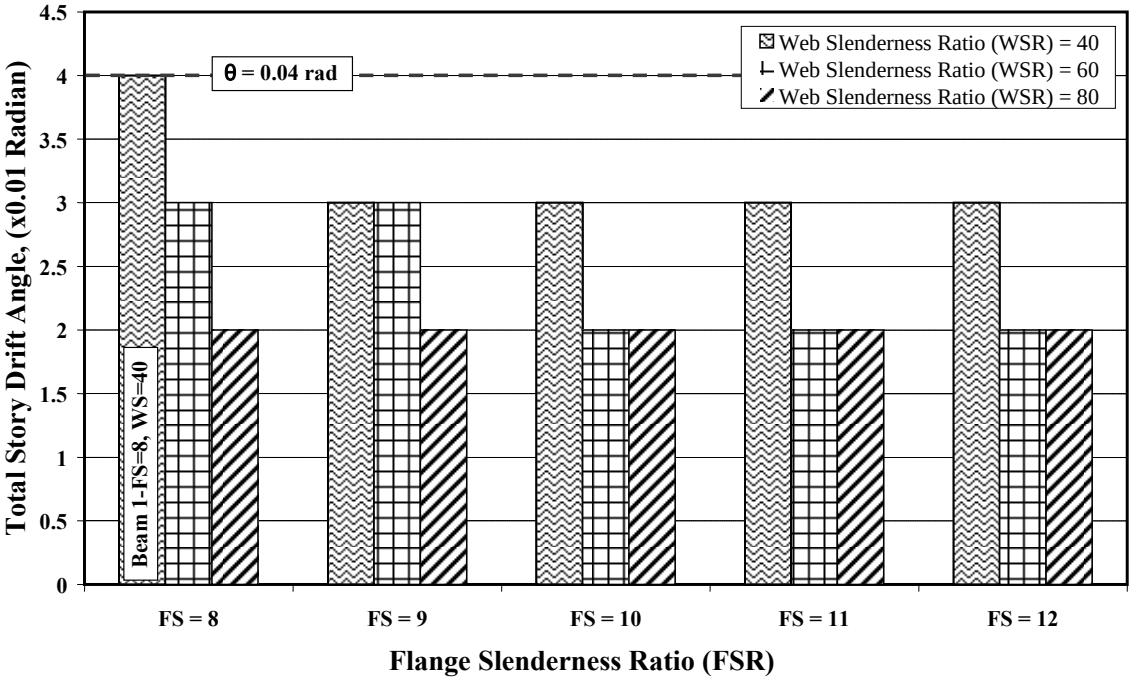

Figure 4.19. Comparisons of Story Drift Ratio

In total, all specimens modified with WH beneath the beam bottom flange reach their full plastic moment away from the column face and local buckling in the beam flanges and web occurred outside of the haunch. Figure 4.20 represents the plastic hinge region with local buckling in Beam 12 modified with WH.

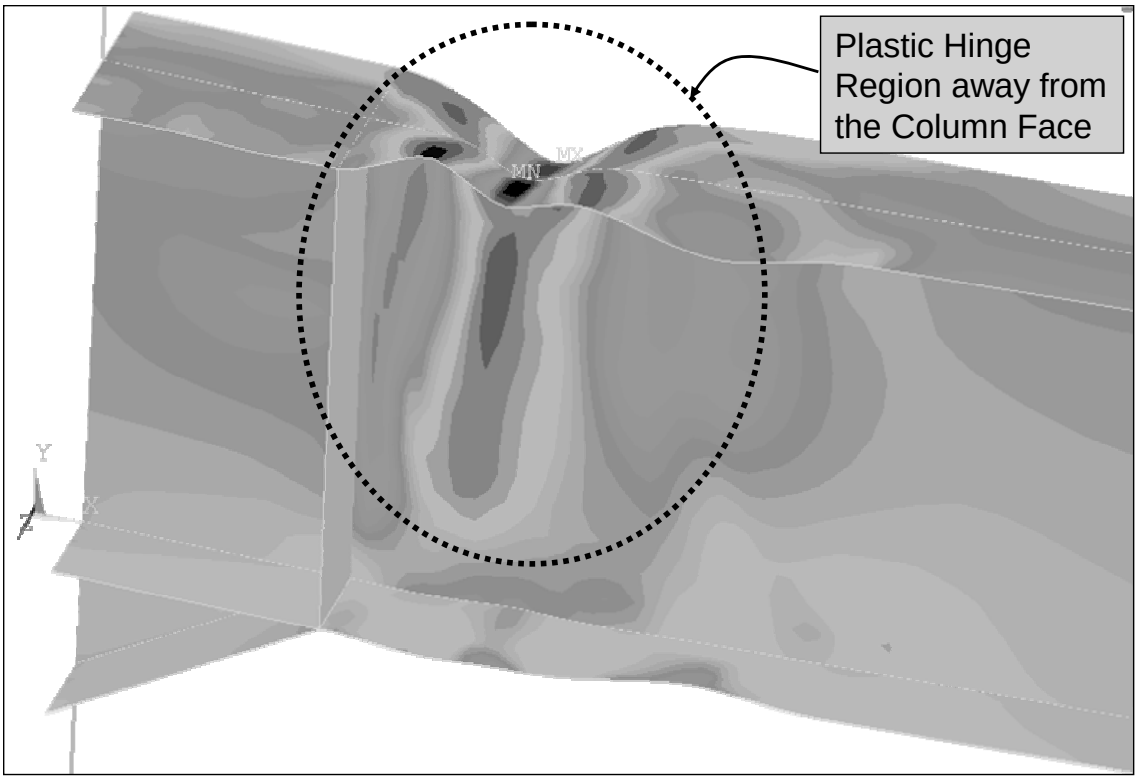

Figure 4.20. Plastic Hinge Region of Beam 12 (FS=11, WS=80)

Table 4.2 tabulates positive and negative bending behavior of all specimens. In positive bending top flange is in compression and bottom flange is in tension, in negative bending top flange is in tension and bottom flange is in compression. For all beams except Beam 7, 11, and 15, strength degradation due to local buckling was less severe in positive bending than in negative bending because of WH existence. Generally, minor flange local buckling is observed in the lower portion of the beam flange outside the WH region with minor strength degradation. This type of minor FLB results in WLB followed by severe strength degradation. Minor and severe local buckling behaviors of the Beam 8 under the negative bending are briefly shown in Figure 4.21.a and Figure 4.21.b.

Table 4.2. Positive and Negative Bending Behavior of the Specimens

Specimen	b/t_f	d/t_w	Positive Bending			Negative Bending		
			Severe Capacity Loss at θ (%)	Step	Maximum Strength at the Last Step (M/M_p)	Severe Capacity Loss at θ (%)	Step	Maximum Strength at the Last Step (M/M_p)
Beam 1	8	40	4	1	0.89	4	1	-0.86
Beam 2		60	3	2	0.81	3	1	-0.76
Beam 3		80	3	1	0.75	2	2	-0.32
Beam 4	9	40	3	2	0.83	3	2	-0.83
Beam 5		60	3	1	0.78	3	1	-0.77
Beam 6		80	2	2	0.71	2	1	-0.32
Beam 7	10	40	3	2	0.81	3	1	-0.82
Beam 8		60	3	1	0.75	2	2	-0.75
Beam 9		80	2	2	0.57	2	1	-0.31
Beam 10	11	40	3	2	0.76	3	1	-0.76
Beam 11		60	2	2	0.71	2	2	-0.75
Beam 12		80	2	1	0.35	2	1	-0.34
Beam 13	12	40	3	1	0.78	3	1	-0.68
Beam 14		60	2	1	0.72	2	1	-0.69
Beam 15		80	2	1	0.32	2	2	-0.65

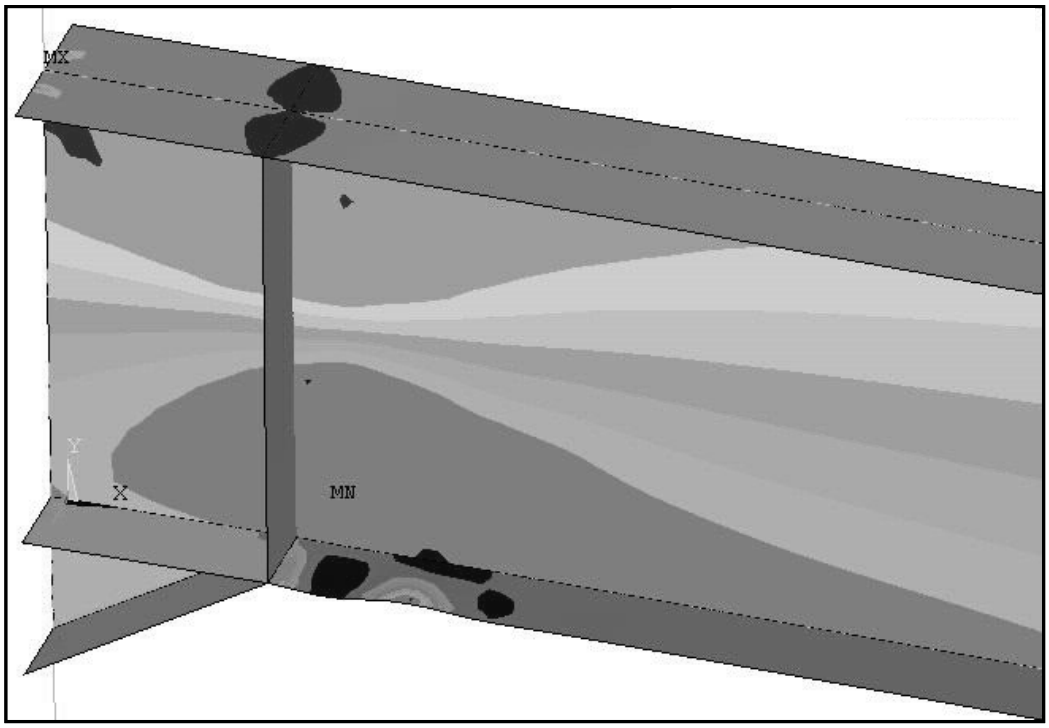

(a)

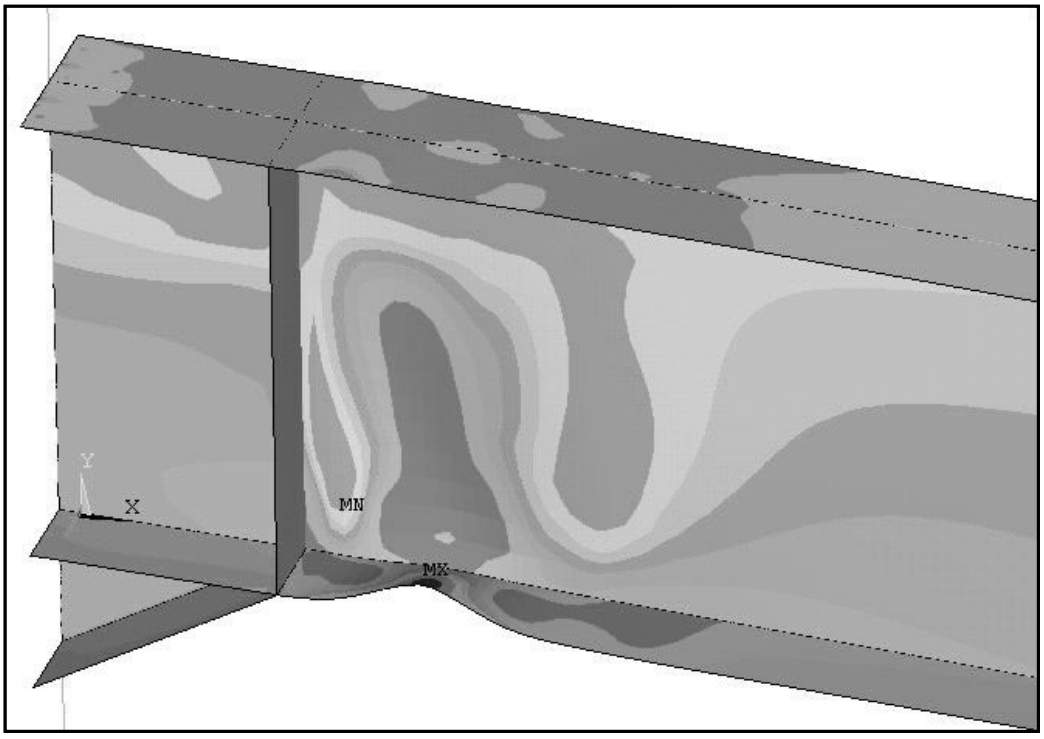

(b)

Figure 4.21. Local Buckling Representation of Beam 4; a) Minor Flange Local Buckling, b) Severe Flange and Web Local Buckling

The results of the analyses showed that all beams reached their full plastic moment into the beam away from the face of the column by using the WH type connection. On the other hand, twelve of the fifteen specimens are not adequate to reach the target story drift rotation amplitude with at least 80% moment capacity stipulated in ANSI/AISC-341-05 (AISC 2005b). In addition, all specimens experienced severe local buckling before reaching the inter-story drift angle of 0.04 rad.

4.3.3. FEA Results of Beams with GFRP

4.3.3.1. Introduction

For the first step of beam-GFRP application, GFRP material was taken as an isotropic material with an elastic modulus of 10 GPa and a layer thickness of 1.5 mm. The ideal dimensions and location of GFRP were determined utilizing this model. After obtaining the actual dimensions and location of GFRP, orthotropic material model was used to see actual behavior of steel-GFRP systems.

The results are evaluated for each beam section with GFRP as normalized moment at the column face (M/M_p) versus total (elastic plus plastic) story drift ratio (radian).

In order to obtain an ideal form of beam-GFRP application it is needed to determine the length, thickness, and width of the GFRP materials that will be applied to the beam flanges along with the location of the GFRP materials on the beam flanges. Length, width, and location of GFRP will be the same for all fifteen beams to be analyzed. In other words, once these variables will determined by analyses in one beam, they will become the optimum values for all beam sections. These optimum values are determined by running several analyses on Beam 8 with FSR of 10 and WSR of 60. The interlaminar shear stress or shear forces at the steel-GFRP interface binding will not investigated in these analyses. These stresses will be checked after the optimum length, width, and location are found.

Because shear stresses will not checked in that level, GFRP materials were modeled as an isotropic material by using the SHELL 181 composite element and

thickness of one layer was taken as 1.5 mm for economy of time (Figure 3.1). When the interlaminar shear stress will be checked, GFRP materials will be modeled as orthotropic materials with the same shell element and the thickness of one layer will be taken as 0.9 mm based on conducted GFRP tests.

4.3.3.2. Determination of Optimum Length, Width, and Location of GFRP

Beam having FSR of 10 and WSR of 60 was used to determine the optimum length, width, and location of GFRP materials. In order to come up with an easy to follow nomenclature the length of the GFRP were depicted as a ratio of beam depth (ex: $L_{GFRP} = 1d_b$, $2d_b$, or $3d_b$), and the width of the GFRP were named as a ratio of flange width for each half of flange (ex: $b_{GFRP} = 0.19b_f$, $0.40b_f$, or $0.47b_f$). The illustration of these values is presented in Figure 4.22.

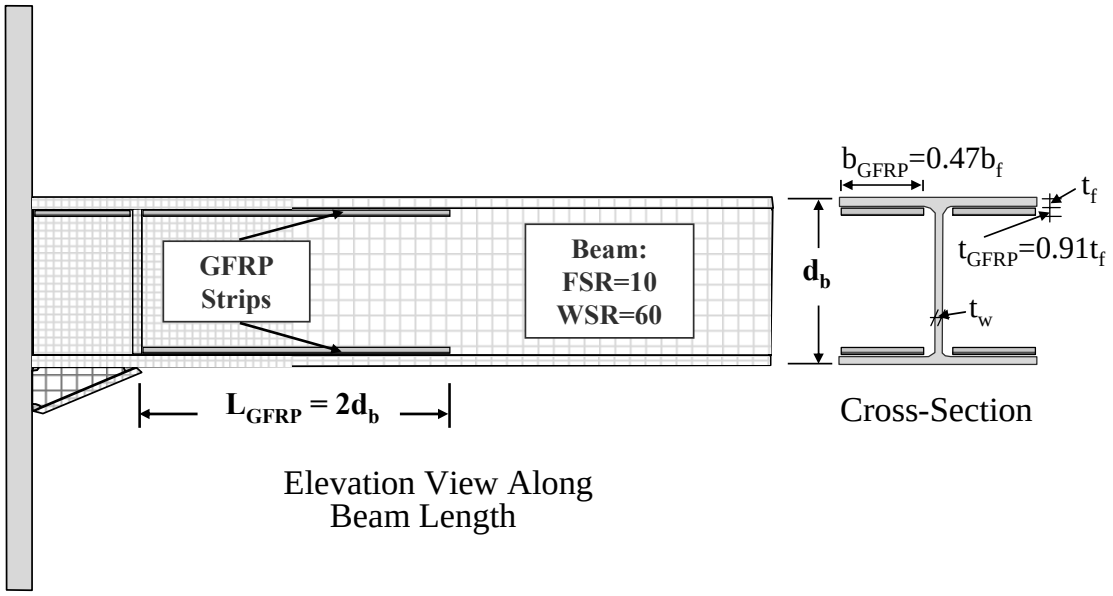

Figure 4.22. Values of Width and Length of the GFRP Strips

In addition, three options were considered for the location of GFRP. The first option was to place the GFRP strips outside the welded haunch region on top of the bottom flange, and bottom of the top flange; considering the presence of a concrete slab over the top flange in a real structure (Figure 4.23). The second option was to place the GFRP strips not only outside but also inside the welded haunch region on top of the bottom flange, and bottom of the top flange (Figure 4.24). The last option was to place the GFRP strips on top of the bottom flange, and bottom of the top flange outside the WH region and on bottom of the top flange inside the WH region (Figure 4.25).

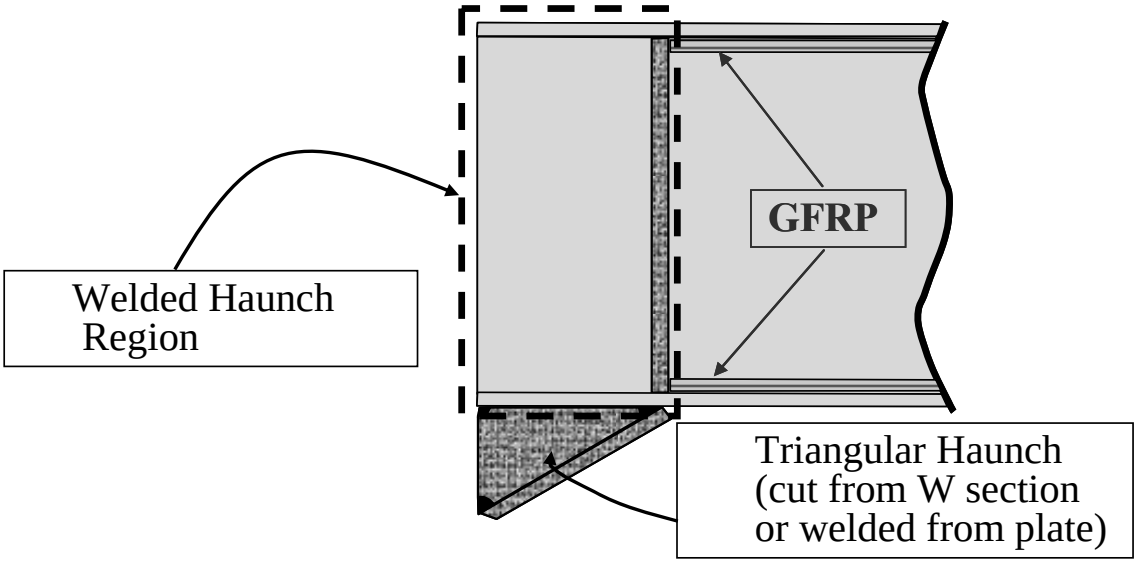

Figure 4.23. Location of GFRP: Out of the WH Region

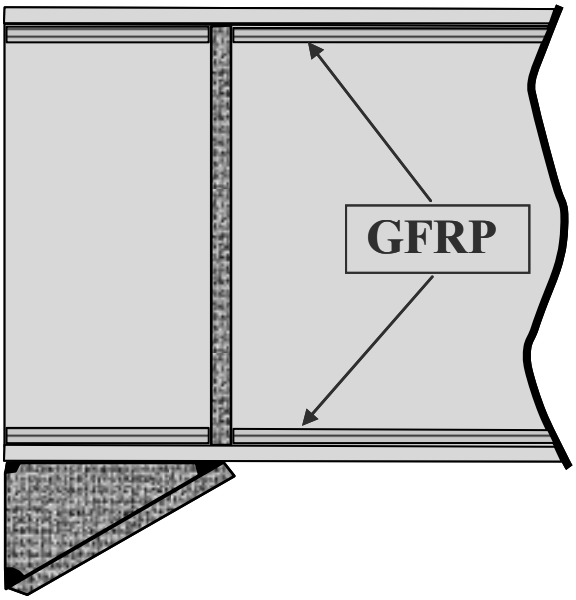

Figure 4.24. Location of GFRP: In and Out of the WH Region

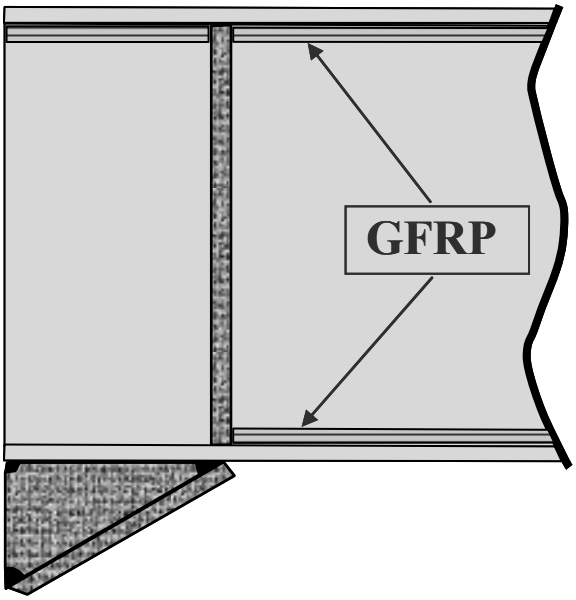

Figure 4.25. Location of GFRP: In and Out of the WH Region (There is no GFRP on top of the Bottom Flange)

Normalized moment at the column face (M/M_p) versus total (elastic plus plastic) story drift ratio (radian) behavior of bare beam and beam models with different L_{GFRP}

and b_{GFRP} values and location of GFRP were compared. The results of the comparisons are tabulated in Table 4.3, Table 4.4, and Table 4.5. The first row in the tables presents values for bare steel section (with FSR of 10 and WSR of 60) in order to highlight the effects of the GFRP strips. In all of the tables the first, second, third, and fourth columns present the number of GFRP layers used, the total thickness of GFRP (as a ratio of beam flange thickness, t_f), the length of GFRP (as a ratio of beam depth, d_b), and the width of the GFRP (as a ratio of beam flange width, b_f), respectively. The fifth and seventh columns present M_{max}/M_p values reached under negative and positive bending, respectively, the sixth and eighths columns present the load step at which local buckling initiates.

Table 4.3 presents results for beams with GFRP strips placed outside the welded haunch region (Figure 4.23). Rows 3, 4, 5, and 6 present results for beam-GFRP systems with GFRP having a thickness of $0.34t_f$ (number of layers = 3). The system with a GFRP length of $2d_b$ and width of $0.19b_f$ showed a similar behavior with the bare beam (comparing row 3 with row 2). The M_{max}/M_p values in the negative region of the bare beam and beam with GFRP are 0.92 and 0.93, respectively. In addition, local flange buckling of both bare beam and beam-GFRP system were observed in the second step of 0.02 radians of rotation. When the GFRP length was increased from $2d_b$ to L_b (L_b = distance from web stiffener to beam end), there was no difference at these values. When the length of GFRP was $2d_b$ and the width of GFRP was $0.47b_f$, or the length of GFRP was L_b and the width of GFRP was $0.47b_f$, it was observed that the behavior of the beam-GFRP system was again similar to the behavior of bare beam. Therefore, the thickness of GFRP was increased.

Rows 6, 7, 8, and 9 present results for beam-GFRP systems with GFRP having a thickness of $0.91t_f$ (number of layers = 8). Increasing the thickness of GFRP did not contribute much to the behavior. The only difference was in the load step where local buckling initiated. In the bare beam local buckling was observed in the second step of 0.02 radians of rotation, where in the beam-GFRP system local buckling was observed in the first step of 0.03 radians of rotation. Furthermore, it can also be understood from Table 4.3 that the behavior of the beam does not change by increasing the length of the GFRP from $2d_b$ to L_b.

Table 4.3. Location of GFRP: Out of the WH Region (Figure 4.23)

	1	2	3	4	5	6	7	8
	Number of Layer	t_{GFRP}	L_{GFRP}	b_{GFRP}	Negative Bending		Positive Bending	
					Max (M_{max}/M_P)	Local Flange Buckling	Max (M_{max}/M_P)	Local Flange Buckling
1	**BARE**	**t_f = 13.25 mm**	**L_b = 3500 mm**	**b_f = 265 mm**	**0.92**	**0.02/2. Step**	**0.99**	**0.02/2. Step**
2	**3 Layers (4.5 mm)**	**0.34 t_f**	$2d_b$	$0.19b_f$	0.93	**0.02/2. Step**	1.00	**0.02/2. Step**
3			L_b	$0.19b_f$	0.92	**0.02/2. Step**	1.00	**0.02/2. Step**
4			$2d_b$	$0.47b_f$	0.94	**0.02/2. Step**	1.01	**0.02/2. Step**
5			L_b	$0.47b_f$	0.94	**0.02/2. Step**	1.01	**0.03/1. Step**
6	**8 Layers (12 mm)**	**0.91 t_f**	$2d_b$	$0.19b_f$	0.95	**0.02/2. Step**	1.01	**0.03/1. Step**
7			L_b	$0.19b_f$	0.95	**0.02/2. Step**	1.01	**0.03/1. Step**
8			$2d_b$	$0.47b_f$	0.94	**0.03/1. Step**	1.03	**0.03/1. Step**
9			L_b	$0.47b_f$	1.00	**0.03/1. Step**	1.05	**0.03/1. Step**

From the first set of analysis it can be understood that the GFRP located only out of the WH region (Figure 4.23) is not affecting the behavior of the beam very much. Therefore, in the second set of analyses GFRP materials were located in and out of the WH region. Table 4.4 presents results for beams with GFRP strips placed inside (bottom of top flange and top of bottom flange) and outside the welded haunch region (Figure 4.24). Rows 2 and 3 present results for beam-GFRP systems with GFRP having a thickness of $0.34t_f$ (number of layers = 3). The system with a GFRP length of $2d_b$ and width of $0.47b_f$ showed a similar behavior with the bare beam (comparing row 2 with row 1). The M_{max}/M_p values in the negative region of the bare beam and beam with GFRP are 0.92 and 0.95, respectively. These values are 0.99 and 1.03 in the positive bending region, respectively. In addition, local flange buckling of both bare beam and beam-GFRP system were observed in the second step of 0.02 radians of rotation, both in negative and positive bending. When the GFRP length was increased from $2d_b$ to L_b (L_b = distance from web stiffener to beam end), there was no difference at these values

(comparing row 3 with row 1). As it was observed in the first set of analyses, increasing the length of the GFRP from $2d_b$ to L_b did not have a contribution to the behavior of the beam (comparing row 3 with row 2).

Analyses were continued with increasing the thickness of GFRP. Rows 4, 5, and 6 present results for beam–GFRP systems with GFRP having a thickness of $0.91t_f$. The behavior of the beam-GFRP systems, with GFRP strips having a length of $2d_b$ and width of $0.19b_f$ showed little difference from the behavior of bare beam (comparing row 4 with row 1). Increasing the length of the GFRP strip from $2d_b$ to L_b also did not change the behavior. Keeping the thickness and length of the GFRP at $0.91t_f$ and $2d_b$, respectively, and increasing the width to $0.47b_f$ bumped up the load where buckling initiated one step; from the second cycle of 0.02 rad of rotation to first cycle of 0.03 rad of rotation. The increase in length also increased the M_{max}/M_p value; from 0.92 to 1.03 in negative bending and from 0.99 to 1.18 in positive bending. Rows 7 and 8 present results for beam–GFRP systems with GFRP having a thickness of $1.47t_f$ and length of $2d_b$. Keeping the width at $0.19b_f$ gave almost the same results as the beam-GFRP system presented in row 6 ($t_{GFRP} = 0.91t_f$, $L_{GFRP} = 2d_b$, $b_{GFRP} = 0.47b_f$). Although the stresses in the GFRP are not evaluated, using a thinner GFRP with a width of $0.47b_f$ will be more efficient than using a thicker GFRP with a width of $0.19b_f$; due to the fact that more surface area will reduce the stress demands to transfer shear forces. Keeping the thickness and length of the GFRP at $1.47t_f$ and $2d_b$, respectively, and increasing the width to $0.47b_f$ increased the maximum achieved moment more than 20%, which is greater than what is allowed; but also increased the load cycle at which local buckling initiates. The analyses presented in rows 9 and 10 were conducted to determine the required thickness of GFRP in order to achieve no buckling. No buckling was achieved with the following GFRP dimensions: $t_{GFRP} = 2.49t_f$, $L_{GFRP} = 2d_b$, $b_{GFRP} = 0.47b_f$. However, the maximum achieved moment at the face of the column far exceeded the limit.

Table 4.4. Location of GFRP: In and Out of the WH Region (Figure 4.24)

	1	2	3	4	5	6	7	8
	Number of Layer	t_{GFRP}	L_{GFRP}	b_{GFRP}	Negative Bending		Positive Bending	
					Max (M_{max}/M_P)	Local Flange Buckling	Max (M_{max}/M_P)	Local Flange Buckling
1	BARE	t_f = 13.25 mm	L_b = 3500 mm	b_f = 265 mm	0.92	0.02/2. Step	0.99	0.02/2. Step
2	3 Layers (4.5 mm)	0.34 t_f	$2d_b$	$0.47b_f$	0.95	0.02/2. Step	1.03	0.02/2. Step
3			L_b	$0.47b_f$	0.95	0.02/2. Step	1.03	0.02/2. Step
4	8 Layers (12 mm)	0.91 t_f	$2d_b$	$0.19b_f$	0.97	0.02/2. Step	1.02	0.03/1. Step
5			L_b	$0.19b_f$	0.97	0.02/2. Step	1.03	0.03/1. Step
6			$2d_b$	$0.47b_f$	1.03	0.03/1. Step	1.18	0.03/1. Step
7	13 Layers (19.5 mm)	1.47 t_f	$2d_b$	$0.19b_f$	1.00	0.03/1. Step	1.17	0.03/2. Step
8			$2d_b$	$0.47b_f$	1.23	0.03/2. Step	1.31	0.04/1. Step
9	17 Layers (25.5 mm)	1.92 t_f	$2d_b$	$0.47b_f$	1.29	0.04/1. Step	1.37	0.04/1. Step
10	22 Layers (33 mm)	2.49 t_f	$2d_b$	$0.47b_f$	1.46	no buckling	1.60	no buckling

Analyses were also conducted to determine whether the GFRP strips on top of the bottom flange inside welded haunch region had any effect on the performance of the system. Table 4.5 presents results for beams with GFRP strips placed inside (only at bottom of top flange) and outside the welded haunch region (Figure 4.25) together with a system with GFRP strips placed inside (both at bottom of top flange and top of bottom flange) and outside the welded haunch region (Figure 4.24). The results in Table 4.5 show that using GFRP at top of the bottom flange inside the welded haunch region has no contribution to the behavior of the system.

As a result, the optimum values for length and width of GFRP strips were chosen as: $L_{GFRP} = 2d_b$, $b_{GFRP} = 0.47b_f$. The thickness will change depending on the slenderness ratios of the flanges and the web.

Table 4.5. Location of GFRP: In and Out of the WH Region (There is no GFRP on top of the Bottom Flange) (Figure 4.25)

	1	2	3	4	5	6	7	8
					Negative Bending		Positive Bending	
	Number of Layer	t_{GFRP}	L_{GFRP}	b_{GFRP}	Max (M_{max}/M_P)	Local Flange Buckling	Max (M_{max}/M_P)	Local Flange Buckling
1	BARE	t_f = 13.25 mm	L_b = 3500 mm	b_f = 265 mm	0.92	0.02/2. Step	0.99	0.02/2. Step
2	13 Layers (19.5 mm) (There is GFRP on Bottom Flange in WH Region)	1.47 t_f	$2d_b$	$0.47b_f$	1.23	0.03/2. Step	1.31	0.04/1. Step
3	13 Layers (19.5 mm) (There is no GFRP on Bottom Flange in WH Region)		$2d_b$	$0.47b_f$	1.22	0.03/2. Step	1.31	0.04/1. Step

Figure 4.26 shows the normalized moment at the column face versus story drift ratio behavior of both bare beam with FSR of 10 and WSR of 60, (represented by solid line) and the same beam with GFRP having thickness of $0.91t_f$, length of $2d_b$, and width of $0.47b_f$ (represented with dash lines). As can be seen from the figure the upper limit of M_{max}/M_p = 1.2 is satisfied and local buckling initiates at the first cycle of 0.03 rad of rotation, compared to second cycle of 0.02 rad of rotation for the bare steel beam. Figure 4.27 represents the M/M_p-θ (rad) behavior of beam-GFRP system, which did not experience any local buckling (thickness of GFRP = $2.49t_f$).

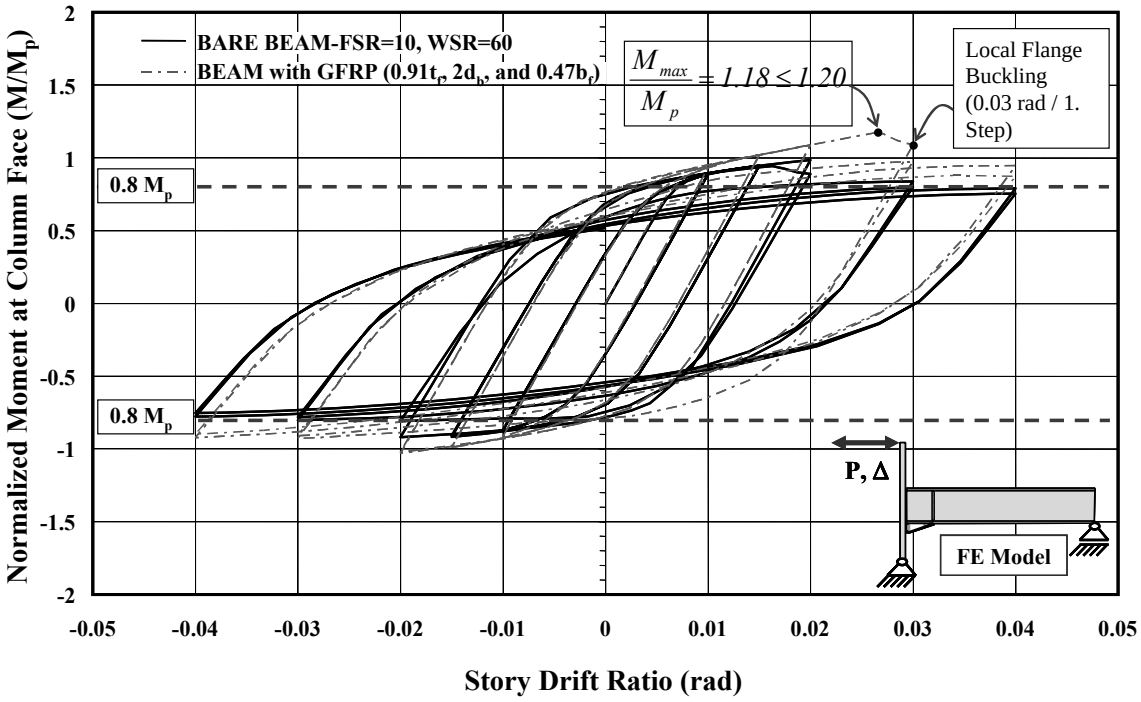

Figure 4.26. Moment-Rotation Behavior of Beam retrofitted by GFRP (FSR = 10, WSR = 60, GFRP dimensions = $0.91t_f$, $2d_b$, and $0.47b_f$)

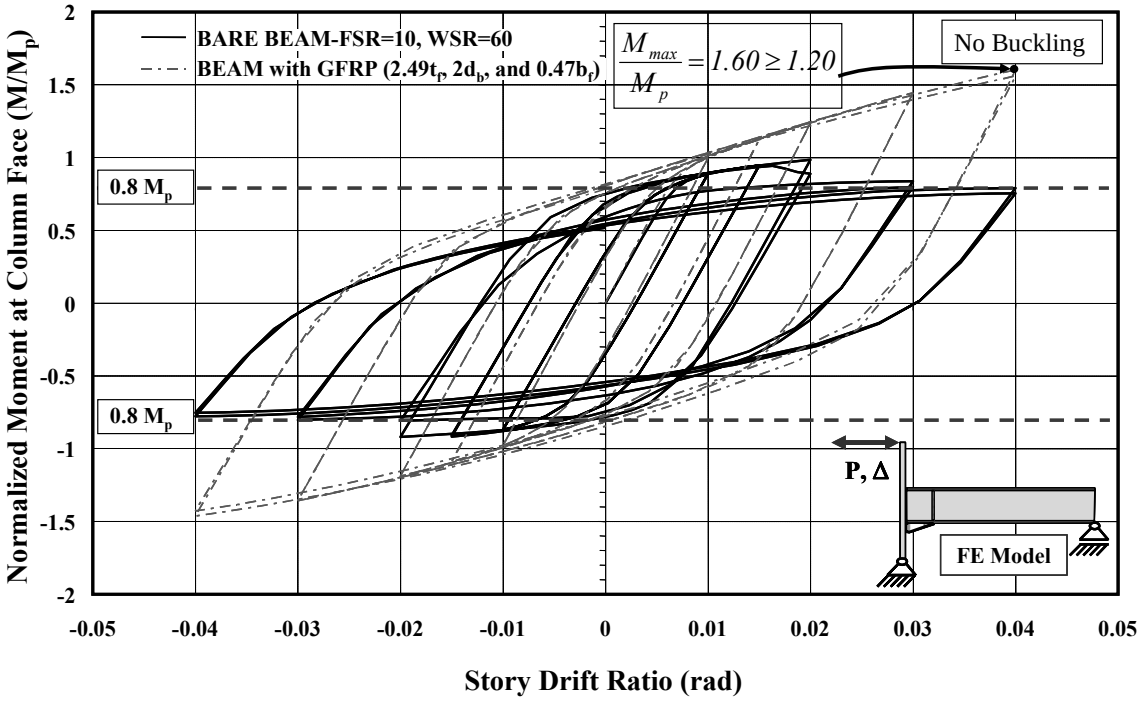

Figure 4.27. Moment-Rotation Behavior of Beam retrofitted by GFRP (FSR = 10, WSR = 60, GFRP dimensions = $2.49t_f$, $2d_b$, and $0.47b_f$)

Figure 4.28 and Figure 4.29 show the deformation profile of bare steel beam and steel-GFRP system (: $t_{GFRP} = 0.91t_f$, $L_{GFRP} = 2d_b$, $b_{GFRP} = 0.47b_f$) for the beam with FSR of 10 and WSR of 60, respectively, at 0.02 or the rad of rotation. The comparison clearly shows the effect of GFRP retrofitting.

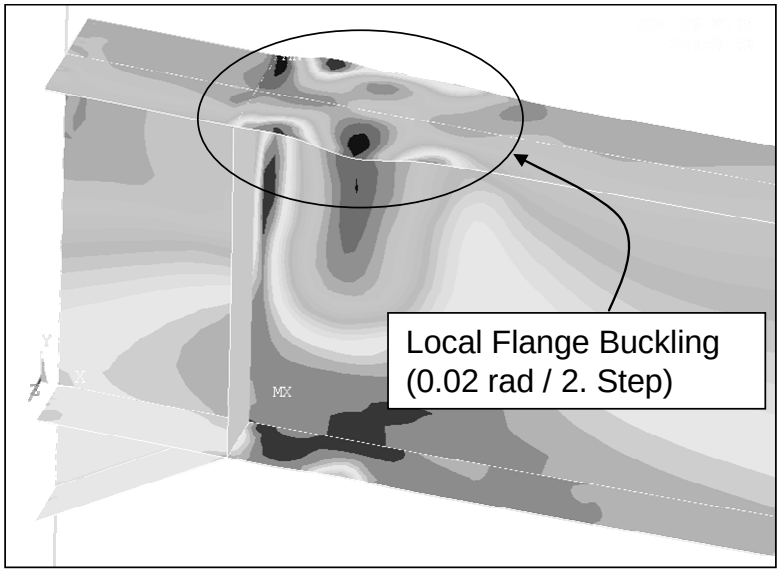

Figure 4.28. Behavior of Bare Beam at 0.02 rad/2. Step (FSR = 10, WSR = 60)

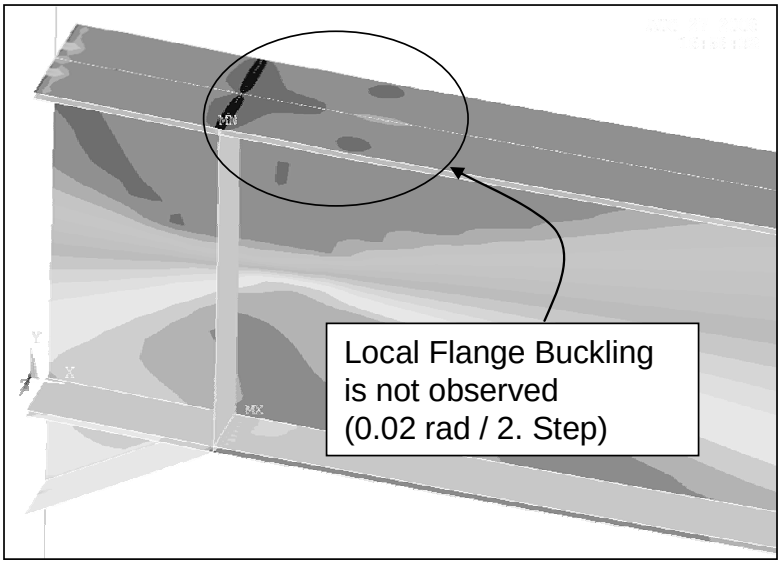

Figure 4.29. Behavior of Beam retrofitted by GFRP at 0.02 rad/2. Step (FSR = 10, WSR = 60, GFRP dimensions = $2.49t_f$, $2d_b$, and $0.47b_f$)

4.3.3.3. Analyses with Orthotropic GFRP Material Properties

After determining the ideal length ($2d_b$), ideal width ($0.47b_f$), and locations (on top of the bottom beam flange out of the WH region and on bottom of top beam flange in and out of WH region) of GFRP by using isotropic material properties for GFRP analyses were conducted by using orthotropic material properties for GFRP strips. In these analyses the thickness of one layer of GFRP was taken as 0.9 mm to be consistent with GFRP production scheme. The orthotropic material properties used in the analyses are given in Table 3.1 (elastic modulus, tensile strength of GFRP and polymer matrix) and Table 3.2 (shear modulus of GFRP in 3 directions).

In order to compare the behavior of GFRP modeled as an isotropic material with GFRP modeled as an orthotropic material, analyses were conducted for beam having FSR of 10 and WSR of 60 with both isotropic GFRP model and orthotropic GFRP model. The results of the analyses are presented in Table 4.6. The system with isotropic properties showed similar behavior as the system modeled using orthotropic material properties (comparing row 2 with row 3). The M_{max}/M_p value is 1.03 in the negative region for the beam-GFRP system with isotropic material properties and 1.04 for the beam-GFRP system with orthotropic material properties. The same is valid in the positive bending case. The similarities can also be observed in the load cycle when local buckling initiates.

Table 4.6. Comparison of GFRP modeled as an Isotropic Material with GFRP modeled as an Orthotropic Material

	1	2	3	4	5	6	7	8
					Negative Bending		Positive Bending	
	Number of Layer	t_{GFRP}	L_{GFRP}	b_{GFRP}	Max (M_{max}/M_P)	Local Flange Buckling	Max (M_{max}/M_P)	Local Flange Buckling
1	BARE	t_f = 13.25 mm	L_b = 3500 mm	b_f = 265 mm	0.92	0.02/2. Step	0.99	0.02/2. Step
2	8 Layers (1.5x8=12 mm) (Isotropic Material Model)	0.91 t_f	$2d_b$	0.47b_f	1.03	0.03/1. Step	1.18	0.03/1. Step
3	14 Layers (14x0.9=11.7 mm) (Orthotropic Material Model)	0.95 t_f	$2d_b$	0.47b_f	1.04	0.03/1. Step	1.17	0.03/1. Step

Analyses were continued for beam sections named as Beam 9 (FSR=10, WSR=80) and Beam 15 (FSR=12, WSR=80). Both Beam 9 and Beam 15 sections were strengthened by orthotropic GFRP material. The results of the analyses are tabulated in Table 4.7 and Table 4.8. The first rows of the tables include the information related to bare beams named as Beam 9 and Beam 15. For both beams only two analyses were conducted with GFRP strips (rows 2 and 3). It was observed in both beams that local buckling initiates in the webs, rather than in the flanges; due to the high web slenderness ratio. Adding GFRP postponed local buckling initiation one load cycle. However, further increase in the thickness of GFRP does not seem to affect the behavior, since buckling progresses in the webs. Further finite element analyses are being conducted and will be presented in another student's master's thesis.

In addition, in order to see the behavior of GFRP materials, the maximum tensile strength and interlaminar shear stress values of GFRP, which were taken from the FE analyses, were compared with the failure values observed in small scale standard tests in Table 4.9. It can be seen that the stress values determined from the analyses are well below the failure stresses of GFRP strips. Further investigation of the problem is currently being done by another master's student.

Table 4.7. Behavior of Beam-GFRP Systems (Beam 9 - FSR = 10, WSR = 80)

	1	2	3	4	5	6	7	8
	Number of Layer	t_{GFRP}	L_{GFRP}	b_{GFRP}	Negative Bending		Positive Bending	
					Max (M_{max}/M_P)	Local Flange Buckling	Max (M_{max}/M_P)	Local Flange Buckling
1	BARE	t_f = 13.25 mm	L_b = 3500 mm	b_f = 265 mm	0.91	0.02/1. Step	0.98	0.02/2. Step
2	19 Layers (17.1 mm)	1.29 t_f	$2d_b$	$0.47b_f$	1.08	0.02/2. Step	1.13	0.02/2. Step
3	20 Layers (18 mm)	1.36 t_f	$2d_b$	$0.47b_f$	1.08	0.02/2. Step	1.13	0.02/2. Step

Table 4.8. Behavior of Beam-GFRP Systems (Beam 15 - FSR = 12, WSR = 80)

	1	2	3	4	5	6	7	8
	Number of Layer	t_{GFRP}	L_{GFRP}	b_{GFRP}	Negative Bending		Positive Bending	
					Max (M_{max}/M_P)	Local Flange Buckling	Max (M_{max}/M_P)	Local Flange Buckling
1	BARE	t_f = 12.05 mm	L_b = 3500 mm	b_f = 265 mm	0.88	0.015/2. Step	0.92	0.02/1. Step
2	21 Layers (18.9 mm)	1.57 t_f	$2d_b$	$0.47b_f$	1.09	0.02/2. Step	1.15	0.02/2. Step
3	22 Layers (18 mm)	1.64 t_f	$2d_b$	$0.47b_f$	1.10	0.02/2. Step	1.15	0.02/2. Step

Table 4.9. Comparison of Interlaminar Shear Stress with Failure Values

Thickness of GFRP	Maximum Interlaminar Shear Stress (Mpa)		Maximum Tensile Strength of $0^o/-45^o/90^o/+45^o$ Oriented GFRP with 1250 gr/m^2 Unit Weight (MPa)
	XY direction	YZ direction	
Failure Values taken from the Results of Laboratory Tests	43.6	13	230
$0.95t_f$ (Beam 8 with FSR of 10, WSR of 60)	6.4	6.7	158.7
$1.36t_f$ (Beam 9 with FSR of 10, WSR of 80)	6.2	5.3	165.0
$1.64t_f$ (Beam 15 with FSR of 12, WSR of 80)	6.6	5.3	157

CHAPTER 5

CONCLUSIONS

This study presents an analytical study on both bare beams, which have flange slenderness ratios of 8 to 12 and web slenderness ratios of 40-60-80, modified by WH and three steel I-beams strengthened with GFRP strips subjected to inelastic reversed cyclic loading. The major observations from the analyses are summarized as follows:

1. As discussed in Chapter 4, all bare beams that modified with WH beneath the beam bottom flange reach their full plastic moment away from the column face and local buckling in the beam flanges and web occurred outside of the haunch region. On the other hand, twelve of the fifteen specimens are not adequate to reach the target story drift rotation amplitude with at least 80% moment capacity stipulated in ANSI/AISC-341-05 (AISC 2005b). Besides, all specimens experienced severe local buckling before reaching the inter-story drift angle of 0.04 rad.

2. The results of analysis conducted on bare beams shows that as the part of weld control, the maximum strength (the largest strength obtained during all the cycles) of all specimens was smaller than the design moment of the connections, as expected.

3. The analyses also showed that strength degradation rate and total (elastic and plastic) story drift ratio are strongly dependent on the slenderness ratio of WLB, not FLB.

4. For the beam-GFRP systems, the ideal dimensions of GFRP were determined as length of $2d_b$ and width of $0.47b_f$. Also, the optimum locations of GFRP are determined as adding the GFRP on top of the bottom beam flange out of the WH region and on bottom of top beam flange in and out of WH region; considering the presence of a concrete slab over the top flange in real structure.

5. The ideal thickness of GFRP, which satisfies the maximum moment criterion, were found as $0.91t_f$, $1.29t_f$, and $1.64t_f$ for Beam 8, Beam 9, and Beam 15, respectively (these beams were retrofitted by the ideal length and width of the GFRP).

6. In addition, the interlaminar shear stresses of all GFRP laminates were considerably smaller than the interlaminar shear stress failure values (43.6 MPa in YZ

(XZ) direction and 13 MPa in ZX (ZY) direction obtained from the results of laboratory tests).

7. As a result of FEA studies, it can be concluded that GFRP strips can postpone local buckling and improve the energy dissipation capacity of beam-column connections.

REFERENCES

Accord, N.B. and Christopher J. Earls. 2006. Use of Fiber Reinforced Polymer Composite Elements to Enhance Structural Steel Member Ductility. *Journal of Composites for Construction*, *ASCE* 10(4):337-344.

AISC 1994. *Load and Resisting Factor* (LRFD) *Manual of Steel Construction*. Chicago, IL: American Institute of Steel Construction (AISC).

AISC 2001. *Modification of existing welded Steel Moment Frame Connections for Seismic Resistance*. *Steel Design Guide Series 12*. Chicago, IL: American Institute of Steel Construction (AISC*)*.

Aktan, A.E., Karlson, B.I., and Sozen, M.A. 1973. *Stress-Strain Relationships of Reinforcing Bars Subjected to Large Strain Reversals. A Report on a Research Project Sponsored by the National Science Foundation, Research Grant GI 29934.* Urbana, Illinois: 397.

ANSI/AISC. 2005a. *Pre-qualified Connections for Special and Intermediate Steel Moment Frames for Seismic Applications,* AISC-358-05. Chicago, IL: American Institute of Steel Construction (AISC*)*.

ANSI/AISC 2005b. *Seismic Provisions for Structural Steel Buildings.* Chicago, IL: American Institute of Steel Construction (AISC*)*.

ANSI/AISC 2005c. *Specification for Structural Steel Buildings,* AISC 360-05. Chicago, IL: American Institute of Steel Construction (AISC*)*.

American Society for Testing and Materials (ASTM) 2005. *Standard Test Methods and Definitions for Mechanical Testing of Steel Products*, ASTM A 370-02. Philadelphia: American Society for Testing and Materials.

ANSYS User Manual 2007. *Swanson Analysis Systems*, Inc.

BİB 2006. *Specification for Structures to be Built in Disaster Areas.* Turkey, Ankara: Ministry of Public Works and Settlement Government of Republic of Turkey (BİB).

Bruneau, M., Engelhardt, M.D., Filiatrault, and A., Goel, S.C., eds. 2005. Review of Selected Recent Research on US Seismic Design and Retrofit Strategies for Steel Structures. *Progress in structural Engineering and Materials* 7:103–114.

Buyukozturk, O., Gunes, O., and Karaca, E. 2004. Progress on Understanding Debonding Problems in Reinforced Concrete and Steel Members Strengthened Using FRP Composites. *Construction and Building Materials* 18(1):9-19.

Cadei, J.M., Stratford, T.J., and Hollaway, T.C., eds. 2004. *Strengthening Metallic Structures Using Externally Bonded Fiber-Reinforced Polymers. Publication C595, Construction Industry Research and Information Association* (CIRIA), London, UK: 233.

Chen, W.F. and Han, D.J. 1988. *Plasticity for Structural Engineers.* New York: Springer-Verlag.

Civjan, S.A., Engelhardt, M.D., and Gross, J.L. 2000. Retrofit of Pre-Northridge Moment–Resisting Connections. *Journal of Structural Engineerin*g 126(4):445-452.

Dawood, M. and Rizkalla, S. 2006. Bond and Splice Behavior of High Modulus CFRP Materials Bonded to Steel Structures. *Third International Conference on FRP Composites in Civil Engineering, December*, Miami, Florida.

Ekiz, E., El-Tawil, S. Parra-Montesinos, G., and Goel, S. 2004. Enhancing Plastic Hinge Behavior in steel Flexural Members using CFRP Wraps. *Proceedings of the 13th World Conference on Earthquake Engineering*: 2496.

Engelhardt, M.D. and Husain, A.S. 1992. *Cyclic Tests on Large Scale Steel Moment Connections. Phil M. Ferguson Structural Engineering Laboratory Report* (PMFSEL). Austin, TX: Report No.92-2.

Engelhardt, M.D. 1998. Reinforcing of Steel Moment Connections with Cover Plates: Benefits and Limitations. *Engineering Structures* 20(12):1030-1038.

Eurocode-8 2003. *Design of structures for Earthquake Resistance – Part-1: General Rules, Seismic Actions, and Rules for Buildings.* Brussels, Belgium: *European Committee for Standardization (CEN).*

FEMA (Federal Emergency Management Agency) 2000a. *Recommended Seismic Design Criteria for New Steel Moment-Frame Buildings.* Washington, D.C: Federal Emergency Management Agency (FEMA) Publication No. FEMA-350.

FEMA 2000b. *Recommended Seismic Evaluation and Upgrade Criteria for Existing Welded Steel Moment-Frame Buildings.* Washington, D.C: Federal Emergency Management Agency (FEMA) Publication No. FEMA-351.

Gibson, R.F. 1994. *Principles of Composite Material Mechanic*s. New York: McGrawHill.

Guven, C.A. 2008. *Experimental Study on Improving Local Buckling Behavior of Steel Plates Strengthened with Glass Fiber Reinforced Polymers.* Turkey: Master Thesis Draft of İzmir Institute of Technology (IYTE).

Hull, D. and Clyne, T.W. 2000. *An Introduction to Composite Materials*. Cambridge: Cambridge University Press, 2nd Edition.

Jones, R.M. 1998. *Mechanics of Composite Materials*. Philadelphia, PA: Taylor & Francis, 2nd Edition.

Jones, S.L., Try, G.T., and Engelhardt, M.D. 2002. Experimental Evaluation of Cyclically Loaded Reduced Beam Section Moment Connections. *Journal of Structural Engineering* 128(4):441-451.

Jin, J. and El-Tawil, S. 2004. Seismic Performance of Steel Frames with Reduced Section Connections. *Journal of Constructional Steel Research* 61:453-471.

Kim, K. and Engelhardt, M.D. 1995. *Development of Analytical Models for Earthquake Analysis of steel Moment Frames. Phil M. Ferguson Structural Engineering Laboratory Report* (PMFSEL). Austin, TX: Report No. 95-2.

Lee, C.H., Jeon, S.W., Kim, J.H., and Uang, C.M. 2005. Effects of Panel Zone Strength and Beam Web Connection Method on Seismic Performance of Reduced Beam Section Steel Moment Connections. *Journal of Structural Engineering* 131(12):1854-1865.

Lenwari, A., Thepchatri, T., and Albrecht, P. 2005. Flexural Response of Steel Beams Strengthened with Partial-Length CFRP Plates. *Journal of Composites for Construction* 9(4):296–303.

Nakashima, M., Suita, K., and Morisako, K. 1998. Tests of Welded Beam-Column Subassemblies I: Global Behavior. *Journal of Structural Engineerin*g, ASCE 124(11):1236-1244.

Nakashima, M., Kanao, I., and Lui, D. 2002. Lateral Instability and Lateral Bracing of Steel Beams Subjected to Cyclic Loading. *Journal of Structural Engineering*, ASCE 128(10):1308-1316.

Nakashima, M., Liu, D., and Kanao, I. 2003. Lateral-Torsional and Instability of Steel Beams Subjected to Large Cyclic Loading. *Journal of Steel Structures*, *Korean Society of Steel Construction* 3(3):179-189.

Okazaki, T., Liu, D., Nakashima, M., and Engelhardt, M.D. 2006. Stability Requirements for Beams in Seismic Steel Moment Frames. *Journal of Structural Engineering*, ASCE 132(9):1334-1342.

Photiou, N.K., Hollaway, L.C., and Chryssanthopoulos, M.K. 2006. Strengthening of an Artificially Degraded Steel Beam Utilizing a Carbon/Glass Composite System. *Construction and Building Materials* 20:11-21.

Popov, E.P., Yang, T.S., and Chang, S.P. 1998. Design of Steel MRF Connections Before and After 1994 Northridge Earthquake. *Engineering Structures* 20(4-6):510-520.

Richard, D.H. 2004. *Mechanical Properties of Materials Data* MK-HDBK-5E:9-23. http://www.engr.ku.edu/~rhale/ae510/elasticity/sld009.htm (accessed May 15, 2008).

SAC. (1996). *Experimental Investigation of Beam-Column Subassemblages. Technical Report SAC-96-01, Parts 1 and 2,* Sacramento. CA: *SAC Joint Venture*.

SAC. (1999). *Local and Lateral-Torsional Buckling of Wide Flange Beams. Technical Report SAC-99-20.* Sacramento, CA: *SAC Joint Venture*.

Sayed-Ahmed, E.Y. 2004. Strengthening of Thin-Walled Steel I-Section Beams using CFRP Strips. *Proceedings of the 4th Advanced Composites for Bridges and Structures Conference*, Calgary, Canada.

Schwartz, M.M. 2002. *Composite Materials*. New Jersey: Prentice Hall PTR.

Schnerch, D., Dawood, M., Rizkalla, S., and Sumner, E. 2007. Proposed Design Guidelines for Strengthening of Steel Bridges with FRP materials. *Construction and Building Materials* 21:1001-1010.

Setunge, S., Kumar, A., and Nezamian, A., eds. 2002. *Review of Strengthening Techniques Using Externally Bonded Fiber Reinforced Polymer Composites.* Report 2002-005-C-01. Australia: CRC for Construction Innovation.

Taib, A.A., Boukhili, R., Achiou, S., Gordon, S., and Boukehili, H. 2006a. Bonded Joints with Composite Adherends. Part I. Effect of Specimen Configuration, Adhesive Thickness, Spew Fillet and Adherend Stiffness on Fracture. *International Journal of Adhesion and Adhesives* 26(4):226-236.

Taib, A.A., Boukhili, R., Achiou, S., and Boukehili, H. 2006b. Bonded Joints with Composite Adherends. Part II. Finite Element Analysis of Joggle Lap Joints. *International Journal of Adhesion and Adhesives* 26(4):237-248.

Fawzia, S., Riadh Al-Mahaidi,and Zhao, X.L. 2006. Experimental and Finite Element Analysis of a Double Strap Joint between Steel Plates and Normal Modulus CFRP. *Composite Structures* 75:156-162.

Tavakkolizadeh, M. and Saadatmanesh, H. 2003. Strengthening of Steel-Concrete Composite Girders Using Carbon Fiber Reinforced Polymers Sheets. J*ournal of Structural Engineering*, ASCE 129(1):30-40.

Uang, C.M., Yu, Q.S., Noel,S., and Gross, J.L. 2000. Cyclic Testing of Steel Moment Connections Rehabilitated with RBS or Welded Haunch. *Journal of Structural Engineering* (ASCE) 126(1):57–68.

Uang, C.M. and Fan, C.C. 2002. Stability Criteria for Steel Moment Connections with Reduced Beam Section. *Journal of Structural Engineering* 127(9):1021-1027.

Yu, Q.S., Uang, C.M., and Gross, J.L. 2000. Seismic Rehabilitation Design of Steel Moment Connection with Welded Haunch. *Journal of Structural Engineering* (ASCE) 126(1):57–68.

APPENDIX A

DESIGN CALCULATION FOR THE WELDED HAUNCH MODIFICATION

A.1 Design Example for Beam 8

The design of the welded moment connections is based on the American Institute of Steel Construction (ANSI/AISC 358-05) Seismic Provisions (2005a), AISC Design Guide Series (DGS) 12, Modification of Existing Welded Steel Moment Frame Connections for Seismic Resistance (AISC 2001), FEMA 2000a, FEMA 2000b, AISC Load and Resisting Factor Design (LRFD) Specification (Load 1994), Yu et al. (2000).

Step-by-step design calculation of the specimens with triangular haunch at the bottom side of the beam is summarized in conjunction with the procedure presented in Chapter 3 as follows:

Properties of Beam 8:

- d = 753 mm
- b_f = 265 mm
- t_f = 13.25 mm
- t_w = 11.56 mm
- h = 693.50 mm
- k = 25 mm
- A_b = 15601.5 mm^2
- I_x = 1355046248.13 mm^4
- S_x = 3599060.42 mm^3
- Z_b = 4189831.05 mm^3
- F_y = 345 MPa
- E = 205000 MPa
- L = 7000 mm

All notations used in the design calculation are presented in the APPENDIX B.

Step 1: Determination of a, θ and b values:

Design of the haunch is started with the suggestions of the length of the haunch, a, and the angle of the haunch, θ, as follows (AISC 2001; Yu, et al. 2000):

$$a \approx (0.5 \sim 0.6)d\,, \tag{A.1}$$

$$\theta \approx 30^o \pm 5^o\,, \tag{A.2}$$

$a \approx (0.5 \sim 0.6)d$: Choose a = 376.5 mm

$\theta \approx 30^o \pm 5^o$: Choose θ = 31 mm

The b value that is the vertical component of the haunch length may be checked as follows (AISC 2001; Yu, et al. 2000):

$$b = a \tan\theta\,, \tag{A.3}$$

$b = a \tan\theta$: Choose b = 226.2 mm

Step 2: Calculation of maximum moment (M_{pr}) expected in the plastic hinge region of beam:

The expected plastic moment, containing the strain hardening and other factors, is calculated as follows:

$$M_{pr} = 1.2F_y Z_b\,, \tag{A.4}$$

$M_{pr} = 1.2F_y Z_b = 1.2 * 345 * 4189831.05 = 1734590055$ N-mm

Step 3: Calculation of shear force, V_{pr}, in plastic hinge region of beam: (Consider a uniform gravity load, w =8.76 N/mm)

After the expected plastic moment, M_{pr}, is calculated, the corresponding beam shear, V_{pr}, at the plastic hinge region is determined as follows:

$$L' = L - 2a = 7000 - 2 * 376.5 = 6247 \text{ mm}$$

$$V_{pr} = \frac{M_{pr}}{(L'/2)} + \frac{wL'}{2} = \frac{1734590055}{\left(\frac{6247}{2}\right)} + \frac{8.76 * 6247}{2} = 582697.2 \text{ N}$$

Step 4: Calculation of required minimum β value: (Consider strength of weld metal, F_{EXX} = 600 MPa)

In order to limit the top flange groove weld stress to an allowable stress value, F_w, the minimum value of β can be calculated as follows (AISC 2001; Yu, et al. 2000):

$$\beta_{min} = \frac{(M_{pr} + V_{pr} a)/S_x - F_w}{\frac{V_{pr} a}{S_x} + \frac{V_{pr}}{I_b \tan\theta}\left(\frac{d^2}{4} - \frac{I_b}{A_b}\right)}, \quad \text{(A.5)}$$

$$F_w = 0.8 F_{EXX} = 0.8 * 600 = 480 \text{ MPa}$$

$$\beta_{min} = \frac{(1734590055 + 582697.2 * 376.5)/3599060.42 - 480}{\frac{582697.2 * 376.7}{3599060.42} + \frac{582697.2}{1355046248.13 * \tan 31}\left(\frac{753^2}{4} - \frac{1355046248.13}{15601.5}\right)}$$

$$\beta_{min} = 0.63$$

Step 5: Sizing of haunch flange:

For the strength requirement, the haunch is sized as follows (AISC 2001; Yu, et al. 2000):

$$A_{hf} \geq \frac{P_{hf}}{\phi F_{y,hf}} = \frac{\beta V_{pr}}{\phi F_{y,hf} \sin\theta}, \tag{A.6}$$

$$A_{hf} \geq \frac{P_{hf}}{\phi F_{y,hf}} = \frac{\beta V_{pr}}{\phi F_{y,hf} \sin\theta} = \frac{0.63 * 582697.2}{0.9 * 345 * \sin 31} = 2286.7 \text{ mm}^2$$

For satisfying the stability requirement, the haunch flange area of 4770 mm^2 is selected. The corresponding cross-section dimensions of haunch are 18x265 mm (=t_{hf} x b_{hf}) are selected.

Checking of the compact section requirement as (AISC 2001; Yu, et al. 2000):

$$\frac{b_{hf}}{2t_{hf}} = \frac{265}{2 * 18} = 7.36 \leq \frac{137}{\sqrt{F_{y,hf}}} = 7.38 \quad \text{OK}$$

Selected dimensions of haunch are suitable for compactness requirement.

Step 6: Evaluation of β value for stiffness requirement:

For stiffness requirement, the axial stiffness of the haunch flange should satisfy that the actual β value is not less than the minimum β value. In order to compute the actual β value for the haunch flange stiffness requirement, the minimum vertical component of the reaction, $\beta_{min}V_{pr}$, is computed by considering the deformation compatibility between beam and haunch. The resulting β value is defined as follows (AISC 2001; Yu, et al. 2000):

$$\beta = \left(\frac{b}{a}\right)\left(\frac{3L'd + 3ad + 3bL' + 4ab}{3d^2 + 6bd + 4b^2 + \frac{12I_b}{A_b} + \frac{12I_b}{A_{hf}\cos^3\theta}}\right) > \beta_{min}, \qquad \text{(A.7)}$$

$$\beta = \left(\frac{226.2}{376.5}\right) *$$

$$\left(\frac{3*6247*753 + 3*376.5*753 + 3*226.2*6247 + 4*376.5*226.2}{3*753^2 + 6226.2*753 + 4226.2^2 + \frac{12*1355046248.13}{15601.5} + \frac{12*1355046248.13}{4770*\cos^3 31}}\right) > \beta_{min}$$

$$\beta = 1.25 > \beta_{min} = 0.63 \quad \text{OK}$$

β is larger than the β_{min}. This means that the haunch flange with selected geometry would provide an adequate stiffness requirement. The other words the allowable stress, F_w, is an upper limit for the tensile stress in the flange groove weld at the column face.

After the actual β value is checked for the haunch flange stiffness requirement, the tensile stress in the top flange groove weld is computed and checked for the allowable stress, F_w, as follows:

$$f_{wt} = \frac{M_{pr} + V_{pr}(1-\beta)a}{I_b}\left(\frac{d}{2}\right) - \frac{\beta V_{pr}/\tan\theta}{I_b}\left(\frac{d^2}{4} - \frac{I_b}{A_b}\right) < F_w = 0.8F_{EXX}, \qquad \text{(A.8)}$$

$$f_{wt} = \frac{1734590055 + 582697.2*(1-1.25)*376.5}{1355046248.13} * \left(\frac{753}{2}\right)$$

$$- \frac{1.25*582697.2/\tan 31}{1355046248.13}\left(\frac{753^2}{4} - \frac{1355046248.13}{20476}\right) < F_w = 0.8*600 = 480 \text{ MPa}$$

$$f_{wt} = 417.5 \text{ MPa} < F_w = 480 \text{ MPa} \quad \text{OK}$$

The haunch flange axial stress is checked as follows:

$$\frac{\beta V_{pr}}{A_{hf}\ \sin\theta} \le \phi F_{y,hf}\ , \tag{A.9}$$

$$\frac{\beta V_{pr}}{A_{hf}\ \sin\theta} = \frac{1.25 * 582697.2}{4770 * \sin 31} = 296.8 \text{ Mpa} \le \phi F_{y,hf} = 0.9 * 345 = 310.5 \text{ MPa} \quad \text{OK}$$

The tensile stress in the top flange groove weld and the axial stress in the haunch flange would satisfy the strength requirements.

Under the situation that the beam is subjected to positive bending, the maximum tensile stress in the bottom flange groove weld is checked for the allowable stress, F_w, as follows:

$$\begin{aligned} f_{wb} &= \frac{V_{pr}\left(L'/2 + a\right)}{I_b}\left(\frac{d}{2}\right) - \frac{\beta V_{pr} a}{I_b}\left(\frac{d}{2}\right) - \frac{\left(\beta V_{pr}/\tan\theta\right)(d/2)}{I_b}\left(\frac{d}{2}\right) - \frac{\beta V_{pr}/\tan\theta}{A_b} \\ &= \frac{V_{pr} L'/2 + V_{pr}(1-\beta)a}{I_b}\left(\frac{d}{2}\right) - \frac{(\beta V_{pr}/\tan\theta)}{I_b}\left(\frac{d^2}{4} + \frac{I_b}{A_b}\right) < F_w = 0.8 F_{EXX}\ , \end{aligned} \tag{A.10}$$

$$f_{wb} = \frac{582697.2 * 6247 + 582697.2 * (1 - 1.25) * 376.5}{1355046248.13} * \left(\frac{753}{2}\right)$$

$$- \frac{1.25 * 582697.2 / \tan 31}{1355046248.13}\left(\frac{753^2}{4} + \frac{1355046248.13}{15601.5}\right) < F_w = 0.8 * 600 = 480 \text{ MPa}$$

$$f_{wb} = 285.6 \text{ MPa} < F_w = 480 \text{ MPa} \quad \text{OK}$$

Step 7: Checking of shear capacity of both haunch web and beam web:

For the haunch web width-thickness ratio, compactness requirements can be calculated as follows:

$$\frac{a\sin\theta}{t_{hw}} \le \frac{683}{\sqrt{F_{y,hw}}} \tag{A.11}$$

$$\frac{a\sin\theta}{t_{hw}} = \frac{376.5 * \sin 31}{12} = 16.2 \le \frac{683}{\sqrt{F_{y,hw}}} = \frac{683}{\sqrt{345}} = 36.8 \quad \text{OK}$$

Thickness of the haunch web, t_{hw}(=12 mm) is within the acceptable limit for the compactness requirement.

Shear stress, τ_{hw}, in the haunch web is computed as follows:

$$\tau_{hw} = \frac{aV_{pr}}{2(1+\upsilon)I_b}\left(\frac{L'}{2} - \frac{\beta}{\tan\theta}\left(\frac{d}{2}\right) + \frac{(1-\beta)a}{3}\right) < \phi_v\left(0.6F_{y,hw}\right) \tag{A.12}$$

$$= \frac{376.5 * 582697.2}{2 * (1+0.3) * 1355046248.13}\left(\frac{6247}{2} - \frac{1.25}{\tan 31}\left(\frac{753}{2}\right) + \frac{(1-1.25)376.5}{3}\right)$$

$$\tau_{hw} = 143.7 \text{ MPa} < \phi_v\left(0.6F_{y,hw}\right) = 186.3 \text{ MPa} \quad \text{OK}$$

The shear in the beam web, V_{bw}, is calculated as follows:

$$V_{bw} = (1-\beta)V_{pr} \tag{A.13}$$

$$V_{bw} = (1-\beta)V_{pr} = (1-1.25) * 582697.28 = -146542.24 \text{ N} < V_{pr} = 582697.2 \text{ N}$$

The value of V_{bw} is negative. It means that the direction of the beam shear in the haunch region is reversed. The other words, β is larger than 1. The result of Equation A.13 shows that the critical beam shear force value is significantly larger than the shear force in the beam web. Results clearly show that the designed haunch is very suitable for the purpose that the welded haunch reduces the beam shear at the column face.

Step 8: Designing of the beam web stiffeners depended on the actual β value:

The situation of without beam web stiffeners for the design strength, R_n, is checked for the local web yielding using the following equation as follows:

$$\phi R_n = 1.0(2.5k + N)F_y t_w \quad \text{(LRFD (1993), Equation K.1-3 in Chapter K)}$$

$$= 1.0*(2.5*25 + 18)345*11.56 < \beta V_{pr} = 1.25*582697.28$$

$$\phi R_n = 283619.83 \text{ N} < \beta V_{pr} = 729239.5 \text{ N} \quad \text{(NG)}$$

The design strength, R_n, is less than the concentrated force of βV_{pr}. Therefore, a pair of beam web stiffeners consisted of 132.5x20 mm plates (A572 Gr. 50 steel) are provided at the end of the haunch.

The width-thickness ratio of the stiffeners is checked for a compactness section as follows:

$$\frac{b_s}{t_s} \le \frac{250}{\sqrt{F_{y,s}}}, \tag{A.14}$$

$$\frac{b_s}{t_s} = \frac{132.5}{20} = 6.6 \le \frac{250}{\sqrt{F_{y,s}}} = \frac{250}{\sqrt{345}} = 13.4 \quad \text{OK}$$

For strength requirement of an axially compressed member, including two stiffeners together with a strip of the beam web as shown in Figure 3.10, the Equation 3.29 should be satisfied from the LRFD Specifications (1994), Section E2:

$$A_{eff} = 2*132.5*20 + 12*11.56*11.56 = 6903.1 \text{ mm}^2$$

$$I_{eff} = 132.5*\frac{(20*2+11.56)^3}{12} = 35254048.5 \text{ mm}^4$$

The effective length of the compressed member is $0.75h$.

$$r = \sqrt{\frac{I_{eff}}{A_{eff}}} = \sqrt{\frac{35254048.5}{6903.1}} = 71.5 \text{ mm}$$

$$\frac{KL}{r} = \frac{0.75h}{r} = \frac{0.75*693.5}{71.5} = 7.3$$

$$\lambda_c = \frac{KL}{r\prod}\sqrt{\frac{F_y}{E}} = \frac{0.75*693.5}{71.5*3.14}\sqrt{\frac{345}{205000}} = 0.14 < 1.5$$

$$\phi_c F_{cr} = \phi_c * \left(0.678^{\lambda_c^2}\right)F_y = 0.85\left(0.678^{0.14^2}\right)*345 = 290.93 \text{ MPa}$$

$$\phi_c P_n = \phi_c F_{cr}\left(A_{eff}\right) > \beta V_{pr}$$

$$\phi_c P_n = 0.85*299.93*\left(6903.5\right) > \beta V_{pr} = 11.25*582697.28$$

$$\phi_c P_n = 2008352.5 \text{ N} > \beta V_{pr} = 729239.5 \text{ N} \quad \text{OK}$$

The stiffeners are ensured to the strength requirement. Therefore, the preliminary dimensions of WH are acceptable for designing of Beam 8.

APPENDIX B

NOTATIONS

M_{pr} = maximum moment expected in the plastic hinge region (N-mm)

R_y = ratio of the expected yield stress to the specified minimum yield stress (ANSI/AISC 341-05 (AISC 2005b) Table I-6-1)

Z_e = effective plastic modulus of the section at the location of the plastic hinge (mm^3)

C_{pr} = factor to account for peak connection strength, including strain hardening, local restraint

F_y = specified minimum yield stress of steel (MPa)

F_u = specified minimum tensile strength of steel (MPa)

V_{pr} = maximum shear expected in the plastic hinge region (N-mm)

L' = beam span between critical plastic sections (mm), and

w = uniform beam load (N/mm)

a = length of haunch (mm)

d = beam depth (mm), and

θ = angle of haunch (degree)

b = vertical component of the haunch length (mm)

Z_b = plastic section modulus of beam cross-section (mm^3)

F_y = yield stress of steel, including ratio of expected yield stress to specified minimum yield stress (MPa)

β_{min} = minimum β value to limit beam top flange groove weld stress to F_w

F_w = allowable stress of groove weld ($0.8F_{EXX}$)

F_{EXX} = strength of weld metal (MPa)

S_x = elastic section modulus (mm^3)

I_b = moment of inertia of beam section (mm^4)

A_b = area of beam section (mm^2)

P_{hf} = haunch flange axial force that is equal to $\beta V_{pr}/sin\theta$ (N)

A_{hf} = haunch flange area that is equal to $t_{hf}\, b_{hf}$ (mm^2)

$F_{y,hf}$ = minimum specified yield stress of haunch flange (MPa)

β = minimum β value to limit beam top flange groove weld stress to F_w

ϕ = resistance factor, 0.9

b_{hf} = haunch flange width (mm)

t_{hf} = haunch flange thickness (mm)

f_{wb} = tensile stress at beam bottom flange groove weld (MPa)

t_{hw} = haunch web thickness (mm)

$F_{y,hw}$ = minimum specified yield stress of haunch web (MPa)

τ_{hw} = haunch web shear stress (MPa)

υ = Poisson's ratio of steel (0.3)

ϕ_v = resistance factor, 0.9

V_{bw} = shear force in beam web (N)

$F_{y,s}$ = minimum specified yield stress of beam web stiffeners (MPa)

t_s = beam web stiffener thickness (mm)

b_s = beam web stiffener width (mm)

ϕ_c = resisting factor for compression, 0.85

F_{cr} = critical stress (MPa)

A_{eff} = gross area of compression members consist of cross-section area of two stiffeners and a strip of the beam web having a width of $12t_w$ (mm^2)